UNIVERSITY OF OKLAHOMA

GRADUATE COLLEGE

ROLE OF THE OUTER MEMBRANE CHANNEL TolC IN PHYSIOLOGY OF *ESCHERICHIA COLI*

A DISSERTATION

SUBMITTED TO THE GRADUATE FACULTY

in partial fulfillment of the requirements for the

Degree of

DOCTOR OF PHILOSOPHY

By

GIRIJA DHAMDHERE
Norman, Oklahoma
2010

ROLE OF THE OUTER MEMBRANE CHANNEL TolC IN PHYSIOLOGY OF *ESCHERICHIA COLI*

A DISSERTATION APPROVED FOR THE
DEPARTMENT OF CHEMISTRY AND BIOCHEMISTRY

BY

_____
Dr. Helen I. Zgurskaya, Chair

_____
Dr. Valentin V. Rybenkov

_____
Dr. Ann H. West

_____
Dr. Richard W. Taylor

_____
Dr. Anne K. Dunn

Acknowledgements

Follow your passion, and success will follow you -Terri Guillemets. This is exactly what got me from Pune, India to The University of Oklahoma, USA. This journey was long and would not have been possible without the support of so many people in my life. I want to take this opportunity to thank all of them and for making it possible for me to attain this significant milestone in my life. Writing this part is probably the most difficult part of writing this dissertation, difficult because I do not have enough words to thank everyone who has been there for me.

Firstly, I would like to thank my advisor Dr. Zgurskaya for her help and support throughout my PhD program. I look up to her excellent work ethic and constant strive for success. I would also like to express my sincere gratitude to Dr. Rybenkov. His ideas and suggestions were always thought provoking and helped me look at science with a different perspective. I am greatly indebted to both of them for making me a scientist. I would like to thank my committee members Dr. Ann West, Dr Taylor and Dr. Anne Dunn for giving me valuable suggestions during seminars and annual evaluations. I really appreciate them for taking the time out from their busy schedules to attend evaluation meetings every year. Special thanks to Dr. Elena Tikhonova for teaching me all the basic techniques in the lab and encouraging me to go on when I was feeling down. I would also like to extend my thanks to Dr. Zoya Petrushenko, Dr. Yoichi Yamada and Dr. Lusine Demirkhanyan for providing with their help and support. This would not have been a fun experience without the friends I have made

here. Thank you to Dr. Sze Yi Lau, Dr. Vishakha Dastidar, Yun Liu, Sita Devi Modali, Shuo Lu and Nehul Shah. I have made so many great memories here. I would also like to thank Dr. Ganesh Krishnamoorthy and Dr. Qiang Ge for their great suggestions and support.

Most importantly I would like to thank my parents Savita and Rajeev Dhamdhere. They always taught me that nothing is impossible with hard work and perseverance. It is because of the values they have instilled in me that I stand here today. I thank them for their unconditional love and support. I would also like to thank my brother Vasudev Dhamdhere for being there for me when I needed it. Thank you to my grandparents Hari Dhamdhere, Maliti Dhamdhere, Vishnu Joshi and Malini Joshi. They inspire me and have always encouraged me to "go get it." I want to take this opportunity to thank my parents-in law Dr. Sushama Marathe, Anant Marathe and my sister-in law Yogeshree Marathe for their encouragement and support. Special thanks to my aunt and uncle, Madhura Damle, Dr Nitin Damle and Dr. Bal Vad and Dr. Lata Vad for making me feel at home when I was away from home.

I want to say a big "thank you" to my dear husband, Ameya Marathe. I do not have enough words to express what his support has meant for me. Thank you for believing in me and encouraging me to achieve my goals. I would not have managed this feat without his unwavering love and support.

Finally I would like to thank God for all the blessings he has bestowed upon me and for bringing such wonderful people in my life.

Table of Contents

List of Tables

III. Results

III.1 Inactivation of TolC induces stress on *E.coli* membrane and arrests growth on glucose.

III.2 Understanding the physiological role of *E.coli* TolC-YgiBC operon.

III.3 Investigation of multifunctional interactions between TolC and transporters

List of Figures

I. Introduction

III. Results

III.1 Inactivation of TolC induces stress on *E.coli* membrane and arrests growth on glucose.

III.2 Understanding the physiological role of *E.coli* TolC-YgiBC operon.

III.3 Investigation of multifunctional interactions between TolC and transporters.

Abbreviations

ABC	**ATP binding cassette**
ADHII	**Yeast alcohol dehydrogenase (II)**
ADP	**Adenosine diphosphate**
ATP	**Adenosine triphosphate**
AMP	**Adenosine monophosphate**
BSA	**Bovine serum albumin**
CBB	**Coomassie brilliant blue**
CCCP	**Carbonyl cyanide m-chlorophenyl hydrazone**
CPM	**7-Diethylamino-3-(4'-maleimidylphenyl)-4-methylcoumarin**
DNA	**Deoxyribonucleic acid**
DTT	**Dithiothreitol**
EDTA	**Ethylenediaminetetraacetate**
F5M	**Fluorescein-5-maleimide**
GSH	**Glutathione**
GSSG	**Oxidised glutathione**
GSP	**Glutathionyl spermidine**
IM	**Inner membrane**
IPTG	**Isopropyl-β-D-thiogalactopyranoside**
kDa	**Kilodalton**
LB	**Luria-Bertani**
MBB	**Monobromobimane**
MFP	**Membrane fusion protein**

MFS	**Major Facilitator Superfamily**
MIC	**Minimal inhibitory concentration**
MTT	**3-[4,5-dimethylthiazol-2-yl]-2,5-diphenyltetrazolium bromide**
MW	**Molecular weight**
NAD^+	**Nicotinamide adenine dinucleotide**
NADP	**Nicotinamide adenine dinucleotide phosphate**
NADH	**Nicotinamide adenine dinucleotide hydrogen phosphate**
OD	**Optical density**
OM	**Outer membrane**
ORF	**Open reading frame**
PBS	**Phosphate buffered saline**
PCR	**Polymerase Chain Reaction**
PDB	**Protein data bank**
PMSF	**Phenylmethylsulfonyl fluoride**
PMF	**Proton motive force**
PVDF	**Polyvinylidene Fluoride**
RNA	**Ribonucleic acid**
RND	**Resistance-Nodulation-Cell division**
RPM	**Rotation per minute**
RT	**Room temperature**
RTPCR	**Reverse transcriptase PCR**
SDS-PA	**Sodium dodecyl sulfate-polyacrylamide gel**
SPE	**Spermidine**
TMS	**Transmembrane segment**

TX-100	**Triton X-100**
WT	**Wild type**

Abstract

TolC is a versatile, multifunctional protein and in Gram-negative bacteria such as *E.coli*, it has been shown to participate in several functions like drug efflux, toxin secretion and has also been demonstrated to be important for survival in iron limiting conditions. This multifunctional nature of TolC makes it an attractive target for drug design and therefore it becomes imperative to understand the mechanism of TolC's multifunctional nature.

The first part of this dissertation is focused on understanding the physiological function of TolC in *E.coli*. We found that the loss of TolC induces stress on the cytoplasmic membrane and notably impairs cell division and growth in minimal medium. The TolC-dependent phenotype was further exacerbated by the loss of *ygiB* and *ygiC* genes expressed in the same operon as *tolC* and their homologs *yjfM* and *yjfC* located elsewhere on the chromosome. We found that the growth deficiency of *tolC* mutants is caused by the stress on the membrane, L-serine auxotrophy, and depletion of essential metabolites such as GSH and NAD^+. We conclude that disruption of membrane functions caused by inactivation of TolC makes cells highly vulnerable to the challenges of aerobic glucose metabolism. The membrane stress in Δ*tolC* cells leads to metabolic shut-down and growth arrest. The activity of YgiBC and YjfMC protects membranes from the stress and allows Δ*tolC* mutants to resume growth on glucose.

The second part of this dissertation is focused on understanding how TolC is engaged into protein complexes. For this purpose we constructed chromosomal TolC cysteine mutants with a C-terminal six histidine tag. Cysteine replacements at positions

Q352, D356, S363 and D374 were constructed as these residues have been predicted to lie at the TolC-MFP interaction interface. These chromosomal TolC cysteine mutants were expressed from the chromosomal native promoter and were functional. We used these mutants to study in vivo TolC-MFP interactions. Our co-purification and cross-linking experiments indicate that TolC is in close association with MFP, AcrA. However, all the cysteine residues except for TolCQ352C were readily labeled with fluorescent dye, indicating that TolC is freely available for interaction with MFPs. These in vivo studies strongly indicate that TolC-MFP interactions are highly dynamic and transient in nature.

I. Introduction

Entry and exit of molecules in all cells is tightly regulated by the permeability of the cytoplasmic membrane. Gram-negative bacteria like *E.coli* have two such membranes, an inner cytoplasmic membrane (IM) and an outer membrane (OM). The space between the two membranes is known as the periplasm. Therefore in Gram-negative bacteria molecules need to pass through two membrane barriers. *E.coli* has several different transporter protein complexes that facilitate this process. These complexes usually contain an outer membrane protein (OMP) that facilitates transport across the OM and an inner membrane protein which couples H^+ transport or ATP hydrolysis to transport of substances.

E.coli also possesses three component transport systems that allow transport of substances across the two membranes without periplasmic intermediates. This is facilitated by a third periplasmic component which forms a link to connect the OMP to the inner membrane transporter. Several such three component systems have been well studied. For example *E.coli* uses FepA-TonB-ExbBD transport system for import of colicin B and colicin D. In this system FepA is the outer membrane receptor whereas TonB-ExbBD forms the inner membrane-periplasmic transporter complex (Lazdunski *et al*., 1998). Similar systems such as AcrAB-TolC and MacAB-TolC are used for the export of an array of drugs, dyes, detergents and macrolides respectively (Okusu *et al*., 1996 and Kobayashi *et al*., 2001). In these three-component systems, AcrAB and MacAB form the inner membrane-periplasmic transporter complex and TolC, an outer membrane protein serves as the common exit duct. In *E.coli*, TolC is a

multifunctional export protein engaged in the efflux of xenobiotics, protein secretion and enterobactin export (Wandersman *et al*., 1990 and Bleuel *et al*., 2005). TolC's diverse functionality stems from its ability to interact with several different transporters and their respective periplasmic components.

The following section will highlight the known functions and structure of TolC. It also includes the description of the TolC-YgiBC operon as well as the description of glutathionylspermidine, glutathione and spermidine metabolism in *E.coli*.

I.1.1 Role of TolC in multidrug resistance. Antibiotic resistance poses a major problem in the treatment of bacterial infections and Gram-negative bacteria tend to be more resistant to antimicrobials than the Gram-positive bacteria (Nikaido *et al*., 1998). The combination of the outer membrane (OM) as an additional permeability barrier and expression of drug resistance efflux systems makes Gram-negative bacterial infections difficult to treat. The genome of *E.coli* contains 45 predicted drug efflux transporters (http://www.membranetransport.org) with experimental evidence for only 14 of the predicted drug transporters. To date, at least eight different multidrug transporters belonging to different families have been reported to require TolC for their function. TolC is known to interact with AcrAB, AcrD, AcrEF, MdtEF and MdtABC belonging to the RND (Resistance Nodulation Cell-Division) family of transporters. In addition TolC interacts with two MFS (Major Facilitator Superfamily) drug transport systems, EmrAB, EmrKY and an ABC (ATP binding cassette) drug transporter system, MacAB.

AcrAB-TolC is a well-studied multidrug efflux system in *E.coli*. Inactivation of *acrAB* genes renders cells susceptible to an array of drugs, dyes and

detergents (Okusu *et al*., 1996). Substrates for the AcrAB-TolC pump include drugs such as penicillins, cephalosporins, fluoroquinolones, chloramphenicol, tetracyclines, novobiocin, erythromycin and rifampicin; detergents such as bile salts, sodium dodecyl sulfate and dyes like acriflavine and ethidium bromide (Ma *et al*., 1995 and Nikaido & Takatsuka, 2009). AcrB is an integral inner membrane protein with 12 transmembrane segments (TMS) and large periplasmic loops that interact with AcrA and TolC (Seeger *et al*., 2006). AcrB determines the substrate specificity and uses proton motive force (PMF) to actively export its substrates. Membrane fusion protein (MFP), AcrA is attached to the inner membrane by lipid modification. AcrA acts as a link between the inner membrane transporter AcrB and the outer membrane protein, TolC, by bringing them together and forming a long exit conduit (Ip *et al.*, 2003, Zgurskaya & Nikaido, 1999a and Zgurskaya & Nikaido, 1999). Tikhonova *et al.* showed that constitutively expressed AcrAB-TolC, irrespective of the presence of its substrate, forms a stable complex (Tikhonova & Zgurskaya, 2004) inside the cell (Fig I.1A). The key for the actual export of the substrate is opening of the TolC entrance. It is proposed that conformational changes in AcrA trigger the opening of the TolC channel thus allowing substrates to pass through the channel.

I.1.2 Role of TolC in virulence of pathogenic *E.coli*. Enterohemorrhagic and uropathogenic *E. coli* produce hemolyin toxin, HlyA which is secreted out of the cells. HlyA integrates into the host eukaryotic cells and forms pores causing target cell lysis (Stanley *et al*., 1998). Wandersman *et.al* showed that *E.coli* strains deficient in TolC are defective in secretion of hemolysin toxin (Wandersman & Delepelaire, 1990) indicating that TolC plays an important role in virulence of pathogenic *E.coli*. In *E.coli* HlyA is

expressed as a part of *hlyCABD* operon. Gene product of HlyC helps in posttranslational modification and maturation of HlyA toxin. HlyB is integral membrane protein. Its cytoplasmic ATP binding domain undergoes conformational change on ATP binding and couples ATP hydrolysis to HlyA export (Koronakis *et al*., 1995). HlyD is a membrane fusion protein (MFP) known to interact with HlyB and TolC. Cross-linking data shows that unlike AcrAB, HlyBD only recruits the outer membrane channel TolC in the presence of substrate, HlyA (Balakrishnan *et al*., 2001) (Fig I.1B). Thus the HlyBD-TolC secretion system allows direct translocation of hemolysin toxin from the cytoplasm to the cell surface and extracellular medium. Similar to hemolysin secretion TolC is also involved in secretion of colicinV, an antibacterial peptide toxin (Hwang *et al*., 1997). Colicin V secretion also requires CvaB, an inner member ABC (ATP binding cassette) type transporter and CvaA a membrane fusion protein which forms a link between CvaB and TolC. Like hemolysin toxin secretion, CvaAB-TolC complex is only formed in the presence of substrate colicinV (Hwang *et al*., 1997).

I.1.3 Role of TolC in enterobactin secretion and other functions in *E.coli*. Enterobactin is a catecholate-type siderophore of *E.coli*. Enterobactin is produced and used for iron acquisition in iron limiting growth conditions (Bleuel *et al*., 2005). The outer membrane receptor FepA is required for the import of the Fe-enterobactin complex. Recently it was shown that TolC along with transporter EntS is required for the export of enterobactin outside the cell (Bleuel *et al*., 2005). These results indicate that TolC is important for survival of *E.coli* under iron limiting conditions.

Recently, Wiriyathanawudhiwong *et.al* showed that amino acid L-cysteine was toxic to *E.coli* strains deficient in TolC, indicating that the cysteine

toxicity could be due to the impairment of efflux of cysteine and therefore leading to accumulation of cysteine in the periplasm (Wiriyathanawudhiwong *et al*., 2009).

All of the above examples exemplify the TolC's multifunctional role in *E.coli*. The key factors for this multifunctional nature are 1) TolC structure and 2) ability of TolC to interact with different types of transporters.

I.2 Crystal structure of TolC. TolC was crystallized as a homotrimer and the structure was solved at 2.1 Å resolution by Koronakis and co-workers. (Koronakis *et al*., 2000) The structure revealed TolC as a tapered long hollow cylinder 140 Å in length. It comprises a 40 Å long outer membrane β barrel domain (channel domain) that anchors a contiguous 100 Å long α-helical barrel projecting across the periplasm (tunnel domain) (Fig I.2A). A third domain also known as the equatorial domain is made up of both α-helices and β barrels and lines the mid section of the α-helical barrel. This structure of TolC creates a large solvent-filled interior cavity with a volume of roughly 43,000 $Å^3$.

The β-barrel domain. Like majority of the bacterial outer membrane proteins (OMPs) that contain 8 to 22 β-sheets the channel domain of TolC is also assembled from 12 β-strands (four β strands from each protomer) in an antiparallel orientation (Koronakis *et al.,* 2000). The β-barrel is right twisted. Position of the amino acid residues allow for twisting and curving of the β-strands. Small or unbranched side chains are present periodically on the inside of the barrel, and residues with bulkier side chains lie on the outside of the barrel. The loops at the top end of the β-strands of TolC serve as partial external 'lid'. These loops are highly flexible and serve as sites for colicin and

bacteriophage attachment (German & Misra, 2001). In most OMP the interiors are often partially or completely occluded however, the β-barrel of TolC is wide open and fully accessible to solvent.

The α-helical domain. The α-helical barrel is contiguous with the β-barrel and extends into the periplasm. The α-helical domain, especially the periplasmic entrance of this domain, has been shown to be engaged in interaction with MFP such as AcrA (Lobedanz *et al.,* 2007). This domain comprises of 12 helices (4 from each monomer, an inner pair and an outer pair) in an antiparallel arrangement. Although the inner pair and outer pair of helices have high sequence similarity they are arranged differently. An inner pair of helices (H7 and H8) forms a conventional antiparallel coiled-coil but the outer pair (H3 and H4) comprises a straight helix (H3) around which its partner helix 4 is coiling. All the coiled-coils are stabilized by an intermeshing of side-chains ('knobs-into-holes' packing) (Fig I.3). The upper section of the helical domain (near the β-barrel) is virtually uniform in diameter but tapers to a virtual close. One of these coiled-coils from each monomer folds inwards at the periplasmic end and forms a constriction in the TolC pore.

A.

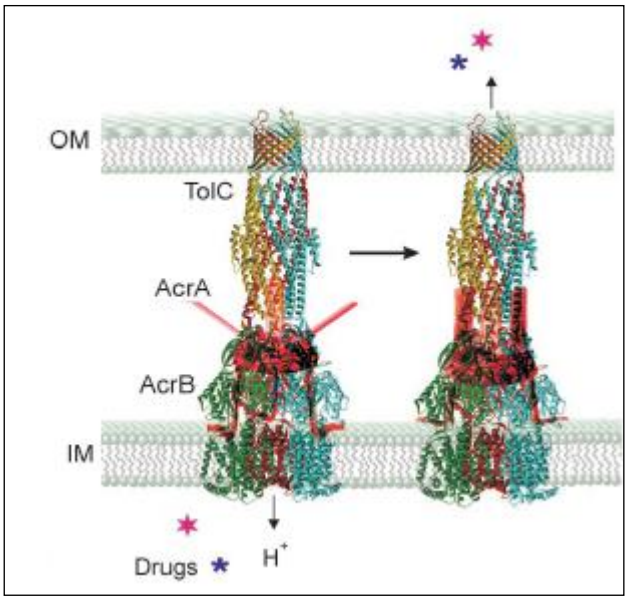

B.

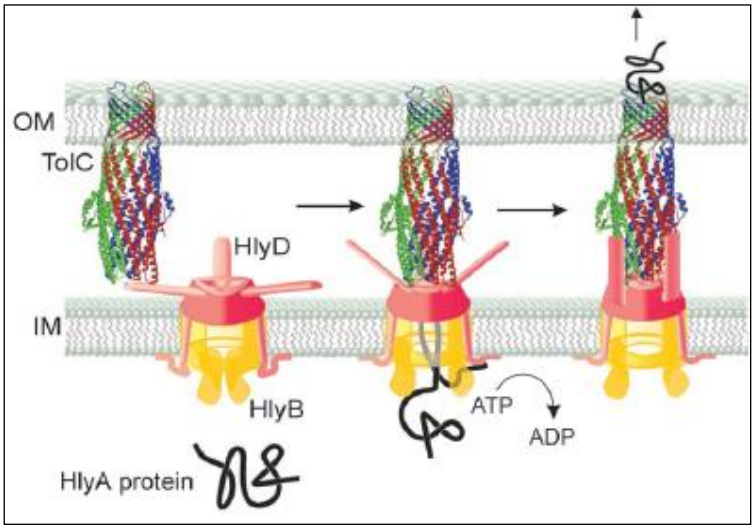

Figure I.1 Recruitment of the TolC channel by AcrAB (Panel A) and HlyBD (Panel B) for efflux of drugs and hemolysin toxin. Figure adapted from Koronakis *et al.*, 2004

This constriction denotes the closed or resting state of TolC and has an effective diameter of approximately 3.9 Å (Anderson, *et al*., 2002) (Fig I.2B). This entrance has to be opened by the MFP-IM transporter to allow the export of substrates. This closed or resting state is stabilized by salt bridges and hydrogen bonds. Figure I. 2D illustrates the fine network of hydrogen bonds and salt bridges. Hydrogen bonds between Asp153–Tyr 362 and Gln136–Glu359 connect each inner coiled coil to the outer coil of the same monomer. Arg367 of the neighboring monomer forms a salt bridge with Asp153 and hydrogen bond to Thr152, thus connecting the inner coil of one monomer to the outer coil of the adjacent monomer (Fig I.2D). Mutations in residues 362 and 367 have shown TolC to remain in constitutively open state thus underlying the importance of H-bond network necessary for closing the periplasmic aperture (Vaccaro *et al*., 2008) (Augustus *et al*., 2004). The periplasmic entrance of the TolC channel is lined by a ring of six aspartic acid residues at positions 371 and 374. Previous studies have shown that these residues are important and can influence selection of substrates (Andersen *et al*., 2002).

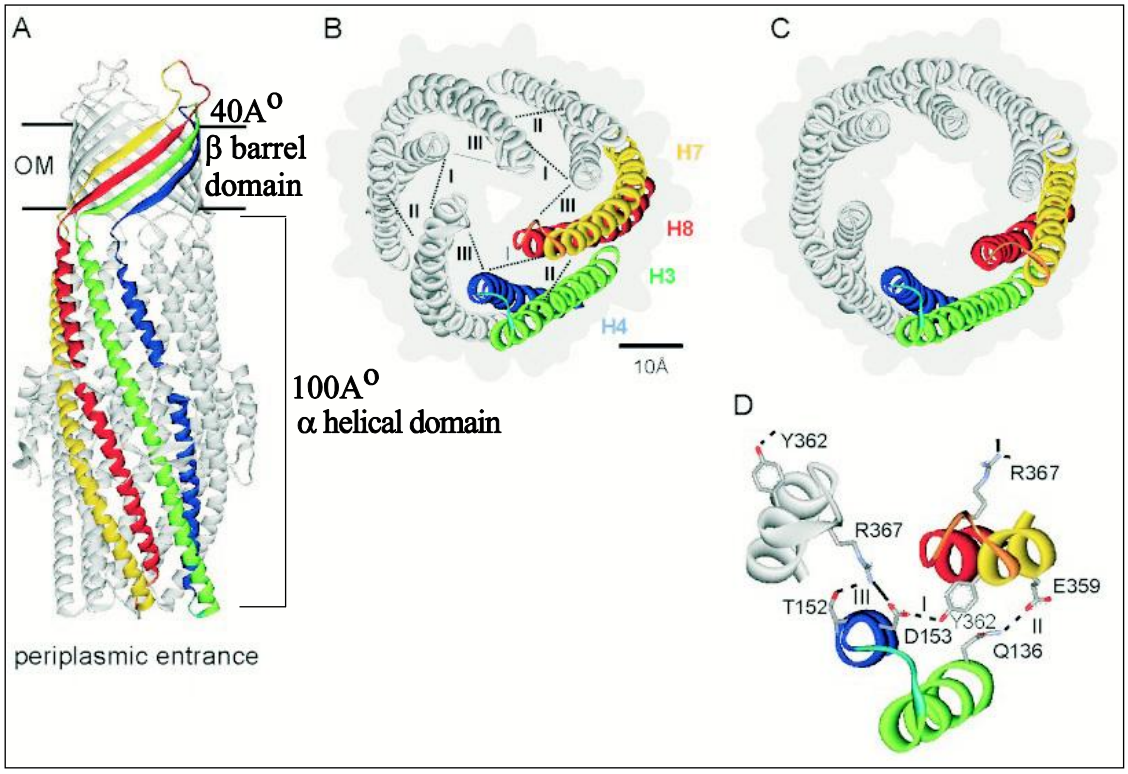

Figure I.2. Structural features of TolC from *E.coli*. Figure adapted from Andersen, *et al*., 2002. (A) TolC was crystallized as a trimer (Koronakis *et al*., 2000). (B) The closed entrance as seen from the periplasmic side. Helices of one monomer are colored. Outer coiled coil helices H3 and H4 are shown in green and blue, respectively. Inner coiled coil helices H7 and H8 are shown in yellow and red, respectively. Intramonomer (I and II) and intermonomer interactions (III) are shown as dotted lines. The gray background shows the surface representation highlighting the small periplasmic entrance. (C) The modeled open state of the entrance derived by realigning the inner coiled coils (H7 and H8) to the same configuration as the outer coiled coils (H3 and H4). (D) Intermonomer and intramonomer network at the tunnel entrance. Intermonomer hydrogen bonds between Asp153-Tyr362 and Gln136-Gln359 shown as dotted lines. Intramonomer salt

bridge between Arg367 of a different monomer with Asp153 shown in solid line. Intramonomer hydrogen bond between Arg367 and Thr152 represented as a dotted line.

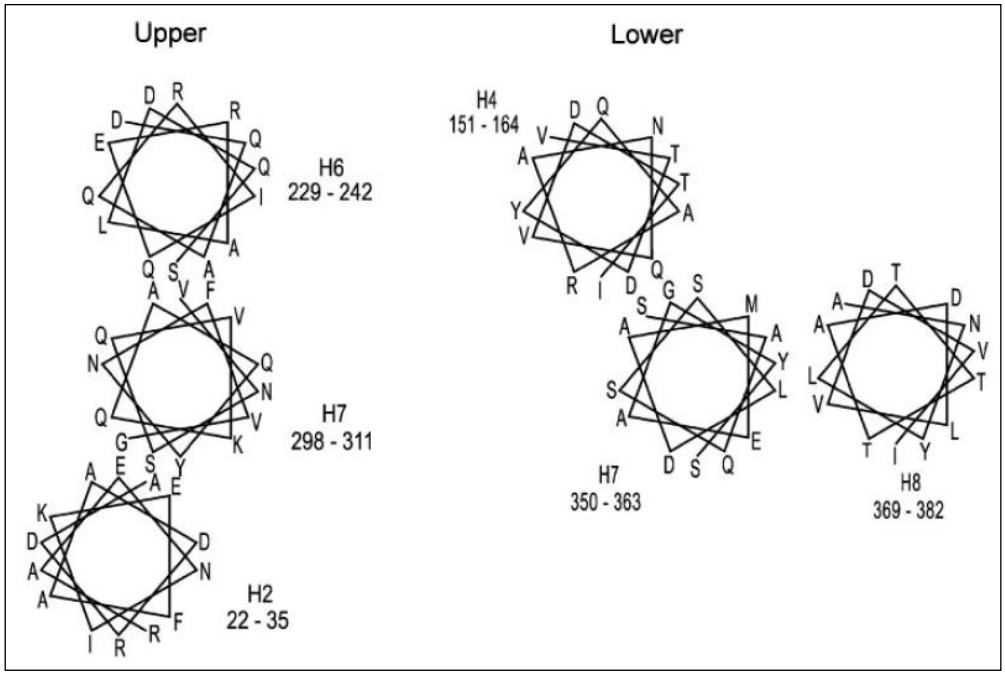

Figure I.3 Helical wheel representations of interhelical interactions of TolC α helical barrel. Upper and lower indicate upper and lower parts of the α helical barrel. Figure adapted from Koronakis *et al*., 2004.

I.3. The TolC-YgiBC operon. In the genome of *E. coli* and other enterobacteria, the chromosomal *tolC* locus contains three genes *tolC*, *ygiB* and *ygiC*, which are said to be expressed in a single operon (Fig. I.4A). However, the functions of YgiB and YgiC as well as any functional link between these proteins and TolC remains unknown.

TolC is a member of the *marA*/*soxS*/*rob* regulon and contains a marbox consensus sequence at position 3176034–3176052 (Martin, *et al*., 1999). MarA, SoxS

and Rob are global stress induced regulators (Martin & Rosner, 2003 and Amabile-Cuevas & Demple, 1991). Recently Zhang and co-workers showed there are four *tolC* promoters (p1-4) (Fig I.4B) (Zhang *et al.*, 2008). Each of the promoters responds to different environmental signals. The p1 promoter has significant constitutive expression under laboratory conditions but is not responsive to EvgAS, PhoPQ, MarA, SoxS or Rob. The p2 promoter is only responsive to EvgAS and PhoPQ and p3 and p4 are activated by MarA, SoxS and Rob (Zhang *et al*., 2008). Both EvgAS and PhoPQ are two-component signal transduction systems. EvgAS upregulates the expression of genes responsible for MDR phenotype (Nishino & Yamaguchi, 2001) and PhoPQ system responds to Mg^{2+} starvation (Kato *et al*., 1999). It is predicted that the presence of four regulatory elements responding to different environmental signals can help tailor the TolC response according to the need of a particular TolC function.

A.

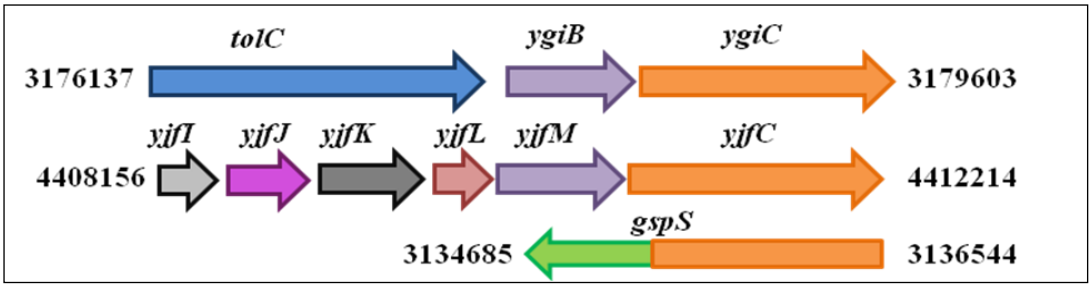

B.

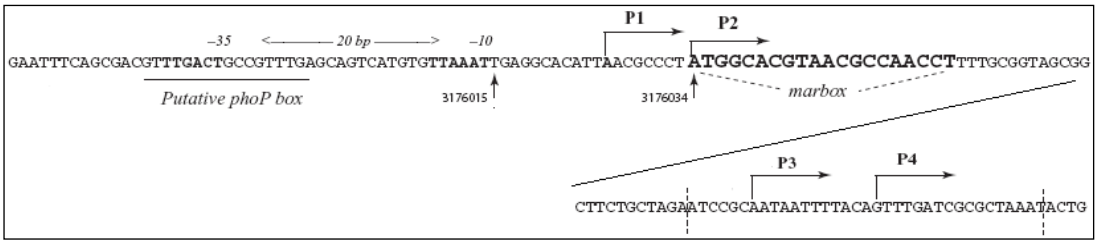

Figure I.4 *E.coli* TolC-YgiBC operon. A. TolC-YgiBC operon structure. **B.** TolC promoter sequences. Figure adapted from Zhang *et al.*, 2008

Kohanski *et al.*'s microarray data shows that expression of YgiB is significantly induced when cells experience oxidative stress indicating that YgiB could play a role in protecting *E.coli* cells against oxidative stress (Kohanski *et al.*, 2007). YgiB is a unique protein and only shares significant homology with YjfM. YjfM is another protein of unknown function expressed elsewhere on the *E.coli* chromosome. YgiB is a 223 amino acid residue protein with a predicted molecular weight of 23.4 kDa and a pI of 9.4. YgiB is highly conserved in other bacteria such as cyanobacteria and proteobacteria and its homologs are also present in some Gram-positive species where they precede the *ygiC*-like genes. Amino acid sequence analysis of YgiB shows the presence of consensus sequence of Leu-Ala-Gly-Cys also known as the lipobox

(Hayashi & Wu, 1990) indicating that YgiB could be a lipoprotein. Post-translational modification prediction programs such as LipoP1.0 and SignalP 3.0 confirm this observation and predict YgiB to be an outer membrane lipoprotein containing a putative type II signal peptide with cleavage site between amino acid positions 36 and 37 (Fig I.5). Residue at position 38, second residue after the predicted cleavage site is glutamic acid indicating that YgiB could be located in the outer membrane. PSIpred a secondary structure prediction program predicts YgiB to be an α/β type of a protein. YgiB is predicted to have four α-helices and five β-sheets. The predicted β-sheets have just two to four amino acid residues indicating that these could be small β-turns. The majority of the protein is predicted to be in an unstructured coil form. Another unique and striking feature of YgiB is the presence of four conserved cysteine residues at positions 53, 64 88 and 97 present in α helices random coil respectively. The role of these charged cysteine residues in the outer membrane remains unknown but could play an important role in inter helical hydrogen bonding (Fig I.5).

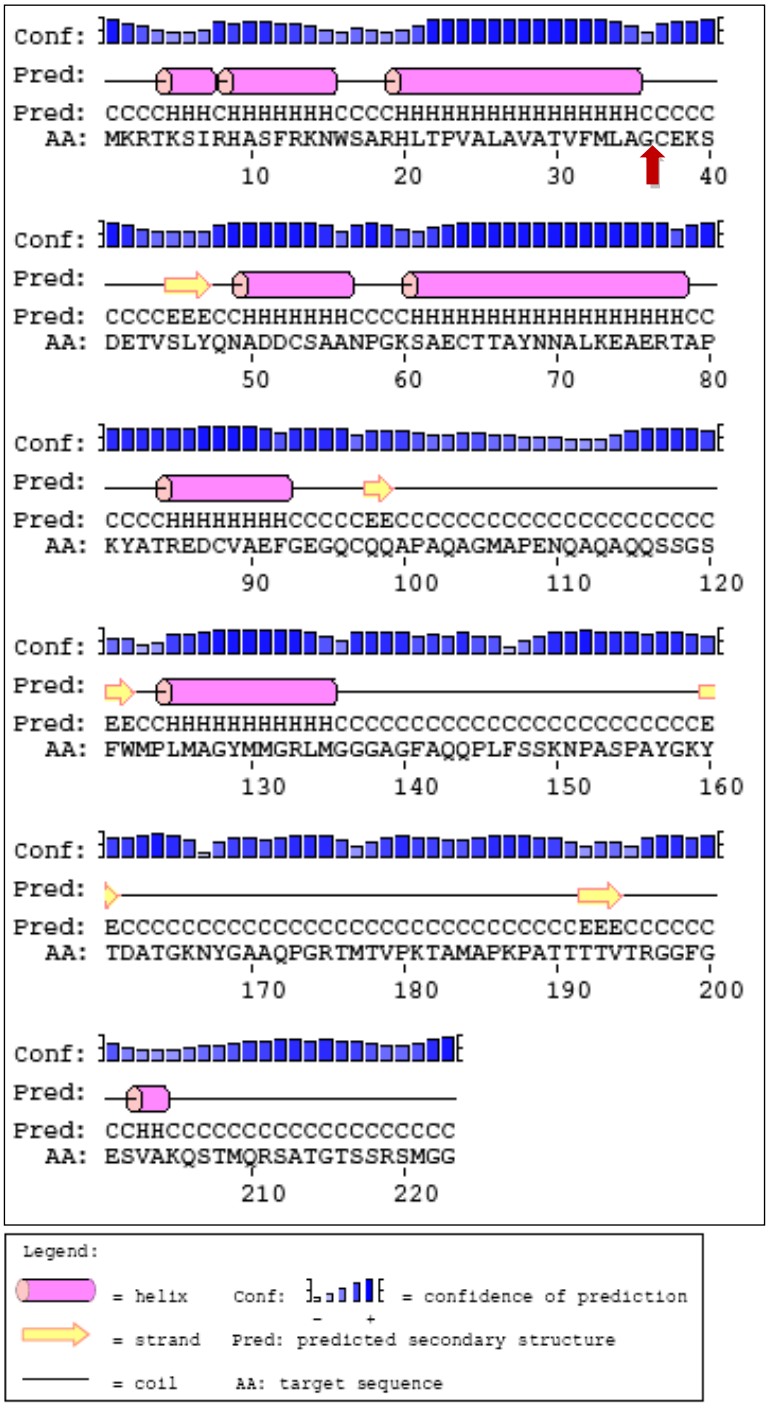

Figure I.5 Secondary structure prediction of YgiB. Predicted cleavage site and cysteine residue modified for attachment of lipid moiety indicated by red arrow.

YgiC is present immediately downstream of YgiB. YgiC is a 386 amino acid residue protein with a predicted molecular weight of 45 kDa and a pI of 4.7. YgiC is predicted to be a cytoplasmic protein and shares significant homology with the C-terminal synthetase domain of *E. coli* GspS and an uncharacterized protein YjfC (Fig I.6). GspS is a bifunctional enzyme possessing both glutathionylspermidine (GSP) synthetase and GSP amidase activities (Bollinger *et al*., 1995). The C-terminal domain of GspS is a GSP synthetase belonging to the ATP-Grasp ATPases family of proteins, which also include the human glutathione synthetase (Pai *et al*., 2006). This domain uses ATP hydrolysis to conjugate glutathione (GSH) and spermidine (SPE) to yield glutathionylspermidine (GSP). The crystal structure of substrate bound GspS and sequence alignment of YgiC with GspS shows that the residues involved in GSH and spermidine binding are conserved. All residues involved in binding and hydrolysis of ATP are also conserved in YgiC. Such high conservation of catalytically important residues in YgiC suggests that this protein could be a GSP synthetase. As YgiC shares 27% identity with GspS we used crystal structure of GspS (PDB ID- 2IO9, chain B) to model the three dimensional structure of YgiC. Programs SWISS MODEL (Arnold *et al*., 2006, Kiefer *et al*., 2009 and Peitsch, 1995) and Frye (Kelley & Sternberg, 2009) were used for this purpose. Both programs predicted similar models, therefore the model generated from SWISS-MODEL was used for further analysis. Figure I.7A shows modeled structure of YgiC. From the predicted structure YgiC has 12 α-helices and 14 β-sheets. Although the overall structure looks similar to GspS synthetase domain there are small differences in the number and orientation of certain α-helices and β-sheets. The presence of an additional amidase domain in GspS can account for the

differences in the orientation of the α-helices and β-strands. Similar to the synthetase domain of GpsS, the overall structure of YgiC is also triangular in shape. The N-terminal domain of YgiC is composed mainly of α-helices and the C-terminal domain of β-sheets. The three main structural units conserved in human glutathione synthetase and GspS are also observed in YgiC even though GspS and YgiC lack any sequence homology with human glutathione synthetase. The three important structural features include an antiparallel β-sheet formed by β12 and β13. In contrast, this domain of GspS structure contains five β strands β 15, β 16, β 29, β 30 and β 31 form the antiparallel β-sheet. The GSH and SPE binding sites are predicted to be centered in this antiparallel β-sheet, in a pocket lined by α-helices 5, 6, 7. The second conserved structural feature is the parallel β-sheet composed of β 2, β 3, β 6 and β 7. The third structural domain is the lid domain and contains β 8, β 9, β 10, β 11, α-12 and the P-loop (Fig I.7A, P-loop indicate in Fig I.8). The ATP binding sites are predicted to be present in the anti-parallel β –sheet of the lid domain. High conservation in predicted structural domains of YgiC, similar to those of human glutathione synthetase and GspS lead us to believe that YgiC belongs to the ATP grasp family of ATPases.

Figure I.6 Sequence alignment of YgiC with GspS (gsp) and YjfC. Conserved and similar residues are marked with *. Amino acid residues involved in GSH binding shown in red, ATP binding residues shown in purple, spermidine binding in green and residues involved in co-ordination of Mg^{2+} ions shown in blue.

A.

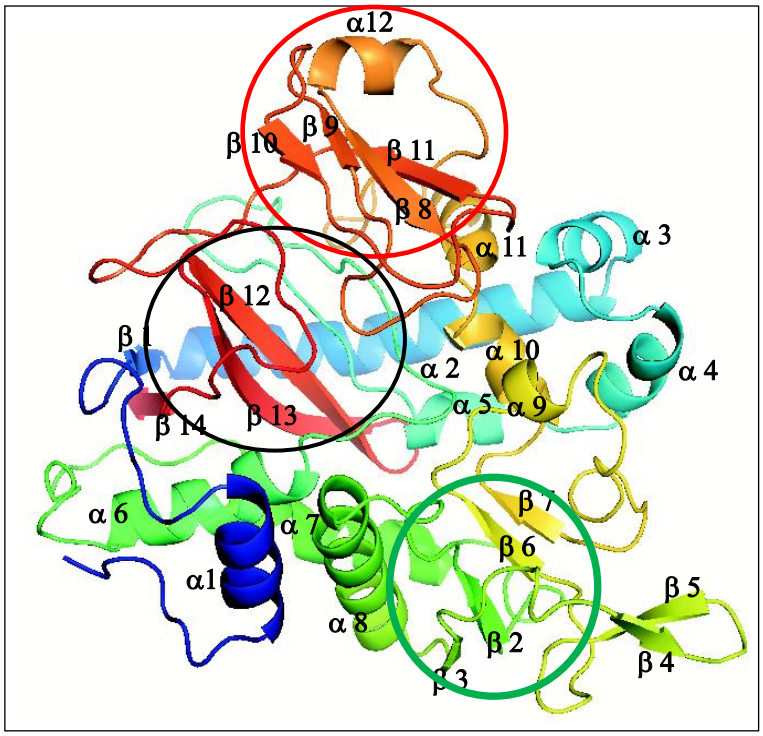

B.

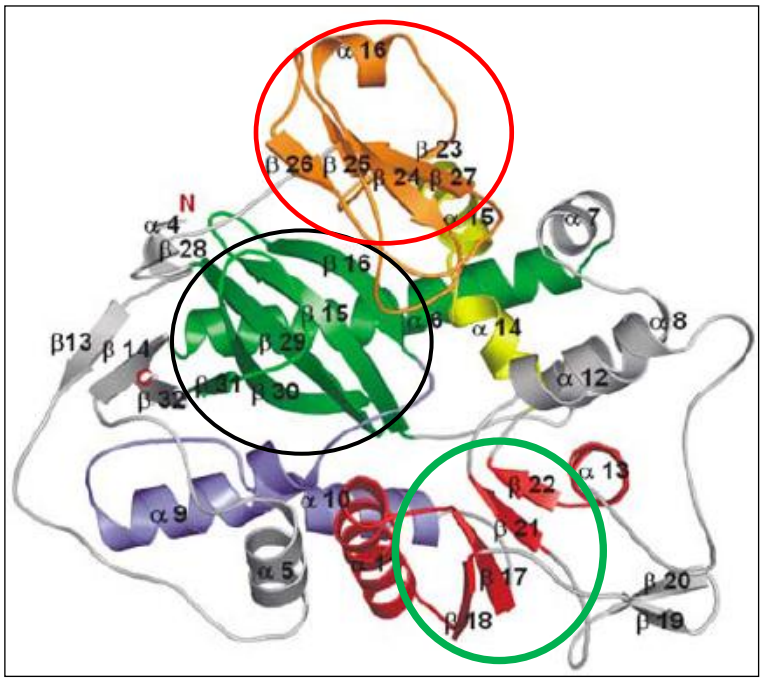

Figure I.7 Predicted tertiary structure of YgiC. A. SWISS-MODEL predicted structure of YgiC. The conserved structural domains are circled as lid domain-red,

antiparallel β sheet circled in black and the parallel β sheet in green. **B.** GspS synthetase domain. Figure adapted from Pai *et al.,* 2006. The three structral domains are higlighted as above, for the predicted structure of YgiC.

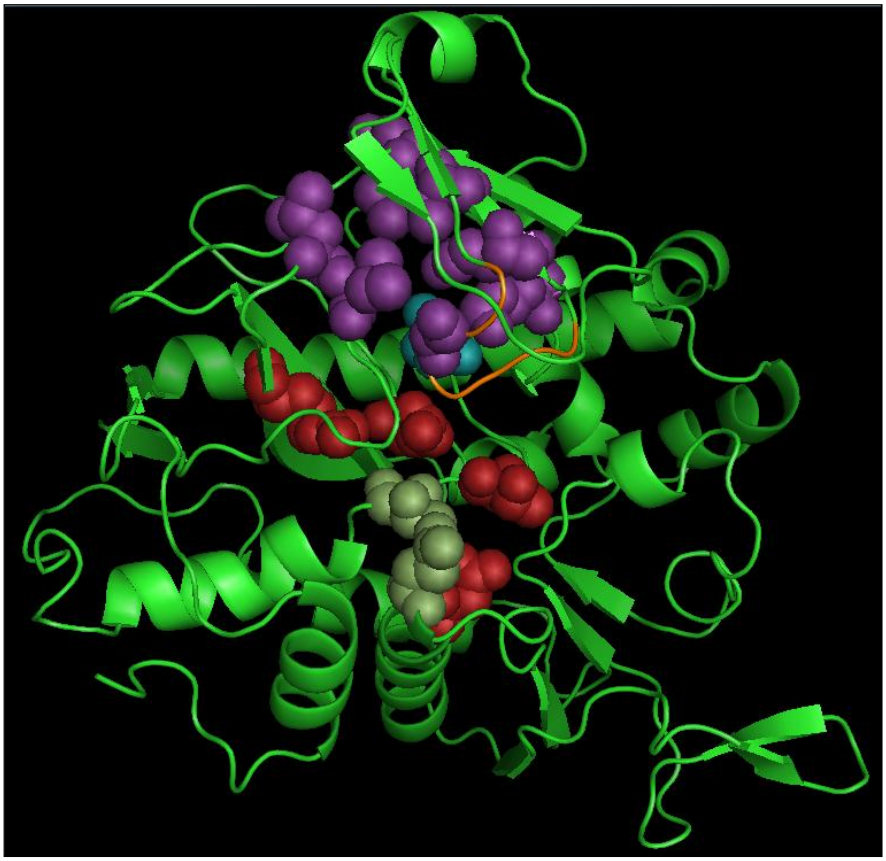

Figure I.8 Predicted YgiC structure indicating binding sites for GSH (R100, T120, D185, R307 and R366) and SPE (T122, E184) shown as spheres in red and green, respectively. Only conserved residues or residues that have conserved substitution are highlighted. Predicted binding sites for ATP (K267, L284, V300, K302, G309, Q377, L371, I372) and Mg^{2+} (E115) are shown in purple and blue, respectively. P-loop indicated in orange.

I.4 The YjfIJKLMC operon. YjfMC proteins share significant sequence homology with YgiB and YgiC, respectively. *yjfMC* genes are expressed as a part of an operon *yjfIJKLMC* and are present elsewhere on the *E.coli* chromosome (Fig I. 4A) . YjfI is a conserved protein 14 kDa in size with pI of 4.0. YjfJ is also a conserved protein and belongs to the phage shock protein A (PspA) /IM30 family of proteins and is predicted to be a 25 kDa protein with a pI of 6.0. The phage shock protein (Psp) response helps maintain the proton motive force (PMF) in cells under PMF-dissipating stress conditions. YjfK is predicted to be a cytoplasmic protein with a molecular weight of 25 kDa. YjfM is also predicted to be a cytoplasmic protein however it is 23% identical to YgiB, a putative outer membrane lipoprotein. Like YgiB, YjfM is a basic protein with a pI of 9.4. YjfC is a glutathionylspermidine synthetase homolog and is 50% identical to YgiC. Sequence alignment of GspS, YgiC and YjfC shows that majority of the catalytic residues are conserved in these proteins. YjfC like YgiC is predicted to be a cytoplasmic protein.

tolC and *ygiBC* genes are predicted to constitute a single operon. Therefore, we hypothesized that YgiBC are functionally linked to TolC. In our research we tried to identify and characterize this functional link between TolC and YgiBC proteins.

I.5. Glutathionylspermidine biosynthesis and metabolism in *E. coli*. Glutathionylspermidine (GSP) is a conjugate of glutathione (GSH) and spermidine (SPE). This conjugate was first detected in *E.coli* in 1959 by Dublin (Dubin, 1959). Previous studies also indicate that major fraction of spermidine is converted to GSP and

that GSP accumulated when *E.coli* is growing in glucose rich medium in stationary phase (Tabor & Tabor, 1975). Later this conjugate was detected in parasitic trypanosomas (Fairlamb *et al*., 1985). Fairlamb and co-workers also showed that in these parasitic trypanosomas, glutathionylsperimide was produced as an intermediate of the metabolic pathway that produces trypanothione, a bis(glutathionyl)spermidine conjugate (Fig I.9) (Fairlamb *et al*., 1985). As these parasites lack GSH reductase and GSH peroxidase activities, trypanothione has appropriated the role as the major and only antioxidant. Since trypanothione appears to have important roles in these pathogens and it is not present in hosts, its metabolism is an obvious target for design of new antiparasitic drugs. However, *E.coli* lacks the enzyme trypanothione synthetase and therefore synthesizes only GSP. The enzyme glutathionylspermidine synthetase/amidase (GspS) has been previously demonstrated to catalyze both the ATP dependent formation of an amide bond between *N*1 of spermidine (*N*-(3-amino) propyl-1, 4-diaminobutane) and the glycine carboxylate of glutathione (γ-Glu-Cys-Gly) and the opposing hydrolysis of this amide bond (Bollinger *et al*., 1995). However its precise physiological role remains unclear to date. Bollinger and coworkers propose that conjugation of glutathione and spermidine could serve as method for modulating the levels of free spermidine and glutathione (Bollinger *et al*., 1995). As GSP possess properties of both GSH and GSP it is postulated that like GSH, GSP also protects the cells against oxidative stress and like SPE could also stabilize/protect DNA the membrane. Since YgiC and YjfC share significant sequence homology with the GspS synthetase domain, we hypothesized that these proteins are involved in GSP biosynthesis in *E.coli*.

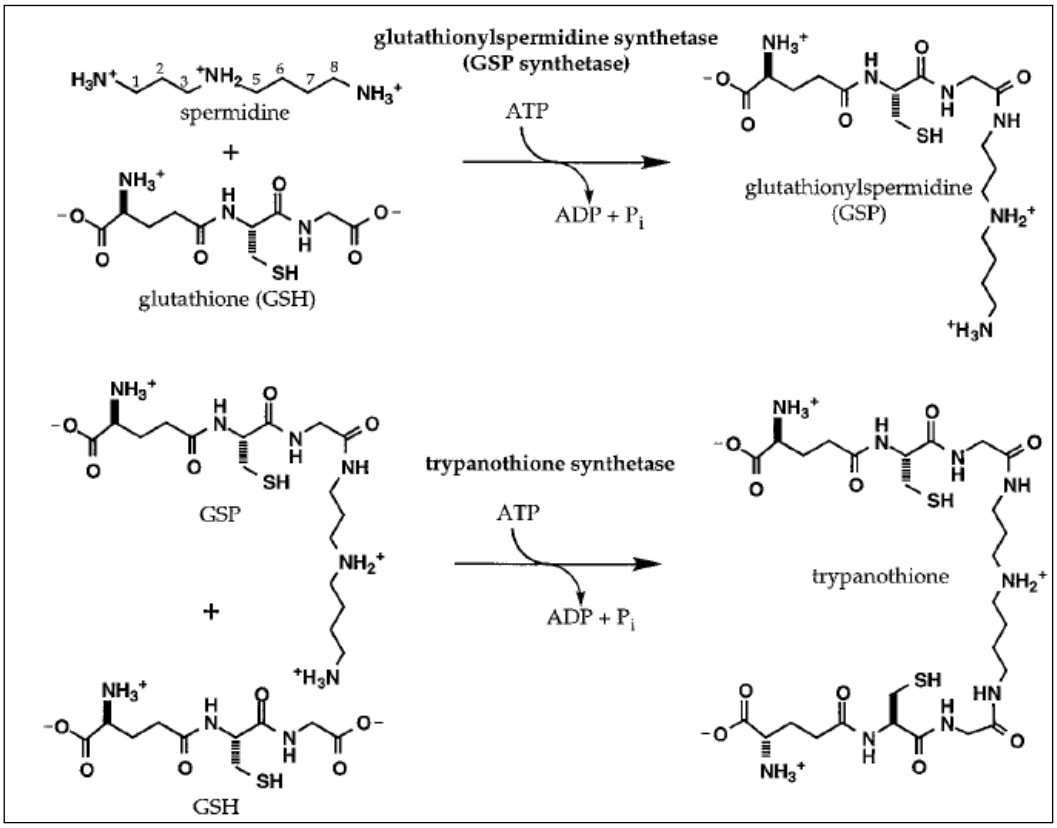

Figure I.9 Trypanothione metabolism of *Trypanosomas sp*. Figure adapted from Kwon *et al.,* 1997.

I.6 Spermidine metabolism in *E.coli*. Polyamines such as spermidine, putrescine, and cadavarine are polycationic molecules and are ubiquitously present in both eukaryotes and prokaryotes. Different cells have different concentrations and different types of polyamines. Prokaryotic cells have higher concentrations of putrescine than spermidine and completely lack spermine. In *E.coli*, polyamine concentrations up to 20 mM have been detected (Tabor *et al*., 1973). Tabor and coworkers showed that *E.coli* cells growing in minimal medium had 17.3 mM of putrescine and 6.3 mM of spermidine (Tabor *et al.,* 1973).

Spermidine is formed by the addition of a propylamine moiety to putrescine. This reaction is catalyzed by enzyme aminopropyl transferase also known as spermidine synthetase, a *speE* gene product (Fig I.10). The propylamine group is obtained from decarboxylated S-adenosyl-L-methionine. Putrescine is formed either by the arginine decarboxylase via agmatine or by the ornithine decarboxylase. In *E.coli* ornithine decarboxylase is the major pathway. Intracellular concentrations of spermidine are tightly regulated by several feedback, recycling, and export/import mechanisms e.g., enzyme spermidine synthetase is feedback inhibited by its product, spermidine (Bowman *et al.*, 1973). Spermidine can also be converted to other forms, e.g. addition of glutathione moiety to yield glutathionylspermidine. Spermidine can also be acetylated to give acetyl spermidine. This reaction is catalyzed by enzyme spermidine acetyltransferase (Fig I.10). However the physiological roles of these forms of spermidine remain unknown.

Polyamines have been attributed a variety of roles; however, little is known about their physiological role. In-vitro experiments have shown polyamines to be associated with membranes and have shown to protect spheroplasts from lysis, indicating their role in stabilizing membranes (Tabor, 1960). Igarashi and co-workers show that major fraction of spermidine in *E.coli* cells is associated with RNA (Igarashi & Kashiwagi, 2000). It was found that presence of polyamines stimulate the association of the 30S subunit of ribosome with 23S particles, thereby enhancing protein synthesis (Yoshida *et al.*, 2004). Igarashi and co-workers demonstrate that polyamines stimulate protein synthesis by 1) changing the secondary structure of mRNA such that in the presence of spermidine, the Shine Dalgarno (SD) sequence and the initiation codon may

become closer during formation of the initiation complex, and this may be important for initiation e.g. structural change of OppA mRNA 2) By stimulating the interaction between unusual initiation codons such as UUG and the anticodon of fMet-tRNA, e.g. UUG–dependent fMet-tRNA binding to adenylate cyclase mRNAribosome complex or 3) suppression of nonsense codon by stimulation of read through of the amber codon UAG–dependent Gln-tRNA^{supE} on ribosome associated RpoS mRNA (Igarashi & Kashiwagi, 2006). Although polyamines have been shown to enhance protein synthesis, stabilize membrane and DNA, polyamines are not essential for growth of *E.coli* as *E.coli* strains completely deficient in polyamine synthesis are able to grow but with reduced growth rates as compared to WT (Chattopadhyay *et al.,* 2009).

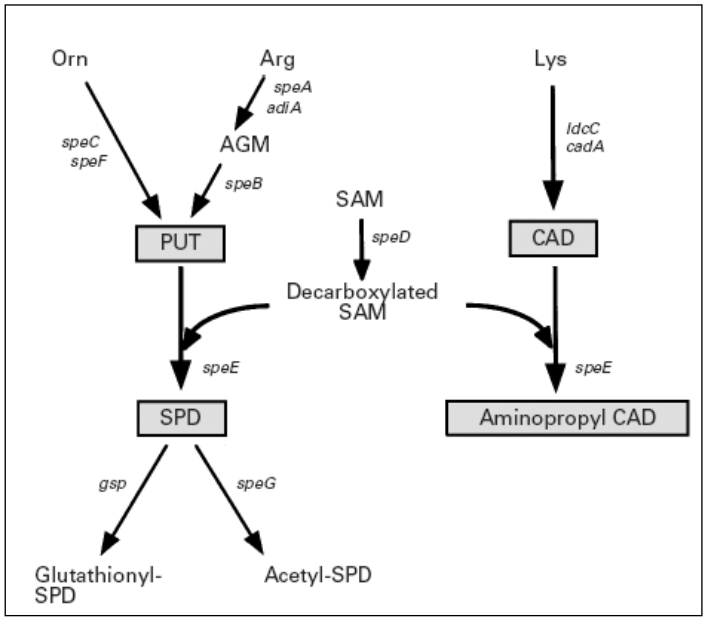

Figure I.10 Spermidine metabolism in *E.coli*. Figure adapted from Igarashi *et al.*, 1999.

I.7 Glutathione metabolism in *E.coli*. Glutathione (GSH), γ -L-glutamyl-L-cysteinyl-glycine is the most abundant non-protein thiol present in all cells. GSH is present in both eukaryotic as well as prokaryotic cells with the exception of some eubacteria or archaebacteria. Intracellular concentration of glutathione ranges from 0.1 mM to 10 mM. With its redox active cysteine thiol, GSH is the primary small molecule antioxidant in many cells and serves to maintain redox state of the cell and scavenge reactive oxygen species. In *E.coli*, GSH plays a critical role in protection against environmental stresses such as osmotic shock, oxidative stress induced by peroxides such as hydrogen peroxide (H_2O_2), protection against toxins like methylglyoxal and chlorine compounds like hypochlorous acid. GSH was also shown to be a negative regulator of the potassium channel KefB and KefC thereby regulating the cytoplasmic K^+ concentrations (Masip *et al.*, 2006).

GSH is synthesized in two steps. The first step is catalyzed by γ -glutamylcysteine synthetase (GCS), product of *gshA* gene that catalyzes the addition of glutamic acid to cysteine to form γ-glutamylcysteine. The second step is catalyzed by the enzyme glutathione synthetase (product of *gshB* gene). Glutathione synthetase catalyzes the addition of glycine to γ-glutamylcysteine to form GSH. Both γ -glutamylcysteine synthetase and glutathione synthetase are cytosolic ATP dependant enzymes (Fig I.11). Intracellular concentrations of GSH are tightly regulated by feedback inhibition of biosynthesis, degradation and oxidation to its dimeric disulfide form GSSG. The enzyme γ -glutamylcysteine synthetase is regulated by feedback inhibition by product GSH. Because of its unique γ linkage, GSH cannot be degraded easily and only one peptidase, γ -glutamyl transpeptidase, is known to degrade GSH.

Surprisingly, this enzyme is localized to the periplasmic space, therefore, degradation of GSH takes place only in the periplasm. However, the transporter protein responsible for transport of GSH from cytoplasm to periplasm is still unknown. The ratio of oxidized and reduced GSH is maintained by glutathione reductase (the product of the *gor* gene) which uses reducing equivalents from NADPH to convert oxidized form of GSH (GSSG) to GSH. Thus, glutathione reductase serves as the key link between the two redox couples (GSH/GSSG and NAD(P)H/NAD(P)) in the cell.

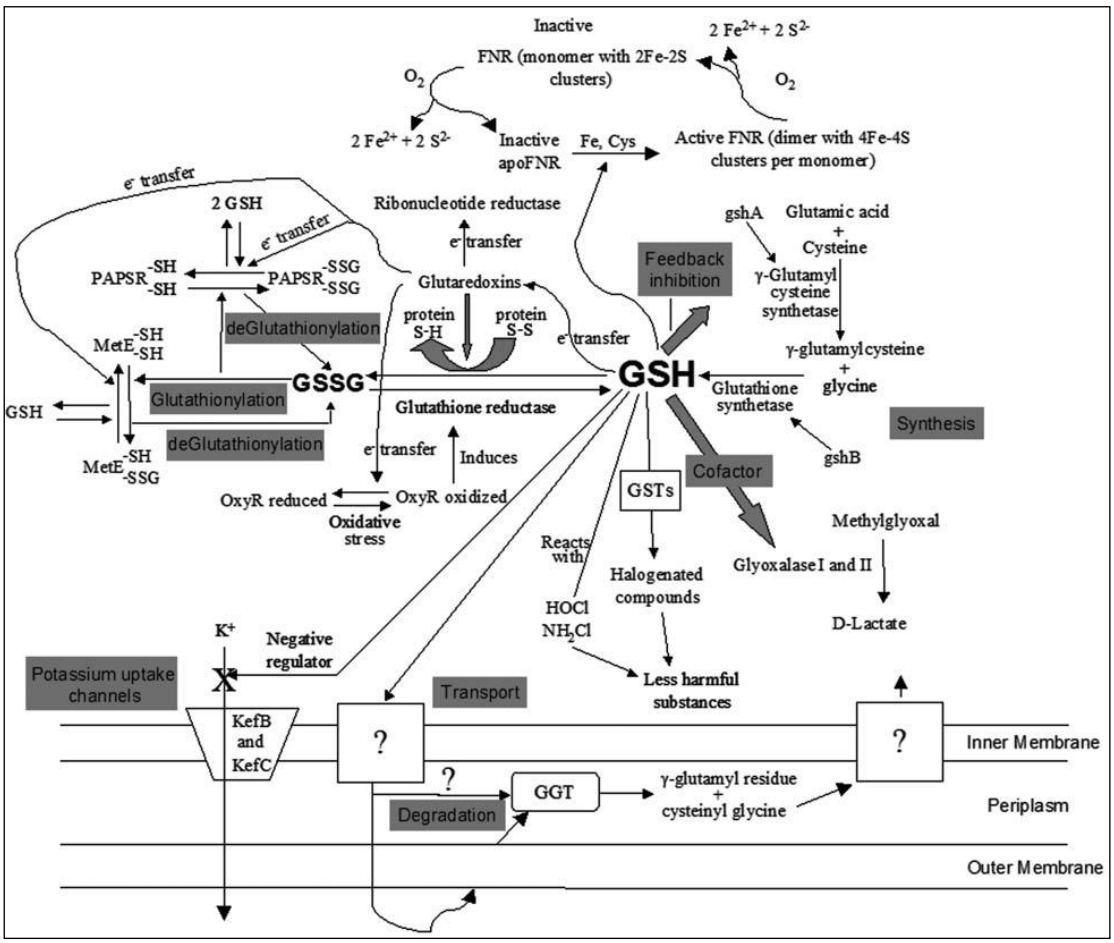

Figure I.11 Glutathione metabolism in *E.coli*. Figure adapted from Masip *et al.*, 2006.

I.8 Aims and Scope of this Dissertation. TolC is required for survival of *E.coli* under conditions that induce stress in cells and its multifunctional nature of TolC makes it an attractive target for designing inhibitors to block the TolC channel. Therefore understanding the mechanism of TolC's interaction with different classes of transporters, the mechanism of export of small molecules like drugs and large protein peptides, and identifying other physiological substrates exported by this channel is necessary. The main goal of this research is to understand the physiological function of TolC in *E.coli*. In order to achieve this goal we aimed to 1) identify and establish a functional link between TolC and YgiB, YgiC and 2) identify proteins interacting with TolC and understand TolC-MFP-transporter interaction dynamics.

II. Experimental Procedures

II.1 Construction of Strains. Strains with deletions in *tolC*, *ygiBC* and *yjfMC* (*ygiBC* homologues) genes were made by the method described by Datsenko and Warner, 2000. All the deletion strains are derivatives of WT, BW25113 strain (*lacI*^{q} *rrnB*$_{T14}$ Δ*lacZ*$_{WJ16}$ *hsdR514* Δ*araBAD*$_{AH33}$ Δ*rhaBAD*$_{LD78}$). This method uses lambda recombinase system to insert a kanamycin resistance gene in the desired locus thus disrupting the gene of interest. Antibiotic resistance genes were removed as described in (Datsenko & Wanner, 2000). All the deletion strains were confirmed with PCR (Appendix A). JW0117-1 (Δ*speE*), JW2914-1 (Δ*gshB*), JW2956-1 (Δ*gspS*), JW2663 (Δ*gshA*) strains are derivatives of WT, BW25113 strain. These strains were obtained from the Keio collection (*Coli*, genetic stock centre, Yale University). These strains were also confirmed with PCR.

II.2 Growth curves and growth rates. Growth rates were measured in Luria-Bertani (LB) medium (10 g of Bactotryptone, 10 g of yeast extract, and 5 g of NaCl per liter) and M9 minimal medium(5X M9 salts (Difco), 0.4% glucose, 2 mM $MgSO_4$ and 0.1 mM $CaCl_2$). Overnight grown cultures were diluted 1:100 into a fresh medium. The change in cell mass was monitored by measuring the optical density (600 nm) of the cultures every hour. The growth rates were calculated as the slope of the graph ($lnOD_{600}$ vs. time (hr)) in exponential phase of growth. Time points corresponding to both lag phase and stationary phase were not included in growth rate calculations. The parent BW25113 (WT) strain was included as a positive control. For experiments related to nutrient deficiencies, strains were grown in M9 medium supplemented with 0.4%

casamino acids or 0.4% glycerol, xylose and fructose. Strains were also grown in M9 medium supplemented with either of the following amino acids or vitamins : 0.2 g/L L-aspartic acid, 0.6g/L L-glutamic acid, 0.1 g/L L-serine, 0.2 g/L L-methionine, 0.2 g/L L-glycine, 0.1 g/L L-cysteine, 1 mg/L thiamine or 1mg/L riboflavin. For growth curves in LB medium supplemented with glutathione, cells were grown overnight in LB medium and then diluted 1:100 in fresh LB medium supplemented with 5 mM, 10 mM and 15 mM glutathione (reduced) (Sigma).

II.3 Phase contrast and fluorescence microscopy. *E. coli* strains were grown overnight in LB medium and diluted 1:100 into fresh M9 medium and grown at 37°C for twenty hours. One microlitre of culture was spread onto a slide and a coverslip was placed on the top. The slides were viewed and photographed with Spot (Insight) camera mounted onto an Olympus BX50 microscope. For fluorescence microscopy, the WT strain along with all deletion strains was grown in M9 medium. Aliquots of the growing cultures were taken at 0.3 OD_{600}, and fixed in PBS/ethanol solution by mixing 400 µl of cell culture with 6.6 ml of ice-cold PBS/ethanol (70%). Cells were washed once with PBS, and resuspended in 400 µl of PBS. Poly-lysine (25µg/ml) was added to the cells. The cells were spread on to clean cover slips and incubated for 5-10 minutes. The excess fluid was washed off. 15 µl of 1x Sypro Orange stain and 100 nM of DAPI (4',6'-diamidino-2-phenylindole) was added onto the cover slip, and viewed with UPlan F1 objective lens on Olympus BX50 microscope.

II.4 SDS-PAGE and immunoblotting. Denaturing SDS-PAGE was performed by standard methods using 12% separating gels. Samples were boiled with 4X sample buffer supplemented with β-mercaptoethanol and loaded onto SDS-PAGE gel. For

immunoblotting analyses, the proteins were transferred onto polyvinylidene difluoride membranes (PVDF) in buffer containing 250 mM Tris-Cl (pH not adjusted) 192 mM glycine and 10% methanol. Transfer was carried out at 70V for 1 hr. The membranes were then stored in blocking buffer (5% dry milk) at 4°C. The membranes were washed and incubated with rabbit primary antibody (Anti-TolC, Anti-AcrA or Anti-AcrB antibody) for 1 hr, washed and then incubated with the secondary anti-rabbit antibody conjugated to alkaline phosphatase (Sigma). Protein bands were visualized by substrates 5-bromo-4-choloro-3-indoyl phosphate and nitro blue tetrazolium.

II.5 Protein Expression Profiles. Strains were grown at 37ºC in 50 ml M9 medium. Cells were collected by centrifugation in exponential phase (0.6 OD_{600}) and stationary phase (48 h after inoculation into fresh M9 medium). Cells were washed and then resuspended in 10 mM Tris-HCl (pH 8.0) and 5 mM EDTA buffer and treated with lysozyme for 40 min. Sonication was used to lyse cells. Unbroken cells were removed by low speed centrifugation and membranes were collected by ultracentrifugation for 1hr at 100,000 ×g Beckman centrifuge (Optima TLX Ultracentrifuge). The membrane pellet was resuspended in buffer containing 50 mM Tris-HCl (pH 8.0), 0.1 M NaCl and 1 mM PMSF. Twenty micrograms of cytoplasmic and membrane proteins were analyzed on 12% SDS PA gels and Coomassie Brilliant Blue staining. Total protein concentration was estimated using the Bradford assay with BSA as a standard.

II.6 Stationary phase viability. Overnight grown cultures were re-inoculated into fresh M9 medium. These cultures were allowed to grow for 10 days. For strains requiring ampicillin, M9 medium was supplemented with 100 µg/ml carbenicillin. Aliquots of the growing cultures were taken at 0 hr, 3 days, 6 days and 10 days. At every time point the

optical density of the culture was measured. The cultures were diluted appropriately and plated onto LB plates. To reduce the error, 2 dilutions (10^3 and 10^2) per culture were used to plate and 2 plates per dilution were used. After incubation at 37°C the colonies were counted**.**

II.7 Norfloxacin killing assay. The method was followed as described previously by Kohanski *et al*.**,** 2007. Briefly, strains were grown overnight in LB medium, diluted 1:1000 into fresh LB medium. The cells were grown up to 0.3 OD_{600}. Bactericidal antibiotic norfloxacin (in DMSO) was added at different concentrations (100 ng/ml, 250 ng/ml, and 600 ng/ml). After every hour the optical density of the culture was measured and 100 µl of aliquot was removed, washed twice with fresh LB medium, diluted appropriately and plated onto LB plates. After incubation at 37°C colonies were counted.

II.8 Hydrogen peroxide disk diffusion assay. All cultures were grown overnight in LB medium. 100 µl of overnight grown cultures were plated onto LB plates. 5%, 15% and 30% of H_2O_2 were used. 4 filter paper disks were placed onto each plate. 20 µl of the above H_2O_2 solutions were added to each of these disks. As a control 20 µl of water was added to fourth disk. After incubating the plates overnight at 37°C, diameters of clearing zones were measured.

II.9 Reverse Transcriptase PCR (RT-PCR). RT-PCR was performed by using QIAGEN OneStep RT-PCR kit. Total RNA was isolated from exponentially growing cells (LB medium) using QIAGEN RNeasy kit. RNA prep was digested with DNase I to digest contaminating DNA. 2 µg of purified total RNA were used for RT-PCR. To detect the *tolC* transcript (reaction 4 in Fig. III.1B), the forward primer tolCstart and the

reverse primer TolCS2 were used to yield a product of 1173 bp (Lane 4 and 5). To detect the *ygiB* and *ygiC* mRNA (reactions 1, 2, and 3 on Fig III.1B) the forward primer TolCD1 and the reverse primers (1) rygiBRT, (2) rygiBRT #2 and (3) rygiCRT were used to yield products of 889 bp, 1184 bp and 1810 bp, respectively.

II.10 Sucrose density gradient fractionation. Cells were grown in 100 ml LB medium supplemented with 100µg/ml ampicillin to an OD_{600} of 0.6. EDTA-lysozyme treatment was performed to prepare spheroplasts (Osborn *et al.*, 1972 and Tikhonova & Zgurskaya, 2004). These spheroplasts were sonicated on ice for 45s. Unbroken cells were removed by centrifugation. Membrane vesicles were collected by ultracentrifugation at 60,000 rpm for 1 h in a Beckman 70Ti rotor. The membrane pellet obtained was resuspended by water bath sonication in buffer containing 20% sucrose and 5 mM EDTA. This membrane fraction was loaded onto a 2 step sucrose gradient (60% and 25%) and centrifuged in a 70-Ti rotor at 40,000 rpm for 3.5 h. Both the outer and inner membrane fractions were collected together, diluted and centrifuged at 40,000 rpm for 40 min to pellet total membranes. Membrane pellet was resuspended and loaded onto a 5 step sucrose gradient (30%, 35%, 40%, 45%, 50%, 55% and 60%) and centrifuged at 40,000 rpm for 12 hr. 250 µl fractions were collected from the bottom of the gradient. The samples were boiled and analyzed by 12 % sodium dodecyl sulfate-polyacrylamide gel electrophoresis (PAGE) and visualized by silver staining.

II.11 Minimum Inhibitory Concentration (MIC) measurements. MIC of various antimicrobial agents was measured in 96 well plates (Tikhonova *et al.,* 2004). Approximately 10^4 exponentially growing cells were inoculated in LB medium supplemented with two-fold increasing concentrations of a drug. In case of MIC

measurements in the presence of glutathione, cells were inoculated into LB medium supplemented with a drug and 15 mM, 10 mM or 5 mM concentration of reduced glutathione.

II.12 Determination of intracellular thiol content. HPLC was used to analyze monobromobimane (MBB) derivatized thiols (Helbig *et al.,* 2008 and Fairlamb *et al.,* 1986). Cells growing in LB medium (OD_{600} ~ 1.0) were collected by centrifugation and either resuspended in the same volume of fresh LB or washed and then resuspended in fresh M9. Cells were incubated at 37°C with shaking (220 rpm) and were collected by centrifugation at one, twelve and twenty hours post reinoculation. Approximately 10^9 cells were washed with fresh M9 medium and resuspended in buffer containing 40 mM HEPES-KOH (pH 7.0) and 5 mM EDTA.

Derivatization with MBB (73.7 μM final concentration) was carried out at 70°C for 3 min. The samples were cooled briefly on ice. The reaction was stopped by adding equal volume of 4 M lithium methanesulfonic acid and further incubated for 30 min. HPLC analyses were done on a Zorbax C-18 column (Hewlett Packard) and Shimadzu LC-10Ai HPLC system with RF-10AXL fluorescence detector. The fluorescence of MBB derivatized thiols was detected at 380 nm excitation and 490 nm emission wavelengths. Mobile phase A contained 0.25% (w/v) d-camphorsulfonate in water, pH 2.7. Mobile phase B contained 0.25% (w/v) d-camphorsulfonate and 25% isopropanol.

II.13 GSSG reductase recycling assay for GSH and GSSG measurements. Procedure was similar to that used by Aslund F, 1999 and Anderson M., 1985. Cells

were grown as described above. Approximately 10^9 cells growing in LB/M9 medium were resuspended in 20 µl of 143 mM sodium phosphate/6.3 mM EDTA, pH 7.4 and 10 µl of 10% 5-sulfosalicylic acid. Samples were centrifuged at 13,000 rpm for 5 min to remove protein precipitates. The assay volume was scaled down to 300 µl. 210 µl NADPH (0.25 mg/ml) and 30 µl 5-5'-dithiobis(2-nitrobenzoic acid) (DTNB) were incubated at 30°C for 15 min and then 60 µl of sample and 3 µl of 266U/ml yeast glutathione reductase enzyme (Sigma) were added to the reaction mix to start the reaction. For GSSG measurements 20 µl of supernatant was treated with 0.4 µl of 2-vinylpyridine. The pH of the reaction was adjusted to 6-7 by adding triethanolamine. Rate of change of absorbance at 412 nm was monitored for 5 min. The assay was calibrated with GSH and GSSG standards using concentrations between 0.15 nmoles and 1.2 nmoles. The same reactions were set to measure GSH and GSSG in culture supernatants, except 25 µl of each supernatant were used in the reaction.

II.14 NAD^+ and NADH measurements. Procedure was similar to that used in Dwyer *et al.*, 2007. Briefly, ~$5X10^9$ cells were taken from cultures growing in LB/M9 medium. Samples were centrifuged at 15,700×g for 2 min and the cell pellets were frozen in dry ice ethanol bath and stored at -80°C until use. 250 µl of 0.2 M NaOH (for NADH extraction) or 250 µl of 0.2 M HCl (for NAD^+ extraction) was added to the ice-cold pellets. Samples were boiled for 10 minutes and then centrifuged at 9,300×g for 5 min. The NAD^+/NADH supernatants were immediately used for assay. The assay reaction mix consisted of 30 µl 1.0 M BICINE-NaOH (pH8.0), 75 µl sample extract, 75 µl 0.1 M NaOH for NAD samples and 0.1 M HCl for NADH samples, 30 µl 16.6 mM phenazine ethosulfate, 30 µl 4.2 mM 3-[4,5-dimethylthiazol-2-yl]-2,5-

diphenyltetrazolium bromide (MTT), 30 µl absolute ethanol and 30 µl 40 mM EDTA (pH 8.0). The reaction mix was pre-incubated for 3 minutes at room temperature and 6 µl of 500 U/ml yeast alcohol dehydrogenase (Sigma) enzyme was added to start the reaction. The rate of reduction of MTT was monitored at 570 nm for 5 min. The rate of reduction of MTT is directly proportional to NAD^+/NADH (Dwyer *et al.,* 2007 and Matsumura & Miyachi, 1980). NAD^+ and NADH standards (Sigma) between 0.125 nmoles and 1.25 nmoles were used to calibrate the assay.

II.15 Construction of chromosomal TolC cysteine mutant strains. TolC mutants containing a single cysteine substitution in positions Q352, D356, S363, D374 and a six histidine tag at the C-terminus were constructed previously by Bobyk and Zgurskaya (unpublished). TolC WT and its Cys-containing derivatives were expressed from a pTrc99a based plasmid.

In order to express WT TolC and TolC cysteine mutants from the *E.coli* chromosome, we first used these plasmids as templates to generate a PCR product for electroporation. Forward primer ftolCstart, containing a sequence homologous to TolC start sequence and reverse primer rtolChis2, containing a sequence homologous to the YgiC downstream sequence was used to generate PCR product. Next the PCR product was cleaned using a PCR clean-up kit. This PCR product was then treated with restriction enzyme DpnI to digest template plasmid. After digestion the PCR products were concentrated to ~100 ng/µl using Zymoclean PCR clean up kit. This PCR product was transformed into GD102 strain (Δ*tolC*Δ*ygiBC::kan*). Colonies with correct insertion were selected by growing on LB plates containing 32µg/ml novobiocin

followed by confirmation with PCR. After PCR confirmation all TolC cysteine mutants as well as $TolC^{his}$ insertions were confirmed by sequencing.

AcrAB deletions in the above mentioned chromosomally expressed TolC cysteine mutants were constructed by first transforming the strains with pKD46 plasmid followed by electroporation of kanamycin gene PCR products into these strains. This PCR product was generated by using pKD4 as template plasmid and primers fAcrABKandisrup and rAcrABKandisrup.

II.16 In vivo whole cell labeling with F5M (fluoresceine-5-malemide). All TolC cysteine mutants along with WT (BW25113) strain as positive control and GD102 strain as negative control were grown until ~1.0 OD_{600} in 50 ml LB medium. Cells were washed with PBS buffer and then resuspended in 1.5 ml PBS. Freshly made fluoresceine-5-malemide was added to a final concentration of 250 µM, and incubated for 30 min at 4°C on the rotator (Dastidar *et al.*, 2007). 1 mM DTT was added to stop the reaction and incubated for 1 min on ice. After centrifugation the pellet was resuspended in 1.5 ml buffer (10 mM Tris-HCl (pH 8.0), 5 mM EDTA). To lyse the cells 100 µg/ml lysozyme was added and incubated for 40 min on ice. Sonication was used to break the cells. Unbroken cells were pelleted and the supernatant was centrifuged at 100,000 ×g for 1 hr to pellet the membranes. The membrane pellet was resuspended in 100 µl buffer (50 mM Tris-HCl (pH 8.0), 100 mM NaCl and 1 mM PMSF). Water bath sonicaton was used to get a homogenized membrane fraction. Protein concentration was measured using Bradford assay (Bio-Rad) with BSA as standard. 20 µg of total protein was loaded onto 12% SDS-PA gel. The gel was scanned on a Storm 840 phosphor imager and fluorescent screen imaging system (Amersham

Pharmacia-Molecular Dynamics) and then stained with Coomassie Brilliant Blue stain to visualize protein bands.

II.17 In vivo cross linking and purification chromosomally expressed TolC^{his} mutants. TolC S363C^{his} strain was grown in LB medium to an OD_{600} 1.2. Cells were washed twice with buffer (20 mM sodium phosphate pH 7.5, 150 mM sodium chloride and 1 mM EDTA), concentrated 7.5 times and incubated 30 min at RT with either DMSO (control) or SPDP. The reaction was stopped with 2.5 mM Tris-HCl (pH 7.4). Cells were centrifuged and washed in buffer containing 0.75 M sucrose, 10 mM Tris-HCl (pH 8.0) and resuspended in 35 ml of the above buffer. Spheroplasts were prepared by adding 100 µg/ml lysozyme and slowly adding 70 ml of 1.5 mM EDTA (pH 8.0) (on ice). Spheroplasts were fragmented into membrane vesicles by sonication for 60-90 sec. Low speed centrifugation was done to remove unbroken cells followed by ultracentrifugation at 100,000 ×g for 1.5 hr to pellet membrane vesicles. Membrane pellet was resuspended in 2 ml buffer containing 0.25 M sucrose, 3.3 mM Tris-HCl (pH 8.0) and 1 mM EDTA (pH 8.0) loaded onto a 2 step sucrose gradient (1.44 M, 0.77 M sucrose) and centrifuged at 100,000 ×g for 4 hr. The outer membrane pellet was resuspended and solubilized in binding buffer (50 mM Tris-HCl (pH 8.0), 500 mM NaCl, 1 mM PMSF, 5 mM imidazole) supplemented with 5% Triton X-100. Insoluble material was removed by centrifugation at 100,000 ×g for 40 min. The soluble fraction was incubated for 2 hr at RT with Cu^{2+} charged His bind resin (Novagen) equilibrated in binding buffer and 0.2% Triton X-100. TolC^{his} was purified by washing column with 20 column volumes of binding buffer supplemented with 5 mM Imidazole, 10 column volumes of binding buffer containing 50 mM Imidazole, 10 column volumes of binding

buffer with 60 mM Imidazole, then washed twice with half column volumes of binding buffer containing 500 mM Imidazole. 500 mM imidazole fractions were concentrated with 10% TCA (trichlotoacetic acid). All fractions were analyzed by SDS-PAGE and western blot analysis using anti-AcrA, anti-AcrB and anti-TolC antibodies.

II.18 Real Time CPM uptake assay. Overnight grown cultures were diluted 1:100 into fresh LB medium and grown to 0.6 OD_{600}. Cells were washed with buffer (50 mM potassium phosphate pH 7.0, 1 mM magnesium sulfate, and 0.5% glucose. Cells were resuspended into appropriate volumes so as to achieve 3.0 OD_{600}, diluted to 0.1-0.2 OD_{600} just before the start of the experiment. 1-5 µM 7-Diethylamino-3-(4'-maleimidylphenyl)-4-methylcoumarin (CPM, dissolved in DMSO, λ_{abs}=384 nm, λ_{em}=469 nm) concentrations used. Fluorescence was measured on a Shimadzu RF 5301-PC spectroflurometer with a slit width 5.0.

II.19.Colicin secretion assay. Respective strains were transformed with pHK11 carrying *cvaABC* and *cvi* genes (Gilson *et al.,* 1990). The colicin sensitive strain BW25113 was grown in LB medium for about 12-14 hr. 100 µl of this culture was spread onto to LB agar plates. With the help of wooden sticks a single colony of strains transformed with pHK11 plasmid were spotted onto these plates. The plates were incubated overnight at 37°C. Diameters of zone of clearing (no cell growth) were measured the next day.

II.20 LIVE/DEAD cell assay. Molecular probes LIVE/DEAD BacLight Bacterial Viability kit was used to score live and dead cells. Cells growing in LB (OD_{600} ~ 1.0) were collected by centrifugation and either resuspended in the same volume of fresh LB or washed and then re-suspended in fresh M9. Cells were incubated at 37°C with

shaking (220 rpm) and were collected by centrifugation at one, twelve and twenty hours post re-inoculation. Cells from 2.5 ml of culture were resuspended in 200 µl 0.85% NaCl. 100 µl of this suspension was added to two tubes containing 2 ml of 0.85% NaCl (for live cells) and as a control to 2 ml of 70% isopropanol (for killed cells). Both the samples were incubated at room temperature for one hour with gentle mixing every 15 minutes. Cells were centrifuged at 10,000 ×g, 4°C for 10 min, washed twice with 0.85% NaCl and finally resuspended in 1 ml 0.85% NaCl. For microscopy, equal volumes of SYTO 9 dye solution (3.3 mM) (as provided in the kit) and propidium iodide (20 mM) (as provided in the kit) were mixed. 0.3 µl of this dye mixture was added to 100 µl of cell suspension and incubated for 15 minutes in the dark at room temperature. 5 µl of the stained bacteria were trapped between a slide and a cover slip, observed and photographed with the help of a Spot (Insight) camera mounted onto an Olympus BX50 microscope through an UPlanF1 X 100/1.3 oil-immersion objective.

II.21 NADH oxidase assay. Cell membrane preparation and the NADH oxidase assay were performed as described before (Tikhonova & Zgurskaya, 2004). Briefly, Cells growing in LB (OD_{600} ~ 1.0) were collected by centrifugation and either resuspended in the same volume of fresh LB or washed and then re-suspended in fresh M9. Cells were incubated at 37°C with shaking (220 rpm) and were collected by centrifugation at one, twelve and twenty hours post re-inoculation. Disruption of cells by EDTA-lysozyme treatment was performed as described previously (Osborn *et al.*, 1972). Sonication was used to lyse cells. Unbroken cells were removed by low speed centrifugation and membranes were collected by ultracentrifugation for 1 hr at 100,000×g. The membrane pellet was resuspended in 10 mM Tris-HCl (pH 8.0), 0.25 M sucrose. Protein

concentration of total membrane was measure using Bradford assay with BSA as a standard. 50 µg total protein was used for the assay. The assay mixture contained 50 mM Tris-HCl-Cl (pH 7.5), 0.3 mM DTT and 0.60 µM NADH (Sigma). Rate of decrease in absorbance at 340 nm was measured for one minute.

III. Results

III.1 Inactivation of TolC induces stress on *E.coli* membrane and arrests growth on glucose.

III.1.1 *tolC, ygiB* and *ygiC* genes are expressed as a part of the same operon. In order to check and establish a functional link between TolC and YgiBC we first wanted to confirm that *tolC, ygiB* and *ygiC* genes constitute a single operon. For this purpose we used reverse transcriptase PCR (RT-PCR). Total RNA was extracted and purified from *E.coli* BW25113 (WT) cells using QIAGEN RNeasy kit. RT-PCR reactions using forward primer annealing to *tolC* locus and reverse primer annealing either to *ygiB* or *ygiC* locus were set up (Fig III.1B lanes 1, 2 and 3). A positive control reaction using forward and reverse primers annealing to the *tolC* was set up (Fig III.1B lane 4). Another control reaction without any reverse transcriptase was also set up to rule out possible DNA contamination (Fig III.1B lane 5). Figure III.1B shows that expected PCR products of sizes 889 bp, 1173 bp, 1184 bp and 1810 bp were obtained only in reactions where reverse transcriptase was present, indicating no DNA contamination in total RNA extracts and confirming that *tolC, ygiB and ygiC* genes are transcribed together.

III.1.2 Deletion of *ygiBC* genes does not affect TolC expression. To investigate the function of *ygiB* and *ygiC* genes in *E.coli*, we created a series of chromosomal deletion mutants. Chromosomal gene deletions were made using the lambda red recombinase system as described by Datsenko & Wanner, 2000. Kanamycin resistance gene insertions into the desired loci were confirmed with PCR. To create strains with two or

more gene deletions, the kanamycin resistance gene was first excised by transforming the strain with pCP20. PCR using primers specific to upstream and downstream regions of the deleted gene was done to confirm that the kanamycin resistance marker was successfully excised. Following confirmation, the same technique of lambda red recombination was used for insertional inactivation of the second locus, thus yielding a strain with two chromosomal gene deletions. A similar strategy was used if more deletions were desired. Kanamycin resistance marker was removed from *tolC* and *ygiBC* locus. Description of all strains created including genotype and PCR confirmations are listed in Appendix A.

yjfM and *yjfC* are close homologues of *ygiB* and *ygiC* genes respectively and could have similar functions as *ygiBC*. Therefore, we made a combination of deletion strains where only *yjfMC* genes were deleted, *yjfMC* and *ygiBC* were deleted and a third strain where *tolC-ygiBC* were deleted together with *yjfMC* genes.

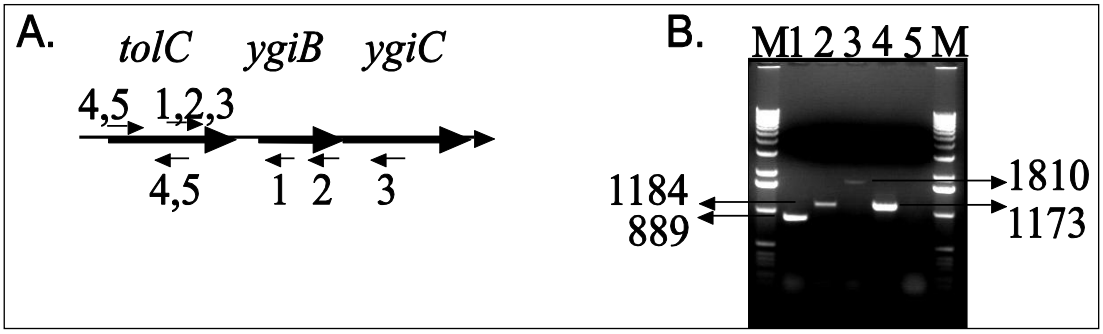

Figure III.1 TolC is expressed along with YgiBC. A. TolC operon with primer positions indicated. B. RT-PCR analysis of RNA isolated from *E. coli* BW25113 (WT) strain. The same RNA sample was used in all reactions. Lanes 1-3: RT-PCR reactions with forward and reverse primers that anneal to *tolC-ygiBC* transcript (primers 1, 2 and

3 in panel A). Lane 4: RT-PCR reaction using forward and reverse primers that anneal to *tolC* transcript (primers 4, 5 in panel A). Lane 5 is the same reaction as in lane 4 but RT was omitted (no DNA control).

We next wanted to test if *ygiBC* genes are involved in regulation of expression or assembly of TolC. Membrane fractions were isolated from WT, Δ*tolC* and Δ*ygiBC* strains. Membrane proteins were separated using 12% SDS-PAGE and then transferred onto PVDF membranes. These membranes were then probed with anti-TolC antibodies. Immunoblotting analysis (Figure III.2) shows the same level of TolC expression and trimerization in Δ*ygiBC* strains as compared to WT, indicating that YgiBC are not required for TolC expression or assembly.

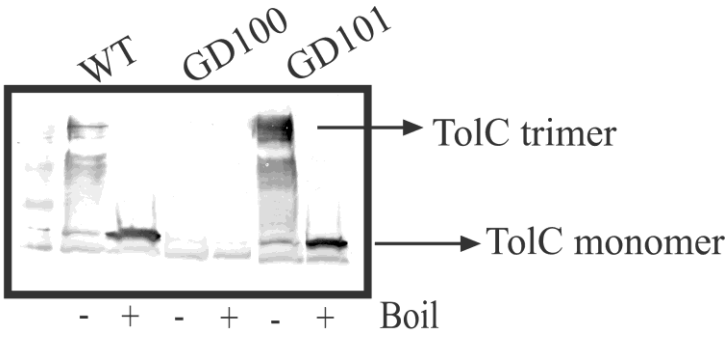

Figure III.2 Deletion of *ygiBC* genes does not affect TolC expression. Immunoblotting analysis of TolC in WT (BW25113), Δ*tolC* (GD100) and Δ*ygiBC* (GD101) strains. 20 µg of total membrane proteins were separated on 12% SDS-PA gel. TolC was visualized using polyclonal anti-TolC antibody. + sign indicates boiled samples and – sign indicates unboiled samples.

III.1.3 Deletion of YgiBC does not affect TolC multidrug resistance (MDR) function. In order to establish a functional link between TolC and YgiBC, we wanted to check if YgiBC proteins participate along with TolC to confer MDR to *E.coli* cells. For this, we measured drug susceptibilities of WT, Δ*tolC*, Δ*ygiBC* and Δ*yjfMC* strains. The MIC data showed that, as expected, all the Δ*tolC* strains were highly susceptible to drugs and the detergent SDS. The Δ*ygiBC* and Δ*ygiBC-yjfMC* strains showed similar levels of resistance for norfloxacin and SDS but showed two-fold increased resistance for erythromycin and four-fold higher resistance for novobiocin as compared to WT (Table 1a). Δ*yjfMC* strain showed two-fold increased resistance to novobiocin and erythromycin and was equally susceptible to norfloxacin and SDS as compared to WT. Both erythromycin and novobiocin are bacteriostatic antibiotics which have different targets in the cell. Novobiocin binds to DNA gyrase inhibiting DNA replication whereas erythromycin binds to the 70S subunit of the ribosome thereby halting protein synthesis.

As Δ*ygiBC* strains showed increased levels of resistance for novobiocin and erythromycin we also measured MIC's of other substrates of the TolC dependant efflux pumps (Tikhonova & Zgurskaya, 2004). WT and Δ*tolC* strains were included as positive and negative controls respectively. MIC results show that Δ*ygiBC* strains show the same level of resistance as WT for all drugs tested (Table 1b). These results indicate that YgiBC are not required for TolC MDR function.

Table 1a: MIC (µg/ml) measurements of WT and mutant strains.

Strain	Genotype	ERY	NOV	NOR	SDS
BW25113	WT	32	32	0.04	>10240
GD100	*ΔtolC*	**1**	**1**	**0.01**	**5**
GD101	*ΔygiBC*	64	**128**	0.04	>10240
GD102	*ΔtolC ΔygiBC*	1	1	0.0025	5
GD103	*ΔyjfMC*	64	64	0.04	>10240
GD104	*ΔygiBC ΔyjfMC*	64	**128**	0.04	>10240
GD105	*ΔtolC ΔygiBC ΔyjfMC*	1	0.25	**0.005**	**5**
GD106	*ΔspeE ΔtolC*	**1**	**1**	**0.005**	5
GD107	*ΔgshB ΔtolC*	**1**	**1**	**0.0025**	5
GD108	*ΔygiBC ΔyjfMC ΔgspS*	64	32	**0.01**	>10240
GD109	*ΔspeE ΔygiBC*	ND	ND	ND	ND
GD110	Δ*speE,* Δ*gshB*	ND	ND	ND	ND
GD111	*ΔyjfMC ΔtolC*	ND	ND	ND	ND

GD112	*ΔgshA ΔtolC*	1	1	0.0025	5
JW0117-1	Δ*speE*	32	64	0.02	>10240
JW2914-1	Δ*gshB*	64	256	0.04	>10240
JW2956-1	Δ*gspS*	64	64	0.02	>10240
JW2663-1	Δ*gshA*	ND	ND	ND	ND

ERY-Erythromycin, NOV- Novobiocin, NOR- Norfloxacin, SDS- sodium dodecyl sulfate. ND-not determined. Values in bold in this table and all other tables indicate that these are significantly different from the WT values.

Table 1b: MIC (µg/ml) measurements of WT and Δ*ygiBC* strains.

Drug	**BW25113 (WT)**	**GD100 (Δ*tolC*)**	**GD101 (Δ*ygiBC*)**
Cholic Acid	>10000	1250	>10000
Ethidium bromide	200	1.5625	200
Oleandomycin	625	4.88	625
Puromycin	32	1	32
Cinoxacin	0.975	0.488	0.975
Nalidixic acid	1.56	0.195	1.56

Chloramphenicol	1.6	0.2	1.6
Tetracycline	0.312	0.078	0.312
Chlortetracycline	0.39	0.049	0.39
Lincomycin	312.5	39	312.5

III.1.4 ΔTolC strains have severe growth defects when grown in M9 medium. To understand the function of *ygiB* and *ygiC* genes we investigated the growth phenotypes of WT, Δ*tolC*, Δ*ygiBC* and Δ*tolC-ygiBC* strains. In Luria-Bertani (LB) medium all the strains had growth patterns and growth rates similar to WT (Figure III.3A). However, in M9 medium Δ*tolC* strain grew with a rate of 0.4 hr^{-1}, approximately 1.5 times slower than WT and showed a delay of growth close to 5 hours before it resumed growth (Figure III.4A). Unlike Δ*tolC* strain, Δ*ygiBC* strain grew with rates similar to WT and Δ*tolC-ygiBC* strain had growth phenotype similar to that of Δ*tolC* strain.

The above mentioned strains along with Δ *yjfMC*, Δ *ygiBC-yjfMC*, Δ *tolC-ygiBC-yjfMC* strains and WT as a control were grown in LB and M9 medium. As observed previously in LB medium all strains had growth rates similar to that of WT (Figure III.3B). In M9 medium Δ *yjfMC* strain grew with rates similar to WT suggesting that YgiBC and YjfMC could have reciprocal functions (Figure III.4A). Δ *ygiBC-yjfMC* strain also had growth rates comparable to those of WT (Figure III.4A). However when *tolC* was deleted in combination with *ygiBC* and *yjfMC* the growth defect worsened. A lag phase of approximately 9 hours was observed and growth rate

was twice lower than WT (Figure III.4A) (Table 2). Therefore these results suggest YgiBC and YjfMC have complimentary functions and that both TolC and YgiBC or YjfMC are required for normal growth of *E.coli* in glucose minimal medium.

A.

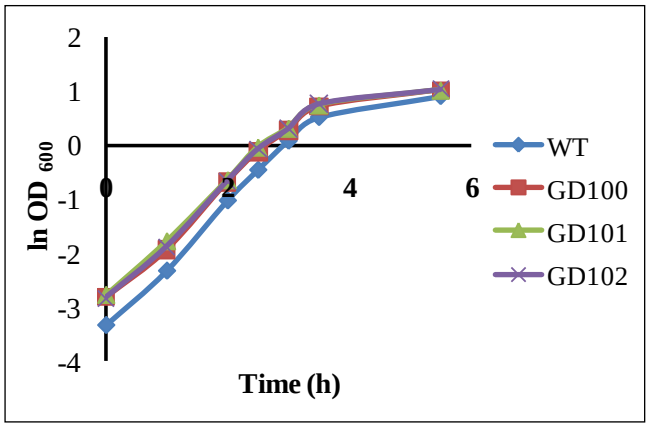

B.

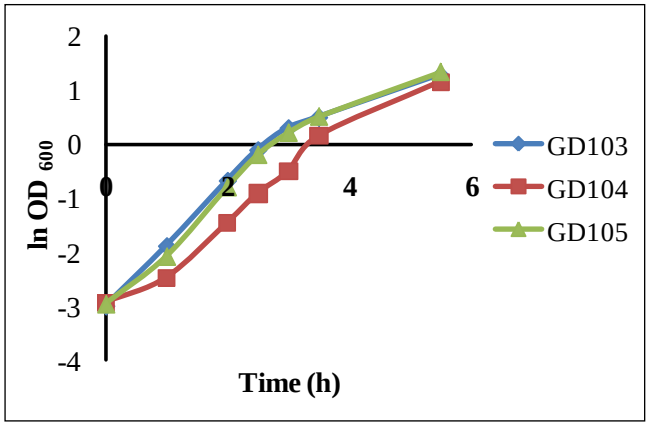

Figure III.3: Growth curves in LB medium. A) Growth curves of WT and Δ*ygiBC* strains. B) Growth curves of Δ*yjfMC* strains. Growth rates (hr^{-1}) are calculated as slope of individual graphs. GD100 (Δ*tolC*), GD101 (Δ*ygiBC)* GD102 (Δ*tolC*Δ*ygiBC*) GD103 (Δ*yjfMC*), GD104 (Δ*ygiBC*Δ*yjfMC*) and GD105 (Δ*tolC*-Δ*ygiBC*Δ*yjfMC*).

A.

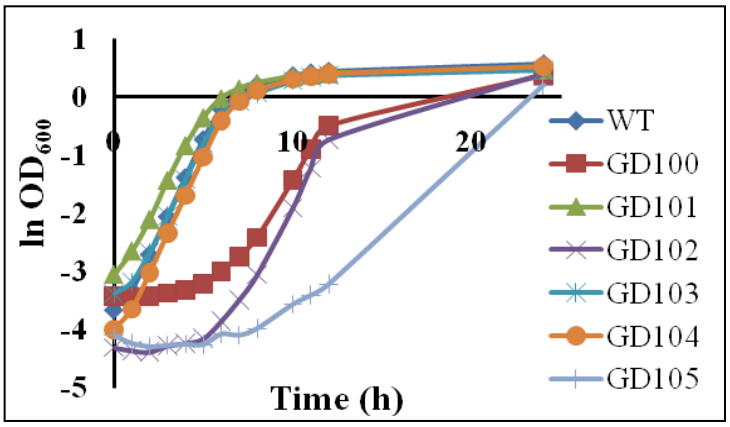

B.

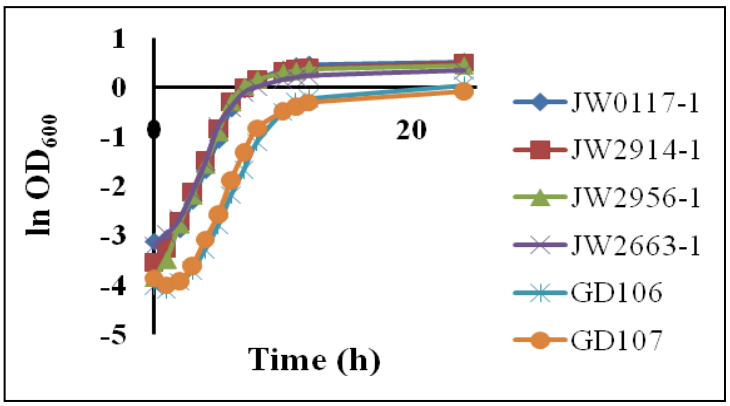

C.

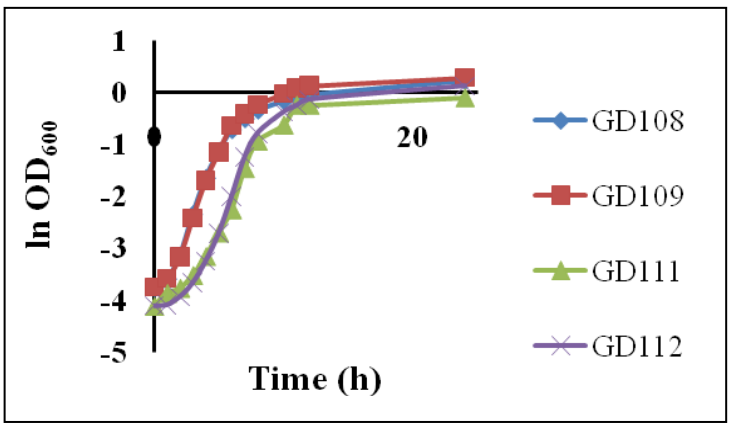

Figure III.4: Growth curves in M9 medium. A) Growth curves of GD100 (Δ*tolC*), GD101 (Δ*ygiBC)* GD102 (Δ*tolC*Δ*ygiBC*) GD103 (Δ*yjfMC*), GD104 (Δ*ygiBC*Δ*yjfMC*) and GD105 (Δ*tolC*Δ*ygiBC*Δ*yjfMC*) strains. B) Growth curves of Δ*speE*, Δ*gshB* and Δ*gspS* strains. C) Growth curves of GSP$^-$ and GSP$^-$ TolC$^-$ strains.

YgiC and YjfC share significant homology with glutathionylspermidine synthetase (GspS) and therefore could be involved in glutathionylspermidine synthesis. We reasoned that the long lag phases and slower growth rates observed in Δ*tolC*, Δ*tolC-ygiBC* and Δ*tolC-ygiBC-yjfMC* strains could be due to the deficiency of glutathionylspermidine and TolC in the cells. To test this hypothesis we requested Δ*speE* (spermidine synthetase), Δ*gshB* (glutathione synthetase), Δ*gshA* (γ-glutamate-cysteine ligase) and Δ*gspS* strains from the Keio collection (Baba *et al*., 2006). Spermidine synthetase is the last enzyme involved in spermidine biosynthesis; therefore Δ*speE* strains do not produce any spermidine in the cells. Similarly GshB synthesizes glutathione (GSH) by ligating precursor γ-glutamyl-cysteine with glycine. Δ*gshB* strains do not produce GSH but accumulate the precursor γ-glutamyl-cysteine (Helbig *et al.*, 2008). GshA is the penultimate enzyme of glutathione biosynthesis pathway. Δ*gshA* strains neither produce the precursor γ-glutamyl-cysteine nor GSH (Helbig *et al.*, 2008). GspS is a well characterized glutathionylspermidine synthetase/amidase.

TolC was deleted in these strains after excising the kanamycin resistance marker from the *speE*, *gshB* and *gshA* locus. We also constructed an *E.coli* strain lacking the two putative glutathionylspermidine synthetases, *ygiBC* and *yjfMC* and the well characterized glutathionylspermidine synthetase/amidase, GspS (GD108).

The above mentioned strains were grown in glucose minimal medium (Figure III.4B). Δ*speE,* Δ*gshB* and Δ*gspS* strains had growth rates slightly lower than WT (Table 2). When TolC was deleted in combination with *speE* or *gshB* these strains

exhibited phenotypes similar to TolC$^-$ strains. These strains demonstrated a lag of growth of approximately three hours and their growth rates ~0.4 hr^{-1} were similar to TolC$^-$ strains. *ΔygiBCΔyjfMCΔgspS*, a strain completely lacking glutathionylspermidine showed no defect when growing in glucose minimal medium and grew at rates similar to those of WT (Figure III.4C, Table 2). These results strongly suggest that the growth defects observed in Δ*tolC-ygiBC-yjfMC* strain is not due to the lack of GSH, SPE or GSP.

Next we wanted to check if the growth defects observed in Δ*tolC* strains can be rescued by expression of TolC. For this purpose we transformed GD100 (Δ*tolC)*, GD102 (Δ*tolC-ygiBC)* and GD105 (Δ*tolC-ygiBC-yjfMC)* strains with a plasmid expressing TolC (pTolC^{his}). Expression of TolC alone could completely rescue the growth defects observed in GD105 strain (Figure III.5) (Appendix B) thus confirming that TolC and *ygiBC*, *yjfMC* have parallel independent functions. Complementation with YgiBC needs to be the done to further confirm the hypothesis.

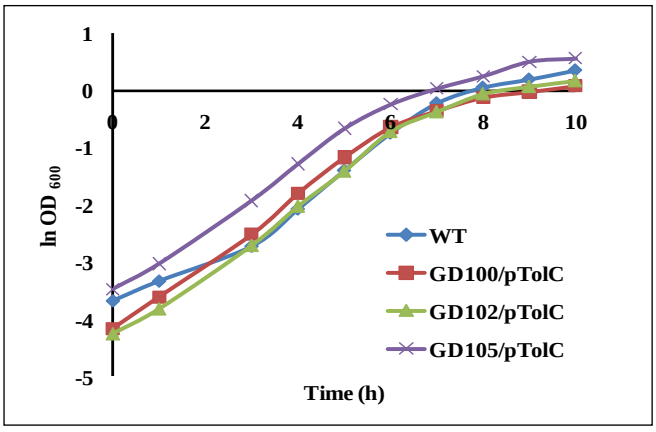

Figure III.5: TolC complements the phenotype observed in M9 medium. Growth curves of ΔTolC strains transformed with plasmid expressing TolC^{his} (pTolC).

Table 2: Growth rates (hr^{-1}) of WT and deletion mutants in LB and M9 medium.

Strain name	Genotype	Growth rate (hr^{-1}) in LB medium	Growth rate (hr^{-1}) in M9medium
BW25113/ WT	*lacI*^{q} *rrnB*$_{T14}$ Δ*lacZ*$_{WJ16}$ *hsdR514* Δ*araBAD*$_{AH33}$ Δ*rhaBAD*$_{LD78}$	1.22 ±0.13	0.62 ± 0.05
GD100	*ΔtolC*	1.12 ±0.08	0.44 ± 0.05
GD101	*ΔygiBC*	1.14 ± 0.18	0.63 ± 0.01
GD102	*ΔtolC ΔygiBC*	1.04 ±0.003	0.55 ±0.05
GD103	*ΔyjfMC*	1.17 ±0.04	0.62 ±0.07
GD104	*ΔygiBC ΔyjfMC*	1.03 ±0.01	0.65 ±0.03
GD105	*ΔtolC ΔygiBC ΔyjfMC*	1.11 ± 0.03	0.34 ±0.1
GD106	*ΔspeE ΔtolC*	ND	0.49 ± 0.06
GD107	*ΔgshB ΔtolC*	ND	0.52 ± 0.06
GD108	*ΔygiBC ΔyjfMC ΔgspS*	ND	0.58 ± 0.03
GD109	*ΔspeE ΔygiBC*	ND	0.61 ± 0.02
GD110	Δ*speE,* Δ*gshB*	ND	0.57 ± 0.04
GD111	*ΔyjfMC ΔtolC*	ND	0.43 ± 0.08
GD112	*ΔgshA ΔtolC*	ND	0.52 ± 0.04

JW0117-1	Δ*speE*	ND	0.52 ±0.04
JW2914-1	Δ*gshB*	ND	0.57 ±0.04
JW2956-1	Δ*gspS*	ND	0.55 ±0.04
JW2663-1	Δ*gshA*	ND	0.58
AG100AX	K-12 *argE3 thi-1* *rpsL xyl mtl galK* *supE441* Δ(*gal-uvrB*) Δ*acrAB*::*kan*	1.0 ± 0.05	ND
W4680	K-12 Δ*acrAB::kan*	ND	0.63±0.007
W4680AE	K-12 Δ*acrAB*::*kan* Δ*acrEF*::*spe*	ND	0.52 ± 0.01
ZK4	MC4100	ND	0.7 ± 0.05
ZK796	MC4100 but Δ*tolC::tet*	ND	0.74 ± 0.001
ECM2112	MC4100 but Δ*acrAB*::*kan* Δ*tolC*::*tet*	ND	0.53 ± 0.02

ND- Not determined. Except otherwise noted, all strains are derivatives of BW25113 (WT).

III.1.5 L-serine can rescue the growth defects observed in M9 medium. Above results show that ΔTolC strains are unable to grow in M9 medium but grow similar to

WT in LB medium. M9 medium is a chemically defined medium containing glucose as carbon source, ammonium, phosphate and sulfate salts as a source of nitrogen, phosphorus and sulfur, respectively. Cells obtain energy by breaking down glucose via glycolysis and tricarboxylic acid cycle (TCA), generating reducing equivalents and important intermediates for amino acid, nucleotide and vitamin biosynthesis. In contrast, LB is a complex medium containing yeast extract, sodium chloride and tryptone. Yeast extract and tryptone provides cells with an abundant supply of vitamins, amino acids, pyruvate and other intermediates of amino acid and nucleotide metabolism. Cells use this supply of amino acids and vitamins and generate energy through gluconeogenesis. Therefore, when growing in LB and M9 medium cells utilize two different pathways to generate energy. We reasoned that the growth defects observed in M9 medium could be due to a nutrient deficiency caused by inhibition or halt of a biosynthetic pathway.

To further investigate the growth defect observed in Δ*tolC* strains, these strains were grown in M9 medium supplemented with 0.4% casamino acids (Figure III.6A). Casamino acids are casein hydrolysates containing a majority of vitamins, trace elements and all amino acids with the exception of glutamine, aspargine and proline. The presence of casamino acids in M9 medium restored normal growth of all Δ*tolC* strains suggesting that the defect in growth could be due to the deficiency of certain vitamins and/or amino acids (Figure III.6A, Appendix B).

To further identify the essential vitamin/amino acid we grew these strains in M9 medium supplemented with either 1 mg/ml riboflavin or 1 mg/ml thiamine.

Riboflavin serves as a precursor for the formation of flavin nucleotides which in turn serve as prosthetic groups for several oxido-reductase enzymes (Sauer *et al.,* 1996) Thiamine is an important co-factor required by several enzymes involved in glycolysis and TCA cycle. Riboflavin and thiamine were not able to restore normal growth in Δ*tolC* strains suggesting that this growth defect could be due to an amino acid deficiency (Figure III.6B) (Appendix B).

Next, we tested different amino acids. These amino acids were chosen based on: 1) If they serve as precursors for the biosynthesis of GSH and spermidine 2) If they serve as precursors for biosynthesis of other amino acids. WT and GD105 strain were grown in M9 medium supplemented with either 0.2 g/L L-aspartate, 0.6 g/L L-glutamate or 0.1 g/L L-serine. L- aspartate serves as a precursor for L-aspargine, L-methionine, L-lysine and L-threonine, which in-turn serves as a precursor for L-isoleucine. L-glutamine, L-proline, L-arginine are synthesized from L-glutamate and L-serine is an intermediate of the L-cysteine and L-glycine biosynthetic pathway. GD105 strain growing in M9 medium supplemented with L-glutamate or L-aspartate did show an increase in growth rate; however, it still had a lag phase of approximately 6 hours (Figure III.6B, Appendix B). Only L-serine was able to completely recue the growth defects of GD105 strain. In the presence of L-serine, GD105 strain resumed growth immediately without a lag phase of 9 hours and growth rate of GD105 strain was similar to WT (Figure III.6C) (Appendix B). Since glycine and cysteine are synthesized from serine we next tested if one of these amino acids could restore normal growth of GD105 strain. Neither glycine nor cysteine was able to rescue growth defects in GD105 strain. In presence of glycine, GD105 strain still showed a lag phase

of 8-9 hours (Figure III.6C) and consistent with previous results (Wiriyathanawudhiwong *et al.,* 2009) cysteine was toxic, to even WT cells. Taken together these results suggest than GD100 and GD105 strains when growing in M9 medium with glucose as carbon source develop an auxotrophy for L-serine.

III.1.6 ΔTolC strains are unable to efficiently metabolize glucose. The next question that we wanted to address was if this growth defect was specific only when glucose is used a carbon source. Therefore we grew WT, GD100 and GD105 in M9 medium with 0.4 % glycerol as the sole carbon source. In *E.coli*, glucose is mainly transported by the phosphoenolpyruvate phosphotransferase system (PTS) (Meadow *et al.,* 1990). As it enters the cell, glucose is immediately phosphorylated to glucose 6-phosphate. Glucose 6-phosphate is subsequently oxidized to pyruvate via glycolysis. Glycerol is transported by GlpF a transporter belonging to the aquaporin channel family of proteins (Stroud *et al*., 2003). Once inside, glycerol is rapidly phosphorylated by glycerol kinase to produce glycerol 3-phosphate. Glycerol 3-phosphate is further oxidized to dihydroxyacetone phosphate by glycerol 3-phosphate dehydrogenase with the reduction of FAD to $FADH_2$. Dihydroxyacetone phosphate enters the glycolytic pathway and the reducing equivalents of $FADH_2$ are transferred ultimately to oxygen through the electron transport chain (Lin, 1976). Surprisingly, in M9 + glycerol medium both GD100 and GD105 strains showed WT phenotype (Figure III.7A, Appendix B). Cells grew with rates equivalent to that of WT and no lag phase was observed. These differences in growth phenotypes suggest that the defects observed when strains are growing in medium with glucose as carbon source could be either due to a defect in transport of glucose into the cells or due to inhibition of enzymes

involved in the early stage of glycolysis namely phosphofructokinase, phosphoglucoseisomerase and aldolase. We, next used M9 medium supplemented with 0.4% fructose (Figure III.7B, Appendix B) or 0.4% xylose (Figure III.7C, Appendix B) as carbon source to grow WT, GD100 and GD105 strains. Like glucose, fructose is transported into the cells in a PTS dependent manner (Meadow *et al.*, 1990). Once inside the cells fructose is phosphorylated to fructose 1- phosphate and fructose 6-phosphate , which then enters the glycolysis pathway. *E.coli* cells express a xylose specific ABC transporter, XylFGH to import xylose (Song & Park, 1998). Growth curve experiments show that fructose was also able to restore normal growth of GD100 and GD105 strains (Figure III.7B). No lag was observed and the growth rates were similar to those of WT. Xylose was unable to completely restore normal growth in GD100 and GD105 strains (Figure III.7C). Although growth rates of both GD100 and GD105 strains were similar to those of WT strain, GD100 strain still showed a lag phase of ~6 hours and GD105 strain showed a lag phase ~1 hour. Taken together these results suggest that glucose metabolism and not uptake of glucose is affected in GD100, GD102 and GD105 strains.

A.

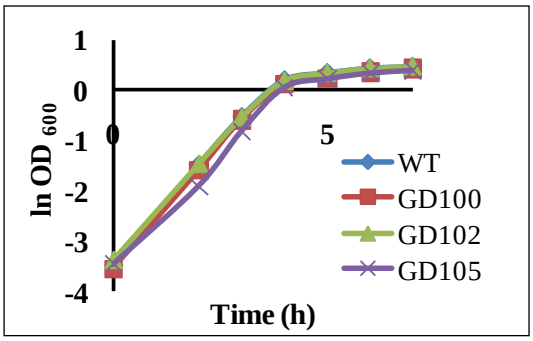

B.

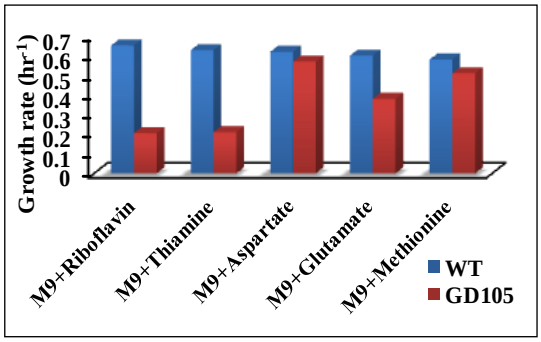

C.

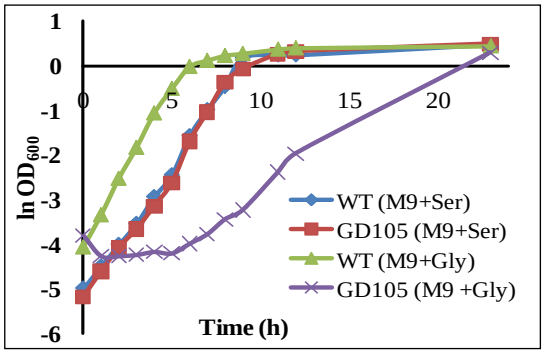

Figure III.6: L-serine in growth medium rescues the defects observed in Δ*tolC-ygiBC-yjfMC* strains. A. Growth curves of WT and Δ*tolC* strains in M9 medium supplemented with 0.4% casamino acids. **B.** Growth rates in M9 medium supplemented with amino acids. **C.** Growth curves in M9 medium supplemented with 0.1g/L serine and 0.2g/L L-glycine.

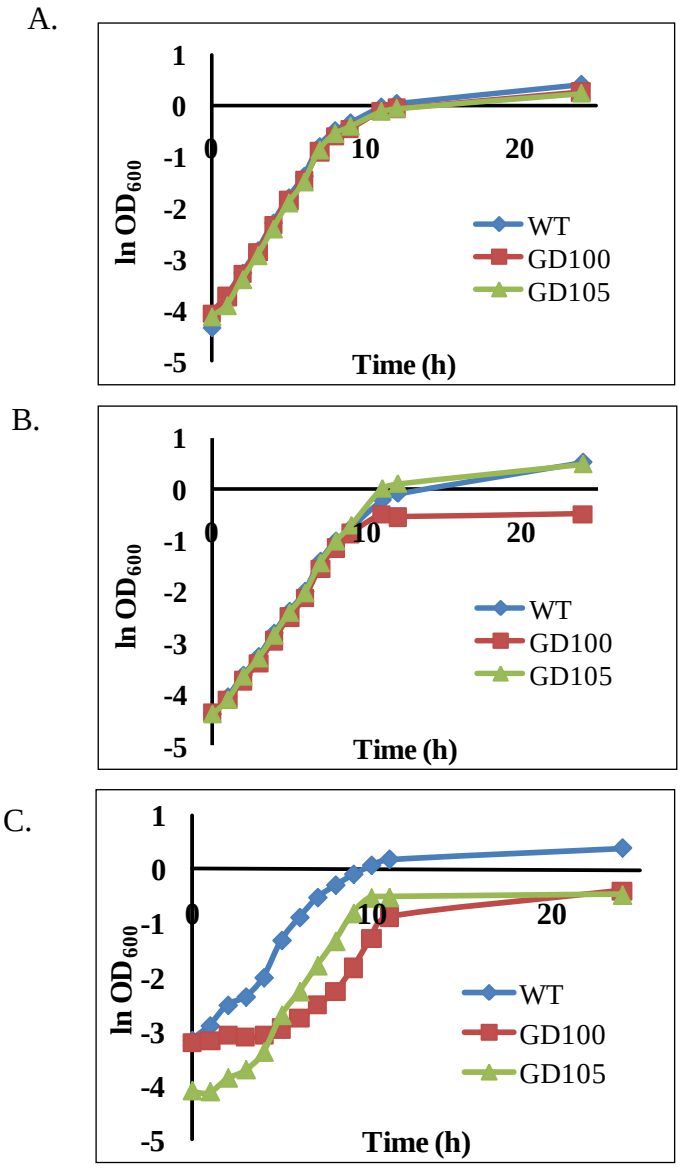

Figure III.7: ΔTolC cells are unable to efficiently metabolize glucose. A: Growth curves of WT, GD100 (Δ*tolC*) and GD105 *(*Δ*tolC-ygiBC-yjfMC*) strains in M9 medium supplemented with 0.4% glycerol. **B:** Growth curves of WT, GD100 (Δ*tolC*) and GD105 (Δ*tolC-ygiBC-yjfMC*) strains in M9 medium supplemented with 0.4% fructose. **C:** Growth curves of WT, GD100 (Δ*tolC*) and GD105 *(*Δ*tolC-ygiBC-yjfMC*) strains in M9 medium supplemented with 0.4% xylose.

III.1.7 ΔTolC cells are filamentous and have anucleate cells in M9 medium. It was shown previously that Δ*tolC* strains growing in M9 medium are filamentous and produce anucleate cells (Hiraga *et al*., 1989). To check this, WT, GD100, GD101, GD102, GD103 and GD105 cells were grown in M9 medium for 12 hours. An aliquot of this culture was spread on to glass slides. The slides were viewed with a 100X phase contrast objective lens. Microscopic observations show that GD101 *(ΔygiBC*), GD103 *(ΔyjfMC)* and GD104 (*ΔygiBC-ΔyjfMC)* strains are similar to WT. However GD100 (Δ*tolC),* GD102 (Δ*tolC-ygiBC)* and GD105 (*ΔtolC- ygiBC-yjfMC)* cells are more elongated than WT (Figure III.8A).

To check if chromosomes were properly segregated in GD100, GD102 and GD105 strains exponentially growing cells in M9 medium were fixed and stained with DAPI and SYPRO orange. SYPRO-orange stains the cell membranes and nucleoids were stained with DAPI. Fluorescence microscopy images show that consistent with previous results Δ*tolC* strains show anucleate cells (Figure III.8B, marked with arrows). Population of anucleate cells reduced significantly when these strains are transformed with plasmid expressing TolC, suggesting that this defect is specific to loss of *tolC* and that TolC is required for normal chromosomal segregation.

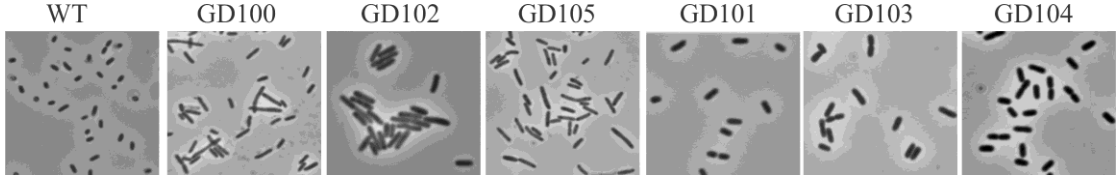

Figure III.8A. Δ*tolC* cells are more elongated than WT when growing in M9 medium. Phase contrast microscopy to determine cell shape and size.

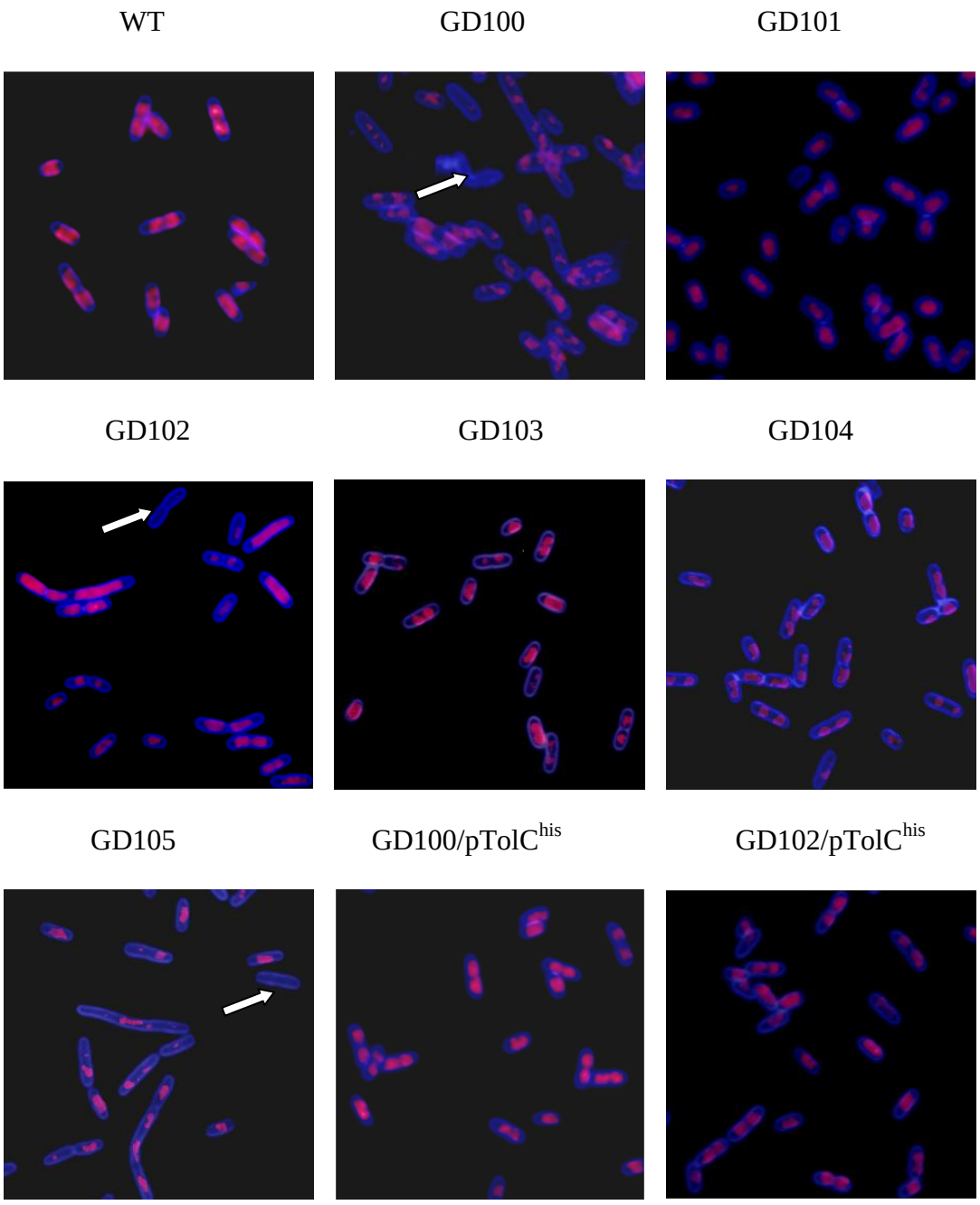

Figure III. 8B. Fluorescence microscopy of DAPI and SYPRO orange stained cells. The Nucleoids stained with DAPI are shown in pink and the SYPRO orange stained cell membranes are shown in blue. Adobe Photoshop was used to generate colored images. Anucleate cells in Δ*tolC* strains are marked with an arrow.

III.1.8 ΔTolC strains when grown in M9 medium overproduce membrane protein PspA in stationary phase. We determined protein expression profiles of cells grown in LB and M9 medium in 1) Exponential phase 2) Stationary phase. No significant differences were observed in both membrane and cytoplasmic fractions when strains were grown in LB medium. Significant differences were observed in membrane protein expression patterns of ΔTolC strains grown in M9 medium. Membrane fractions of ΔTolC strains showed the expression of two unique proteins of molecular weight 27 kDa and 44 kDa (Figure III.9). To gain further insight into the localization of these two proteins, differential solubilization in 1% Sarkosyl was done for one hour on ice. Inner membrane proteins are solubilized with 1% Sarkosyl; however, outer membrane proteins remain insoluble in 1% Sarkosyl (Filip *et al.*, 1973). The soluble and insoluble fractions can then be easily separated by centrifugation at 100,000 ×g for an hour. The 27 kDa protein was readily soluble in 1% Sarkosyl indicating to be an associated/integral inner membrane protein. In contrast the 44 kDa protein remained insoluble in 1% Sarkosyl and therefore was identified as an outer membrane protein. The N-terminal sequencing identified the 27 kDa protein to be Phage shock protein A (PspA). PspA expression is induced when *E.coli* is subject to extracytoplamic stress which leads to dissipation of the proton motive force (Kobayashi *et al.*, 2007). However N-terminal sequencing could not identify the 44 kDa protein. We think that as the 44 kDa is localized in the outer membrane it could be modified at its N-terminal thereby blocking its sequencing.

Our results described above show that presence of serine or other carbon sources such as glycerol and fructose in the growth medium could relieve the defects

observed in ΔTolC strains. Therefore, we wanted to check if membrane damage is caused by growth conditions or if it's caused by deletion of TolC. WT and GD105 strains were grown in M9 medium supplemented with serine or 0.4% glycerol for 48 hours. Membrane protein expression profiles show that when growing in the presence of serine or glycerol GD105 strain still overproduced PspA (Figure III.10). These results suggest that deletion of TolC creates stress on *E.coli* membranes.

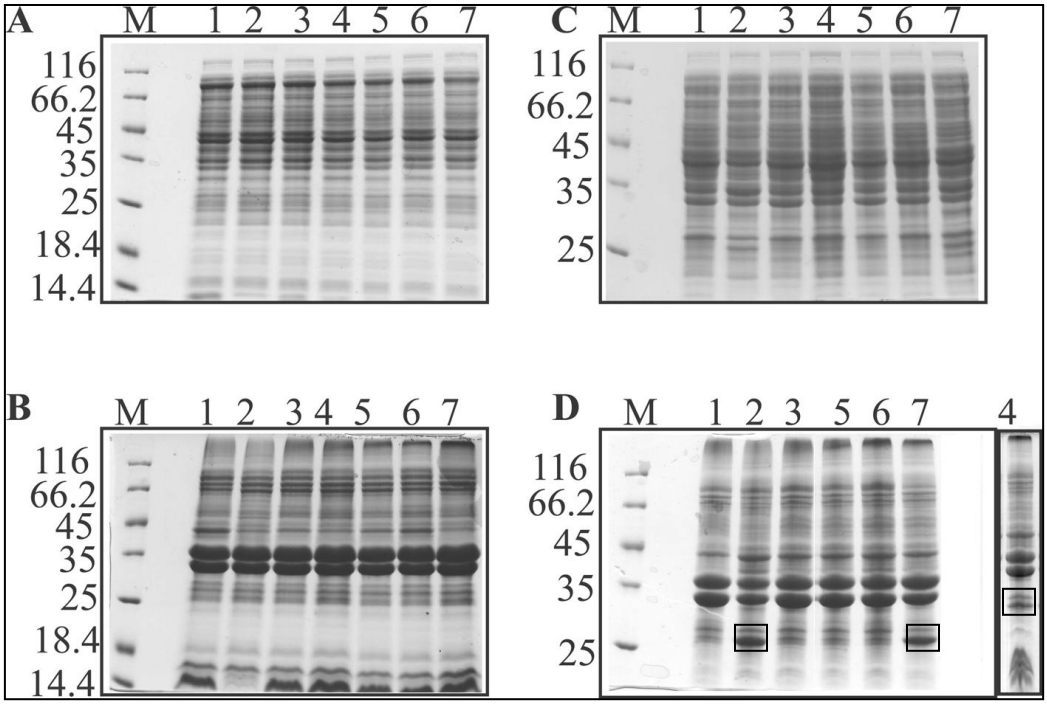

Figure III.9: ΔTolC strains overproduce PspA in stationary phase. All strains were grown in M9 medium and harvested at 0.6 OD_{600} for exponential phase and after 48 hr for stationary phase samples. Panels A and C represent cytoplasmic protein profiles in exponential and stationary phase, respectively. Panels B and D represent membrane protein profiles in exponential and stationary phase, respectively. In all panels: Lane 1- WT, Lane 2- Δ*tolC* (GD100), Lane 3- Δ*ygiBC* (GD101), Lane 4- Δ*tolC-ygiBC*

(GD102), Lane 5- Δ*yjfMC* (GD103), Lane 6- Δ *ygiBC-yjfMC* (GD104), Lane 7- Δ*tolC-ygiBC-yjfMC* (GD105). PspA, the 27 kDa protein indicated in a box.

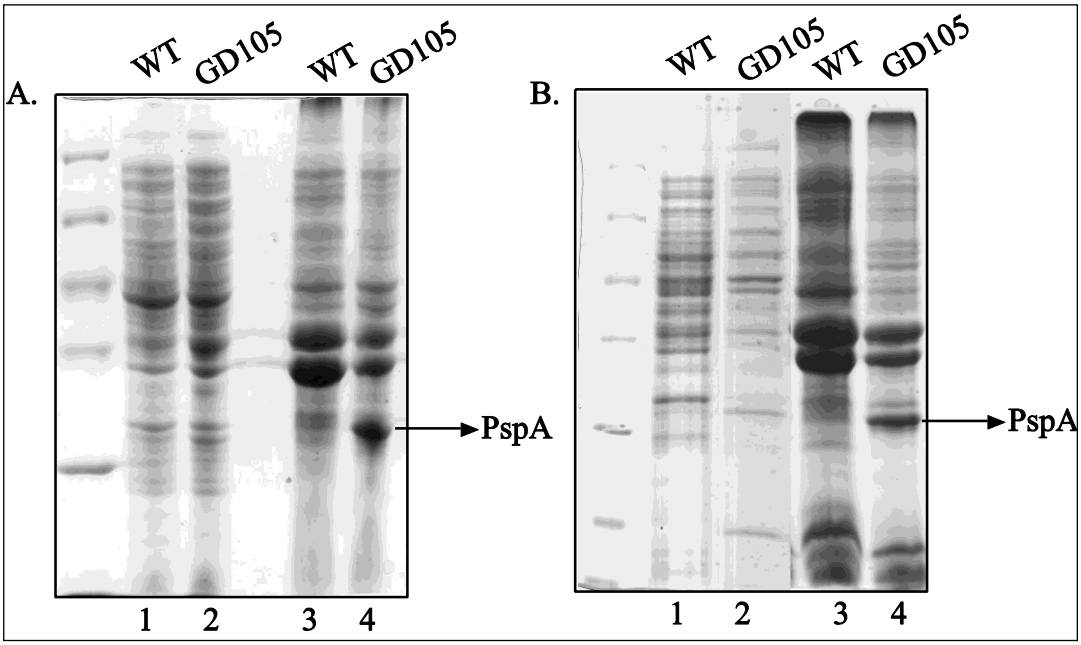

Figure III.10. GD105 (Δ*tolC-ygiBC-yjfMC*) strain overproduces PspA when grown in M9 medium supplemented with L-serine (Panel A) and Glycerol (Panel B) for 48 h (stationary phase). 20 µg of cytoplasmic fractions (Lanes 1, 2) and membrane fractions (Lanes 3, 4) loaded onto 12% SDS-PA gel and stained with Coomasie Brilliant Blue stain.

III.1.9 Deletion of TolC does not affect viability of cells growing in M9 medium. Induction of PspA expression is a strong indication of stress conditions in the cell. Therefore we wanted to check if the viability of ΔTolC strains is affected under these conditions. WT, Δ*tolC* (GD100), Δ*ygiBC* (GD101), Δ*tolC-ygiBC*(GD102), Δ*yjfMC*(GD103), Δ*ygiBC-yjfMC*(GD104), Δ*tolC-ygiBC-yjfMC*(GD105), Δ*speE* (JW0117) and Δ*gshB* (JW 2914) strains were grown in M9 medium. ΔTolC strains transformed

with pTolC^{his} plasmid were used as positive controls. All the strains were grown for 10 days at 37°C with shaking. An aliquot of the growing cultures was removed at 0, 3, 6 and 10 days. At every time point optical density of the culture was measured, culture was diluted accordingly and plated onto LB-agar plates. The graphs represent the number of colony forming units normalized to optical density of the culture plotted against time of incubation. Δ*ygiBC*, Δ*yjfMC*, Δ*ygiBC-yjfMC* and Δ*speE* strains are similar to WT (Figure III.11A and B). Highest number of viable cells was present when cells were in exponential phase (0 day) and there was a decrease in viable cell count as incubation time increased. The only significant difference between the viable cell count of ΔTolC strains and WT is during the exponential growth phase. Both Δ*tolC* and Δ*tolC-ygiBC-yjfMC* strains had ~100-150-fold less number of viable cells at 0 day time point. However at 10 days these strains had similar numbers of viable cells as WT. The three Δ*tolC* strains transformed with pTolC plasmid showed similar patterns as WT. These results confirm that deletion of TolC causes the cells to grow slower, does not affect the viability of cells and that it can be complemented by the expression of TolC.

A. B.

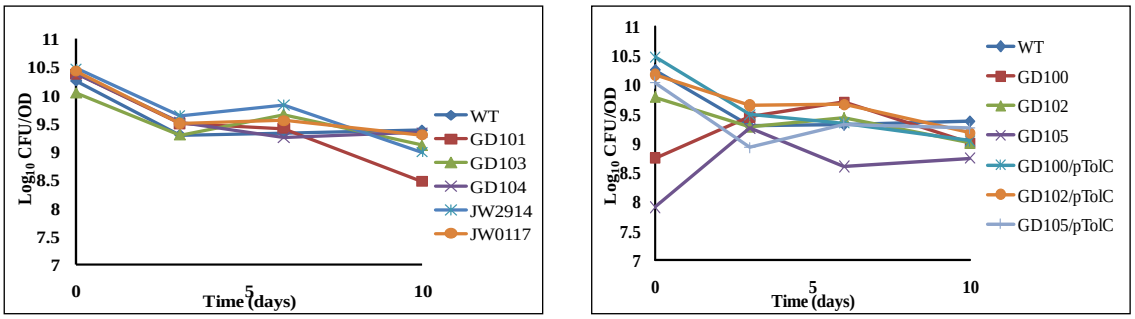

Figure III.11A: Deletion of TolC does not affect cell viability. Panel A: Cell viability profiles of WT and Δ*ygiBC* strains growing in M9 medium. **Panel B**: Cell viability profiles of WT, Δ*tolC* strains and Δ*tolC* strains transformed with pTolC plasmid growing in M9 medium.

Next, we also used the LIVE/DEAD BacLight stain kit (Invitrogen) to determine the number of live cells and the extent of membrane stress in the stationary Δ*tolC* cells. This kit combines nucleic acid stains SYTO9 and propidium iodine. Propidium iodide has been shown to be excluded from cells with structurally intact cytoplasmic membranes because of the size and charge of the propidium molecule (Boulos *et al.*, 1999). As shown on Fig. III.11C, during LB-to-M9 transition and in the stationary phase the vast majority of WT and Δ*tolC* mutant cells remain alive. For all strains, we found that the number of dead cells is less than 5% and remains the same in the exponential and stationary phases.

The results of this experiment are in agreement with the results of determination of colony forming units in the stationary WT and Δ*tolC* mutants. Both these experiments confirmed that in stasis Δ*tolC* cells have the same survival frequency as the WT. However, GD100 and GD105 cells when grown in M9 were notably longer

than the WT cells indicative of cell division defects (Fig. III. 8A, B). Thus, Δ*tolC* cells survive membrane stress and metabolic problems they experience upon transition into the stationary phase in M9 medium. These results further confirm that extended lags and slow growth rates of Δ*tolC* cells upon re-inoculation into a fresh medium (Fig. III.4) are not caused by the low number of live cells but most likely result from the loss of critical metabolites.

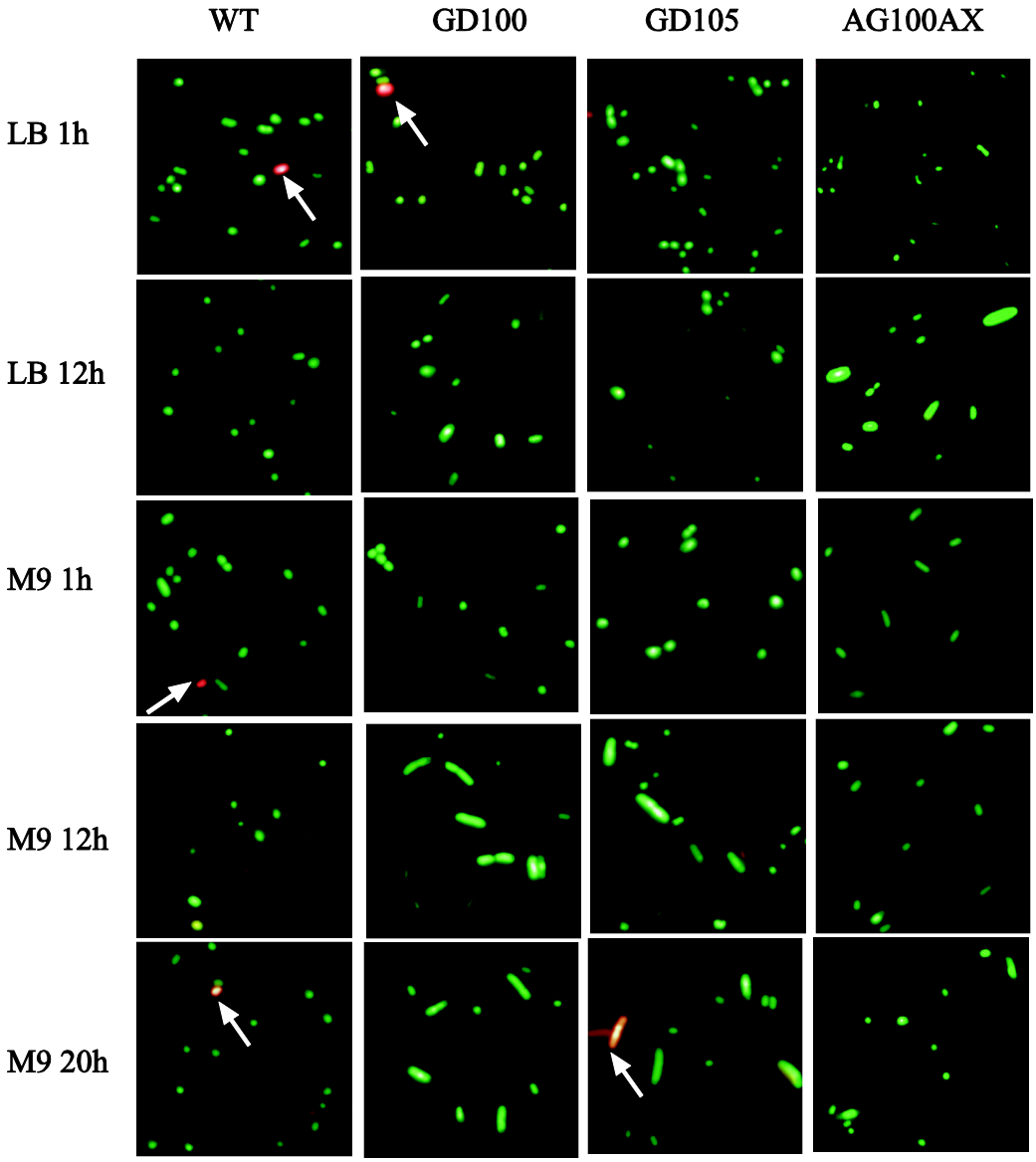

Figure III. 11C. The LIVE/DEAD Bacterial viability kit was used to score live and dead cells. Live cells are seen in green and the dead cells are red and indicated by arrows.

III.2 Understanding the physiological role of *E.coli* TolC-YgiBC operon.

III.2.1 ΔTolC strains have low concentrations of NADH and NAD^+ when growing in M9 medium. Our results indicate that the growth defects observed in ΔTolC strains are specific when glucose is used as carbon source. Therefore, we next measured the NADH, NAD^+ concentrations in cells. NADH and NAD^+ concentrations are strictly regulated and high NADH/NAD^+ ratios inhibit pyruvate dehydrogenase, citrate synthase and α-ketoglutarate dehydrogenase, the key enzymes of TCA cycle (Prüss *et al.*, 1994). TCA cycle converts pyruvate to oxaloacetate with the simultaneous conversion of NAD^+ to NADH. The reducing equivalents of NADH are then finally transferred to electron transport chain to produce ATP (Voet & Voet, 1996). TCA cycle also produces intermediates for amino acid and nucleotide biosynthesis. We hypothesized that ΔTolC strains have high NADH/NAD^+ ratio therefore are unable to grow in M9 medium. We used the NAD^+ cycling assay to measure NADH and NAD^+ concentrations during the LB-M9 transition and in the stationary phase (Leonardo *et al.*, 1996). WT and mutants growing in LB medium had ~ 1 mM concentration of NAD^+ (Table 3a). Even in stationary phase WT and Δ*tolC* cells maintained 1 mM of NAD^+, but in Δ*tolC-ygiBC-yjfMC* cells the concentration of NAD^+ decreased to 0.3 mM.

All strains contained similar concentrations of NAD^+ one hour after the shift into M9 medium (Table 3a). As incubation time in M9 increased NAD^+ concentration dropped significantly in Δ*tolC-ygiBC-yjfMC* cells. Extension of stasis for 20 hours led to three-fold drop to 0.3 mM of NAD^+ in Δ*tolC* cells and NAD^+

concentration further decreased to 0.08 mM in Δ*tolC-ygiBC-yjfMC* cells. These results suggest that when growing in M9, Δ*tolC* cells and Δ*tolC-ygiBC-yjfMC* cells cannot efficiently synthesize NAD^+, which eventually leads to depletion of this cofactor in the stationary phase.

When growing in LB, exponential and stationary phase Δ*tolC-ygiBC-yjfMC* cells contained twice higher concentrations of NADH than WT. High concentrations suggests that Δ*tolC-ygiBC-yjfMC* cells are unable to synthesize amino acids (Prüss *et al.*, 1994). In case of WT, amounts of NADH increased in the M9 12 and 20 hr samples. This increase in NADH concentration reflects the decrease in respiration rate and results in starvation in the stationary phase. However, the amounts of NADH did not change significantly in Δ*tolC* and Δ*tolC-ygiBC-yjfMC* cells. Due to depletion of NAD^+ and the concentration of NADH being constant in Δ*tolC-ygiBC-yjfMC* cells, the NADH/NAD^+ ratio was almost three in M9 20 hr samples as opposed to a NADH/NAD^+ ratio of one in the M9 20 hr samples of WT and Δ*tolC* cells. This result strongly suggests that in M9 medium, Δ*tolC-ygiBC-yjfMC* strain is not only deficient in biosynthetic activities but cannot oxidize NADH as well. As YgiC and YjfC are close homologs of glutathionylspermidine we measured concentrations of NAD^+ and NADH in Δ*gshA* cells that do not synthesize GSH (Helbig *et al.*, 2008) (Table 3a). The amounts of NAD^+, NADH and the NADH/NAD^+ ratio are very similar in *gshA* and WT cells, indicating that the lack of GSH and GSP did not cause the metabolic problems in Δ*tolC-ygiBC-yjfMC* cells.

NAD^+ depletion in the stationary phase Δ*tolC-ygiBC-yjfMC* cells could be completely rescued by plasmid expressing TolC (Table 3b) suggesting that TolC

alone is required to maintain normal metabolism in *E.coli*. In agreement TolC$^+$ cells lacking *ygiBC* and *yjfMC* genes had normal NADH/NAD$^+$ ratios.

Taken together these results strongly suggest that during stationary phase *tolC* cells are depleted of essential metabolites. This metabolite depletion is notably accelerated in Δ*tolC-ygiBC-yjfMC* cells. The high NADH/NAD$^+$ ratio in the stationary phase cells of Δ*tolC-ygiBC-yjfMC* strain indicates that the metabolic shutdown in these cells is caused by depletion of NAD$^+$.

III.2.2. NADH dehydrogenases are inhibited in Δ*tolC* cells. During aerobic metabolism, the major pool of NADH is re-oxidized on the membrane by two membrane-bound NADH dehydrogenases NDH-I and NDH-II (Yun *et al.*, 2005). Thus, either one or both of these proteins could be inhibited in GD105 cells. To further confirm this conclusion we measured the NADH oxidase activity in membrane fractions isolated from WT and Δ*tolC* mutants grown in LB and M9 media. We found that the exponential WT and mutant cells contained similar levels of the membrane bound NADH oxidase activity (Table 4). In the stationary WT and GD100 cells, the NADH oxidase activity decreased by 25-35%. In contrast, the NADH oxidase activity of GD105 membranes dropped 2-3-fold when cells entered stasis in either medium and was 40-60% lower than in the stationary WT cells. Thus, in accord with NADH/NAD$^+$ measurements (Table 4), GD105 membranes cannot efficiently oxidize NADH. We conclude that inhibition of membrane-bound NADH dehydrogenases contributes to metabolic shutdown in Δ*tolC* cells.

Table 3a. NAD^+ and NADH concentrations in WT and Δ*tolC* mutants.

Medium, time of incubation	**BW25113**			**GD100**			**GD105**			**JW2663**		
	NAD^+, mM	NADH, mM	NADH/ NAD^+	NAD^+, mM	NADH, mM	NADH/ NAD^+	NAD^+, mM	NADH, mM	NADH/ NAD^+	NAD^+, mM	NADH, mM	NADH/ NAD^+
LB, 1 hr	1.4 ± 0.28	0.48± 0.2	0.3	1.2±0.3	0.80± 0.4	0.7	1.35± 0.18	0.94± 0.47	0.7	1.1± 0.1	0.41± 0.33	0.4
LB, 12 hr	0.77 ±0.29	0.21 ±0.06	0.3	0.79± 0.2	0.19± 0.06	0.2	0.29± 0.2	0.34± 0.18	1.2	0.7± 0.2	0.26± 0.15	0.4
M9, 1 hr	1.5±0.06	0.38± 0.13	0.2	1.4± 0.08	0.5± 0.09	0.4	1.57± 0.3	0.36± 0.06	0.2	1.41± 0.01	0.34± 0.03	0.2
M9, 12 hr	1.1± 0.15	0.63± 0.08	0.5	1.1± 0.01	0.4± 0.06	0.4	0.47± 0.04	0.29± 0.01	0.6	0.72± 0.01	0.44± 0.05	0.6
M9, 20 hr	0.8 ± 0.29	0.61± 0.27	0.7	0.34± 0.01	0.35± 0.06	1.0	0.08± 0.02	0.23± 0.01	2.9	0.72± 0.09	0.67± 0.01	0.9

Table 3b NAD^+ and NADH concentrations in Δ*ygiBC-yjfMC* (GD104) and Δ *tolC ygiBC-yjfMC*/pTolC (GD105/pTolC) mutants.

Medium, time of incubation	GD104			GD105/pTolC		
	NAD^+, mM	NADH, mM	NADH /NAD^+	NAD^+, mM	NADH, mM	NADH /NAD^+
LB, 1 hr	1.7±0.03	0.97±0.04	0.6	1.51±0.01	1.1±0.01	0.7
LB, 12 hr	0.43±0.01	0.21±0.07	0.5	0.52±0.05	0.26 ±0.05	0.5
M9, 1 hr	1.5±0.1	0.25±0.07	0.2	1.2±0.1	0.3±0.003	0.3
M9, 12 hr	1.1±0.14	0.5±0.007	0.4	0.99±0.01	0.51±0.06	0.5
M9, 20 hr	0.52±0.0007	0.36±0.01	0.7	0.6±0.05	0.51±0.01	0.8

Table 4. NADH oxidase specific activity (U/mg) in membranes isolated from WT and Δ*tolC* mutants.

Medium, time of incubation	**WT**	**GD100**	**GD105**	**JW2663**
LB, 1 hr	0.39 ± 0.06	0.46 ± 0.09	0.39 ± 0.03	ND
LB, 12 hr	0.28 ± 0.02	0.28 ± 0.04	0.13 ± 0.01	ND
M9, 1 hr	0.49 ± 0.09	0.33 ± 0.04	0.52 ± 0.1	0.25 ± 0.02
M9, 12 hr	0.31 ± 0.1	0.36 ± 0.05	0.21 ± 0.01	0.45 ± 0.09
M9, 20 hr	0.35 ± 0.007	0.24 ± 0.07	0.20 ± 0.05	0.30 ± 0.07

ND- Not determined

III.2.3 ΔTolC strains have lower concentrations of intracellular glutathione than WT when growing in M9 medium. As *ygiC* and *yjfC* share close sequence homology with glutathionylspermidine synthetase we hypothesized that the lack of these putative enzymes will lead to a decrease in the levels of GSP in cells. To determine GSH and GSP concentrations in Δ*tolC*, Δ*tolC- ygiBC-yjfMC* strains, we derivitized cell extracts with a thiol specific dye monobromobimane (MBB) (Fairlamb *et.al.*, 1986 and Fahey & Newton, 1987). MBB reacts with thiols to give a fluorescent bimane adduct with an excitation wavelength of 380 nm and emission wavelength of 490 nm. These derivitized extracts were separated by a reverse phase C-18 column and the peaks were detected with a fluorescence detector. WT and Δ*gshA* strains were included as positive and negative controls, respectively. As the growth defects observed in these strains were more pronounced during exit of stationary phase when cells were transferred from LB to M9 medium we wanted to monitor GSH and GSP levels during LB-M9 shift. Aliquots of samples were removed and derivitized when cells were growing for one and twelve hours in LB medium and one, twelve and twenty hours after transfer to fresh M9 medium. GSH and GSP standards were derivitized using the same procedure as that used for other samples.

HPLC profiles show the presence of 4 peaks (Figure III.12). The early peak at 52 min is present all samples including the control samples with dye only, indicating that this peak is a non-specific product which originates from the dye. Comparing GSH standard graphs, the 58 min peak represents GSH as this peak is not present in Δ*gshA* samples (Helbig *et al.*, 2008). The 67 min and 84 min peaks are

present in Δ*gshA* samples indicating that these peaks are non-GSH linked peaks (Figure III.12).

Cells grown for one hour in LB medium have similar levels of intracellular glutathione ~6 mM (Table 5). In case of strains growing for twelve hours in LB medium, WT and Δ*tolC* cells have ~5 mM GSH whereas Δ*tolC- ygiBC-yjfMC* strain contains ~3 mM intracellular GSH. An hour after incubation in fresh M9 medium GSH concentrations remained constant at approximately 7 mM level in WT and Δ*tolC* cells but GSH levels in Δ*tolC- ygiBC-yjfMC* cells decreased further. Twelve hours after shift into M9 medium, GSH concentrations in WT and Δ*tolC* strain remained high, but GSH concentrations in Δ*tolC- ygiBC-yjfMC* strain decreased further to 1.7 mM. Twenty hours of incubation in M9 medium led to the complete drop of GSH below detection limits in both Δ*tolC* and Δ*tolC- ygiBC-yjfMC* cells. In conclusion these results indicate that loss of TolC leads to depletion of the intracellular GSH concentration in stationary phase.

Reasons for the drop of intracellular glutathione concentrations in Δ*tolC* and Δ*tolC-ygiBC-yjfMC* cells after incubation for twenty hours in M9 could either be due to inhibition of GSH biosynthesis or the oxidization of GSH to GSSG. A drawback of the HPLC technique is that MBB can derivitize only reduced thiols therefore GSSG cannot be detected unless the samples are pretreated prior to derivitization. To overcome this problem we used the glutathione reductase assay which measures the total glutathione (GSH+GSSG) in cells (Anderson, 1985). Consistent with HPLC studies, WT cells maintained ~8-10 mM total GSH when incubated in LB medium for one or twelve hours and in M9 medium for 1 hour. GSH+GSSG levels increased to ~18

mM when these cells were further incubated for twelve and twenty hours in M9 medium. Δ*tolC* cells show similar levels of [GSH+GSSG] when grown in LB medium and when incubated for one hour in fresh M9 medium. However [GSH+GSSG] drastically decreases to 1.8 mM when cells are incubated for twenty hours in M9 medium (Table 6). In contrast Δ*tolC-ygiBC-yjfMC* cells after transfer to M9 medium showed decreasing levels of [GSH+GSSG] as the incubation time increased from one to twenty hours.

GSSG concentration in all cells was ~1 μM. Such low concentration of GSSG cannot account for the dramatic drop of GSH in Δ*tolC* strains. This result strongly suggests that the depletion of GSH in GD100 and GD105 strains, probably results from halt in biosynthesis of GSH.

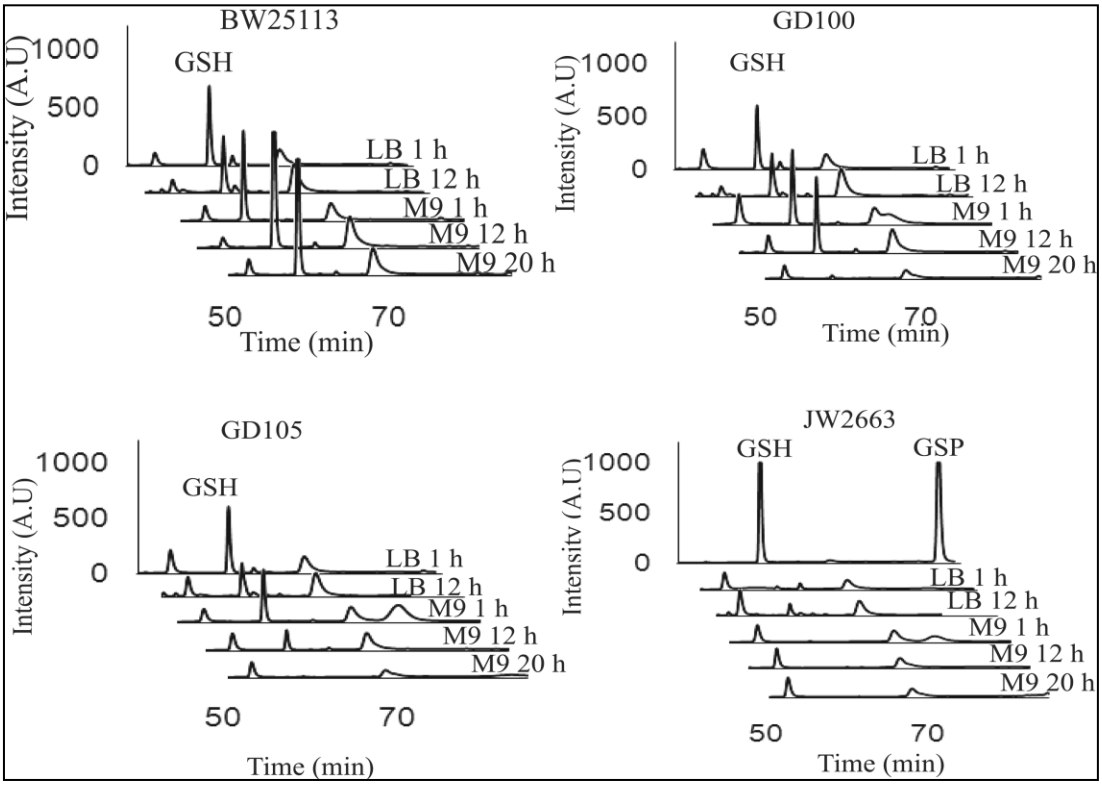

Figure III.12: The M9 grown Δ*tolC* cells deplete endogenous GSH. Intracellular glutathione concentrations in WT, Δ*tolC* (GD100), Δ*tolC-ygiBC-yjfMC* (GD105) and Δ*gshA* (JW2663) strains were detected using HPLC and MBB labeling. Glutathione (GSH) and glutathionylspermidine (GSP) standards shown in JW2663 panel. The intracellular concentrations of GSH when detectable were calculated from peak area using the calibration curve generated with GSH in Table 5.

Table 5. Intracellular GSH concentrations (mM) determined by HPLC and MBB labeling.

Medium, time of incubation	WT	GD100 (Δ*tolC*)	GD105 (Δ*tolC-ygiBC-yjfMC*)	JW2663 (Δ*gshA*)
LB, 1 h	6.3	5.5	5.5	ND
LB, 12 h	4.9	4.5	4.5	ND
M9, 1 h	7.3	6.8	6.8	ND
M9, 12 h	18.2	**6.2**	**6.2**	ND
M9, 20 h	>18.2	**ND**	**ND**	ND

ND: Not detected, below detection limit.

Table 6. Intracellular (in) and excreted (out) concentrations of glutathione in the WT and Δ*tolC* mutants

Medium,	**WT**		**GD100 (Δ*tolC*)**		**GD105(Δ*tolC-ygiBC yjfMC*)**	
time of incubation	GSH+GSSG, mM		GSH+GSSG, mM		GSH+GSSG, mM	
	in	**out**	**in**	**out**	**in**	**out**
LB, 1 h	10.4±0.1	ND	9.7±0.8	ND	7.6±1.9	ND
LB, 12 h	8.1±0.4	ND	8.3±0.01	ND	7.8±1.2	ND
M9, 1 h	8.8±0.7	-	7.1±0.3	-	**4.2±0.3**	-
M9, 12 h	17.7±1.9	0.001± 0.0002	**8.5±0.1**	**0.008 ±0.0003**	**2.4±0.2**	**0.009 ± 0.001**
M9, 20 h	15.1±0.6	0.019± 0.001	**1.8± 0.5**	**0.014±0.001**	**0.3±0.1**	**0.005 ± 0.0004**

ND-Not determined. – below detection limits.

III.2.4 Extracellular glutathione is toxic to ΔTolC strains. Our HPLC profiles show that Δ*tolC* and Δ*tolC-ygiBC* have very low concentrations of GSH in the stationary phase. Furthermore results of GSSG-GSH recycling assay suggest that the biosynthesis of GSH may be affected. To check if the growth defects of Δ*tolC* strains observed in M9 medium are due to the complete lack of GSH in these strains we grew WT, Δ*tolC* and Δ*tolC-ygiB-yjfMC* strains in M9 medium supplemented with 2 mM GSH. Growth curves in figure III.13A show that the presence of 2 mM GSH in the medium was not able to rescue Δ*tolC* and Δ*tolC-ygiB-yjfMC* strains from the growth defects observed in M9 medium. These results suggest that low concentration of GSH is not the sole reason for the observed growth defects (Appendix B). However, we also tested 5 mM, 10 mM and 15 mM concentrations of GSH. Surprisingly 15 mM GSH was toxic to Δ*tolC* and Δ*tolC-ygiB-yjfMC* strains even in LB medium. Δ*tolC* and Δ*tolC-ygiBC-yjfMC* strains show different levels of tolerance towards extracellular GSH concentrations. In LB medium supplemented with 10 mM GSH Δ*tolC-ygiB-yjfMC* already showed a two-fold decrease in growth rate as compared to WT. Although growth rates of WT strain also decreased from 1.0 hr^{-1} in LB medium to 0.7 hr^{-1} in LB medium supplemented with 15 mM GSH, high concentrations of GSH were well tolerated by WT strains (Appendix B) (Figure III.13B).

Previously it was reported that TolC is involved in cysteine tolerance and that Δ*tolC* strains are highly susceptible to 10 mM cysteine (Wiriyathanawudhiwong *et al.,* 2009). Therefore to check if GSH toxicity was due to cysteine we grew WT, Δ*tolC* and Δ*tolC-ygiB-yjfMC* strains in LB medium supplemented with 1 mM and 5 mM of cysteine (Appendix B). Growth rates of Δ*tolC* and Δ*tolC-ygiB-yjfMC* strains were

similar to WT suggesting that the toxicity of high concentrations of GSH was not due to cysteine but due to the lack of *tolC*, *ygiBC* and *yjfMC* gene products.

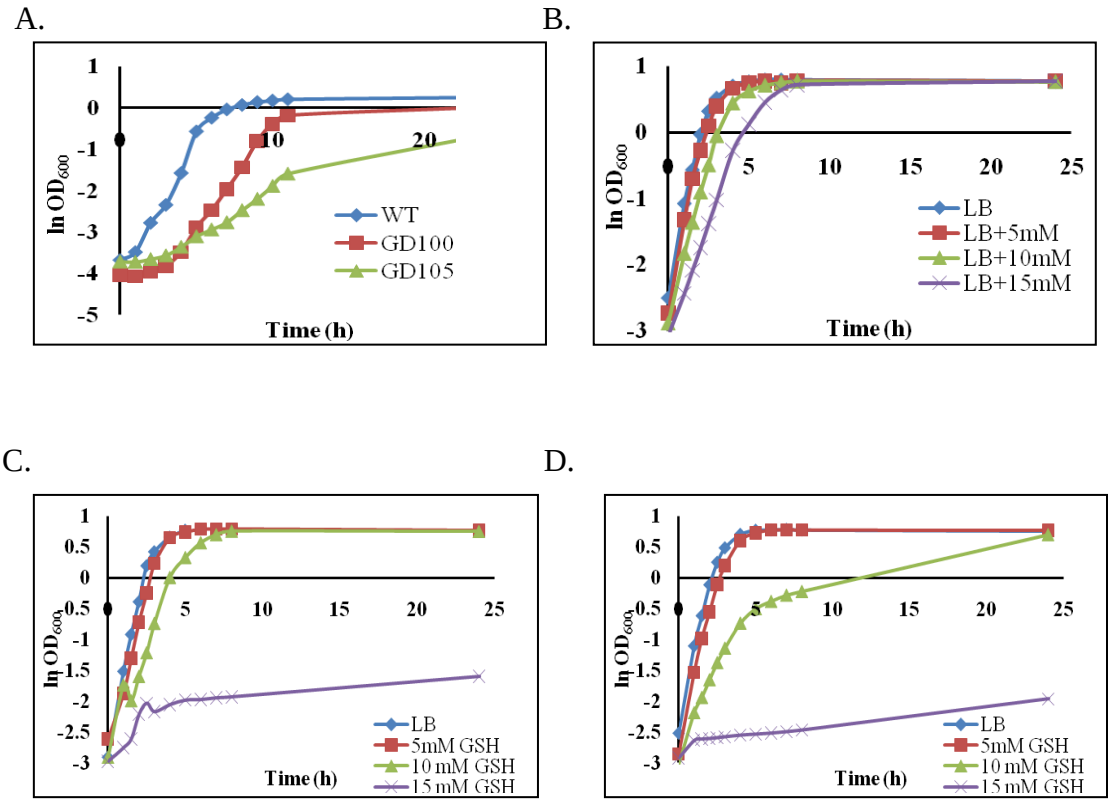

Figure III.13 Extracellular glutathione is toxic to Δ TolC strains : A: M9 + 2 mM GSH **B:** WT growth curves in LB medium with 5 mM, 10 mM and 15 mM GSH. **C:** GD100 growth curves in LB medium with 5 mM, 10 mM and 15 mM GSH. **D.** GD105 growth curves in LB medium with 5 mM, 10 mM and 15 mM GSH

III.2.5 YgiBC and YjfMC do not contribute significantly towards protection against norfloxacin and hydrogen peroxide (H_2O_2). Previously it was demonstrated that bactericidal antibiotics cause oxidative stress in cells (Kohanski *et al.,* 2007).

Kohanski *et al.*'s microarray data also showed the expression of *ygiB* to be up-regulated when cells are treated with bactericidal drugs as opposed to bacteriostatic drugs. To check if deletion of *ygiB* and its homolog *yjfM* alters the sensitivity to bactericidal drugs we treated WT, Δ*ygiBC* (GD101), Δ*yjfMC* (GD103), Δ*ygiBC-yjfMC* (GD104), Δ*speE* (JW0117) and Δ*gshB* (JW 2914) strains with two different concentrations of norfloxacin, 250 ng/ml and 600 ng/ml. Norfloxacin is a bactericidal antibiotic and has been shown to generate damaging free radicals in *E.coli* cells (Kohanski *et al.*, 2007). All the strains were grown in LB medium until 0.3 OD_{600} and different concentrations of norfloxacin were added, aliquots of each culture were removed at 0 h, 1 h, 2 h and 3 h post addition of norfloxacin and plated onto LB-agar plates. A positive control without addition of antibiotic was also included. The graphs in figure III.14 represent colony forming units with respect to time of incubation after the addition of norfloxacin. As expected in the no drug control there was no difference observed in the number of viable cells between WT and *ygiBC*, *yjfMC* and *ygiBC-yjfMC* deletion strains at any time point.

When treated with 250 ng/ml norfloxacin all the strains showed a similar pattern of susceptibility. At 0 hour WT and all other mutants had the same number of viable cells ~10^{10} cells/ml (Figure III.14). The only small difference in the cell count was observed at 3 hour time point. WT and Δ*ygiBC* strains were similar and had $2.2X10^6$ and $1.4X10^6$ viable cells/ml, respectively. Δ*yjfMC*, Δ*ygiBC-yjfMC*, Δ*gshB* and Δ*speE* strains had ~10^7 viable cells/ml. This 10-fold difference may not be significant and could arise due to pipetting, dilution error or both. However different susceptibility patterns were observed when the cells were treated with 600 ng/ml

norfloxacin. Δ*yjfMC* strain was most susceptible as no colonies were observed just one hour post incubation with the antibiotic. After three hours incubation with antibiotic, WT had 10^8 viable cells/ml, Δ*ygiBC* and Δ*ygiBC-yjfMC* strains had ~100-fold less number of viable cells than WT. Δ*speE* strain had ~10^6 viable cells/ml and Δ*gshB* strain was completely susceptible to norfloxacin. Although, Δ*ygiBC* strains are more susceptible to 600 ng/ml norfloxacin than WT more experiments need to be done to conclude that *ygiBC* genes participate in protecting *E.coli* cells against oxidative stress.

To investigate the possible role of *ygiBC* genes in protection against H_2O_2 we treated WT, Δ*tolC* strains, Δ*ygiBC-yjfMC*, Δ*gshB*, Δ*speE* and Δ*gspS* strains with different concentrations of H_2O_2 (Figure III.15). H_2O_2 is a potent oxidizing agent and damages cells membranes and DNA (Imlay & Linn, 1987). Overnight grown cultures were plated onto LB-agar plates. Filter paper discs with 20 µl either of 5%, 15%, 30% H_2O_2 solution or water as a control was placed onto the plates. After overnight incubation at 37°C, a zone of clearing was scored. The graphs represent average diameters of zone of clearing observed for each strain (Figure III.15). As expected the diameter of the clear zone increases with increasing concentrations of H_2O_2. However no significant difference in zone diameters was observed between WT and Δ*tolC* strains, Δ*ygiBC-yjfMC*, Δ*gshB*, Δ*speE* and Δ*gspS* strains indicating that glutathionylspermidine synthetase and glutathionylspermidine synthetase like enzymes (*ygiC* and *yjfC*) do not contribute significantly towards protection against H_2O_2.

A.

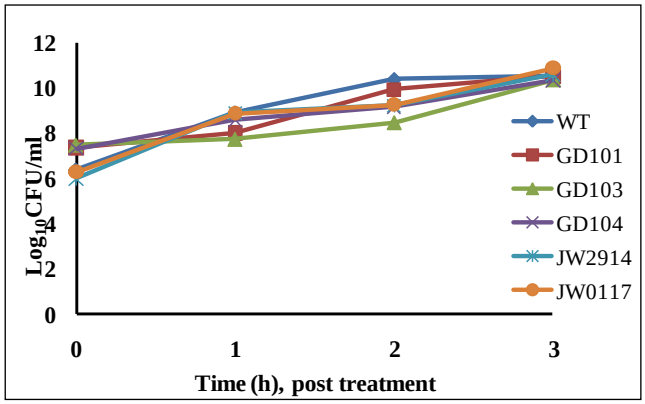

B.

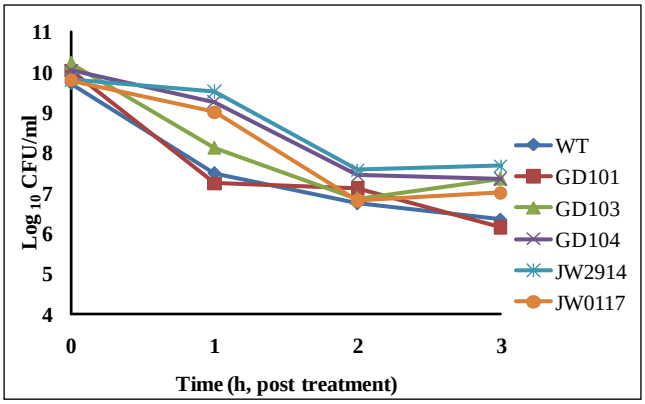

C.

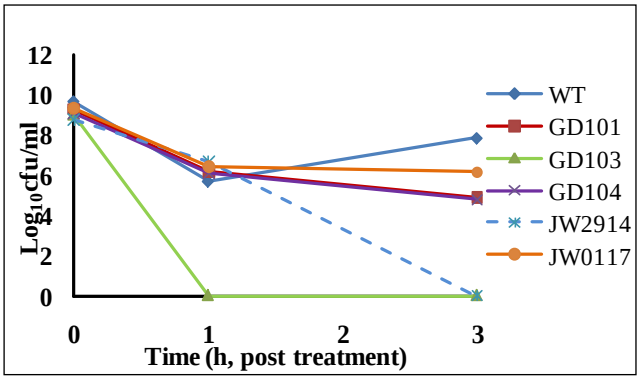

Figure III.14: Treatment with norfloxacin. Number of surviving cells (Log_{10} colony forming units (CFU) per milliliter culture) plotted against time after addition of drug. A: Cells treated with DMSO only. B: Cells treated with 250 ng/ml norfloxacin. C: Cells treated with 600 ng/ml norfloxacin.

A.

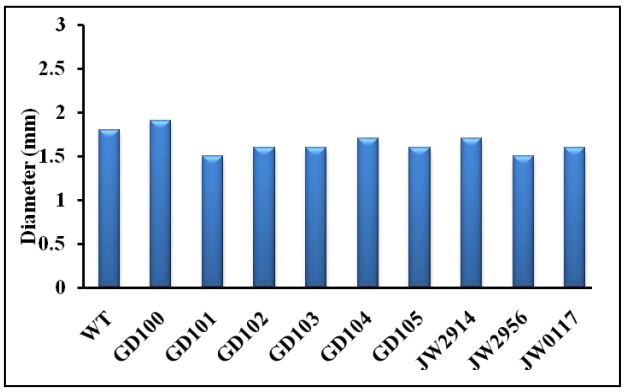

B.

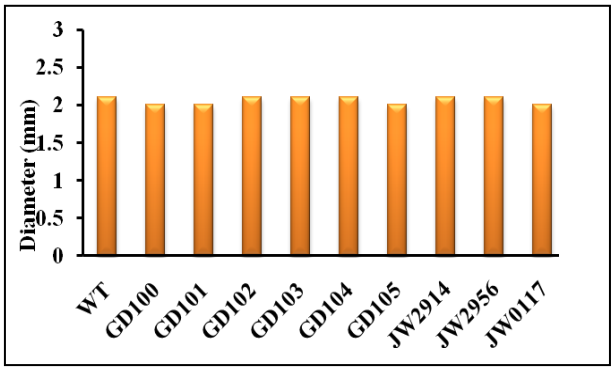

C.

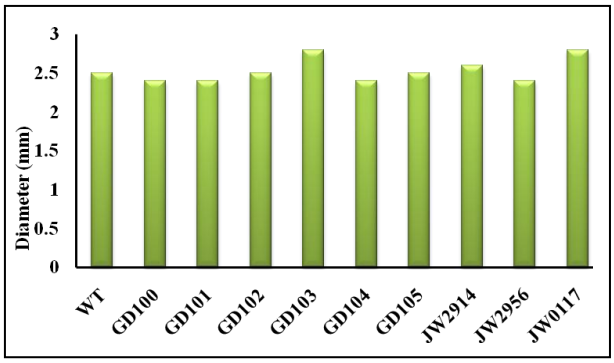

Figure III.15: Hydrogen peroxide disk diffusion assay. Cells exposed to 5% H_2O_2 (A), 15% H_2O_2 (B) and 30% H_2O_2 (C)

III.2.6 YgiBC are not required for GSH mediated protection against antibiotics. Previously it was shown that GSH when added to the extracellular medium protects *E.coli* from aminoglycoside and fluoroquinolone class of antibiotics (Goswami *et.al*

2006). The mechanism of protection proposed is that GSH is a potent antioxidant and neutralizes the free radical species generated by bactericidal antibiotics (Goswami *et al.,* 2006 and Goswami *et al.,* 2007). To check if this protection by GSH is dependent on TolC, glutathionylspermidine synthetase or glutathionylspermidine synthetase like enzymes, we measured bactericidal activity of norfloxacin in the presence of GSH. For this purpose we treated WT, Δ*tolC*, Δ*ygiBC-yjfMC*, Δ*tolC-ygiBC-yjfMC* strains with increasing concentrations of norfloxacin, in the presence of 5 mM, 10 mM and 15 mM of GSH. Controls without GSH and with norfloxacin and vice versa were also set up. Consistent with previously published results, (Goswami *et al.,* 2006) increasing concentrations of GSH protected WT cells from norfloxacin (Table 7, Figure III.16). In the presence of 15 mM GSH MICs of norfloxacin increased up to 32-fold. Δ*ygiBC-yjfMC* strain showed similar level of resistance to norfloxacin as WT. Although notably less than WT, eight-fold protection in presence of 10 mM GSH was also seen in Δ*tolC* strains. Δ*tolC-ygiBC-yjfMC* strain showed four-fold increase in MIC of norfloxacin in presence of 5 mM GSH. From these results we can conclude that glutathionylspermidine synthetase like enzymes are not required for GSH mediated protection against norfloxacin.

To check if TolC's export function is required for GSH mediated protection against norfloxacin we subject Δ*acrAB-acrEF* strain, a strain lacking two major efflux transporters, to norfloxacin in presence of increasing concentrations of GSH. Δ*acrAB-acrEF* strain like WT also shows 32-fold increase in norfloxacin resistance in presence of 15 mM GSH. These results show that AcrAB/EF dependant active efflux is not required for GSH mediated protection against norfloxacin.

Next, to check if this effect is also seen when cells are exposed to bacteriostatic drugs, we treated the above strains with different concentrations of erythromycin in presence of 5 mM, 10 mM and 15 mM GSH. Erythromycin is a macrolide antibiotic and is bacteriostatic in nature. WT cells showed up to 4-fold increase in resistance against erythromycin in presence of 15 mM GSH. Δ*ygiBC-yjfMC* and Δ*acrAB-acrEF* strains showed 8-fold increase in resistance to erythromycin. In contrast, both Δ*tolC* and Δ*tolC-ygiBC-yjfMC* strains were equally susceptible to erythromycin in the presence or absence of GSH. Taken together these results suggest TolC assists in the GSH mediated protection of cells against antibiotics and that GSH protection mechanism is not only restricted to its anti-oxidant property indicating that other mechanisms could also be involved in this process.

III.2.7 Protection against antibiotics is specific to glutathione. We also investigated whether the same phenomenon of protection against antibiotics can be observed with spermidine. Therefore using the same strategy we measured MICs of erythromycin and novobiocin in the presence and absence of increasing concentrations of spermidine. Although novobiocin is bacteriostatic in nature, we chose it because like norfloxacin it inhibits DNA gyrase and thus inhibits DNA replication and cell division. MIC results show that unlike GSH, spermidine in concentrations up to 63.7 mM was well tolerated by Δ*tolC-ygiBC* strain (Table 8). No differences in MIC values of novobiocin were observed in the presence or absence of spermidine in both WT and Δ*tolC-ygiBC* strains. However, four-fold increase in MIC of erythromycin was observed for WT and Δ*tolC-ygiBC* strains in the presence of 63.7 mM spermidine. Although this effect was the same

as that observed for GSH mediated protection of erythromycin the effect was not as dramatic as seen for norfloxacin indicating that the protection against norfloxacin is specific to glutathione. Measurement of MIC of norfloxacin in the presence of spermidine should be done to confirm this result.

A. B.

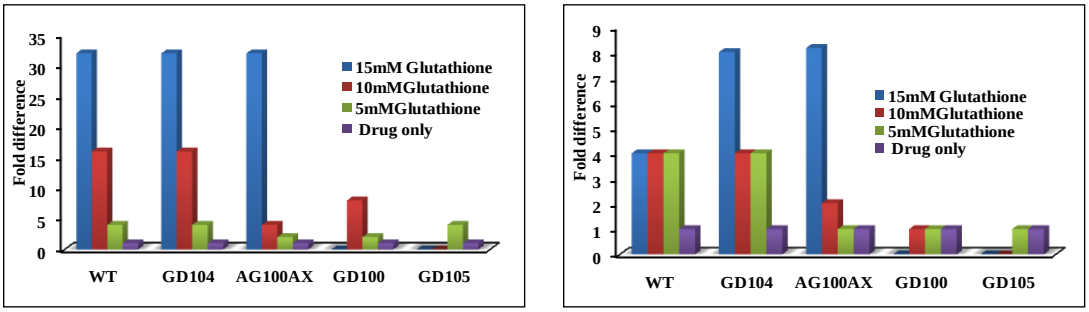

Figure III.16: TolC assists in GSH mediated protection against norfloxacin and erythromycin. A: Fold difference in MIC when cells are treated with norfloxacin. **B:** Fold difference in MIC when cells are treated with erythromycin.

Table 7. MICs of norfloxacin and erythromycin in the presence of glutathione

Strain	Genotype	Norfloxacin (µg/ml)				Erythromycin (µg/ml)			
		No GSH	5 mM	10 mM	15 mM	No GSH	5 mM	10 mM	15 mM
BW25113	WT	0.04	0.16	0.64	1.28	128	512	512	512
GD104	Δ*ygiBC* Δ*yjfMC*	0.04	0.16	0.64	1.28	64	256	256	512
AG100AX	Δ*acrAB* Δ*acrEF*	0.005	0.01	0.02	0.16	4	4	8	32
GD100	Δ*tolC*	0.01	0.02	0.08	-	4	4	4	-
GD105	Δ*tolC* Δ*ygiBC* Δ*yjfMC*	0.005	0.02	-	-	4	4	-	-

Table 8. Susceptibility of WT and Δ*tolC-ygiBC* strains to erythromycin (ERY) and spermidine (SPE).

Minimum inhibitory concentration (MIC)	WT	GD102
ERY	32	2
SPE	>9250	>9250
ERY + 63.7 mM SPE	128	8
Fold difference:(MIC (ERY+SPE)/MIC ERY only	4	4
NOV	64	ND
NOV + 63.7 mM SPE	64	ND
Fold difference for :(MIC (NOV+SPE)/MIC NOV only	1	ND

Minimum inhibitory concentration in µg/ml. ND-not detected, below limit.

III.3 Investigation of multifunctional interactions between TolC and transporters.

III.3.1 Co-purification studies did not identify stable interactions between TolC and other proteins. Our results show that TolC assists in GSH mediated protection against norfloxacin and erythromycin. In addition, we found that this protection is not dependent on AcrAB or AcrEF efflux pumps. Therefore, we hypothesized that other proteins participate with TolC in assisting in the GSH mediated protection against drugs. To identify these protein(s) interacting with TolC we constructed TolC cysteine mutants and expressed them from the chromosomal native promoter of *tolC*. The six histidine tag at the C terminus would aid in the easy one step purification of TolC. Cysteine replacements were created in positions Q352, D356, S363 and D374 (Figure III.17). All of the residues are located in the periplasmic coiled coil domain of TolC, a region previously mapped as the interface of interaction with membrane fusion protein AcrA. Residues Q352, D356, S363 are located on helix 7 whereas residue D374 is located on helix 8 at the periplasmic entrance of TolC. These cysteine residues would help us to study TolC-MFP/protein interaction by in vivo cross linking, thiol labeling to study accessibility etc.

A. **B.**

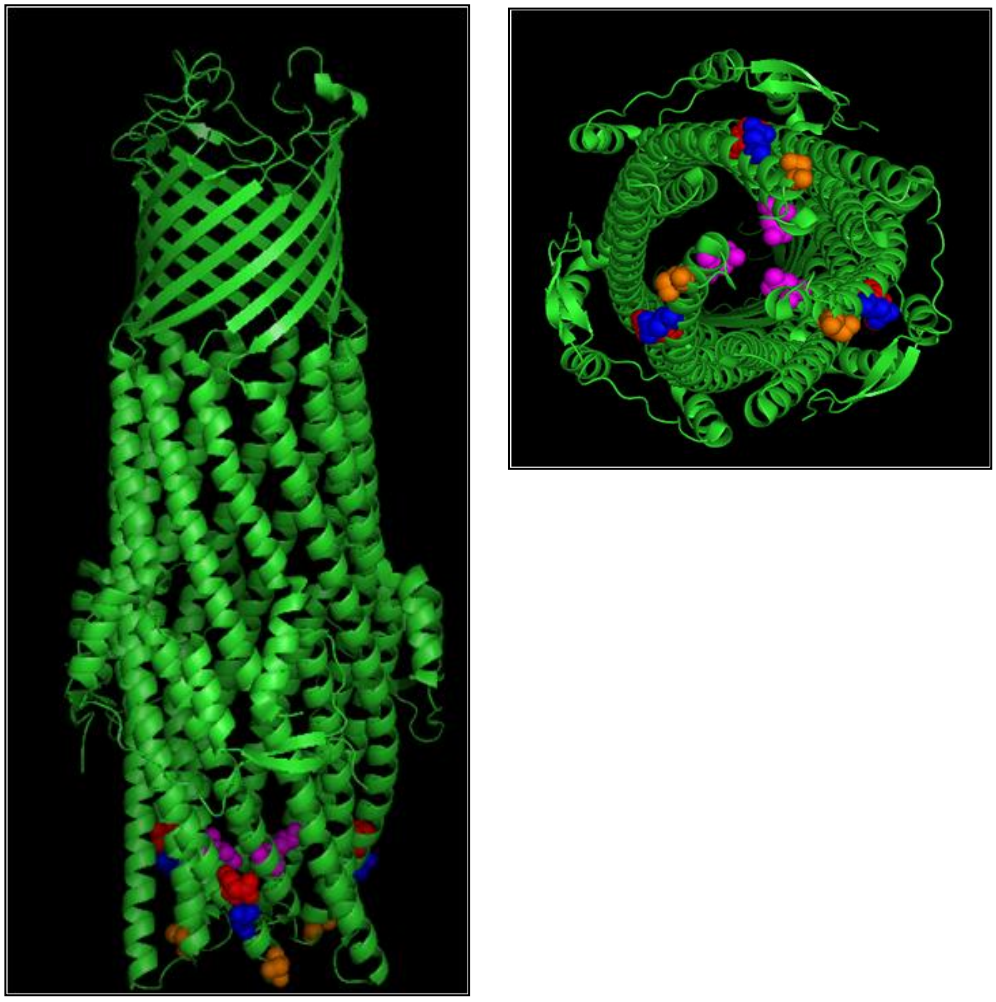

Figure III.17 Crystal structure of TolC with positions of cysteine substitutions shown as spheres. A. Side view of TolC and **B.** Periplasmic view of TolC with residues Q352-Red, D356-Blue, S363C-Pink and D374- Gold. Crystal structure from Koronakis *et al*., 2000.

To avoid non specific signals due to overexpression of TolC we created five strains in which TolC cysteine mutants with a C-terminal his tag and WT

cysteineless TolC^{his} were inserted at the TolC locus. These chromosomal insertion mutants were made using lambda red recombinase method (Datsenko & Wanner, 2000). All the cysteine mutants along with TolC^{his} were expressed from the *tolC* native promoter. Colonies obtained after transformation and selection on LB + novobiocin plates were confirmed with PCR reaction using forward primer TolCstart and reverse primer TolChis (Appendix A). Next, membrane fractions were isolated to check expression of the TolC mutants. The expression profile shows that chromosomally expressed TolC cysteine mutants and TolC^{his} are expressed to a level lower than WT but show similar oligomeric patterns as WT TolC (Figure III.18). To ensure that these chromosomally expressed proteins are functional we measured drug susceptibility and colicinV secretion by these strains. All mutants with the exception of TolCS363C strain showed similar level of resistance (Table 9) and colicin secretion (Table 10) as WT. Surprisingly, TolCS363C strain showed 4-fold increased resistance to novobiocin and lincomycin.

In order to determine if TolC forms a stable complex with any other protein(s), we purified TolCD356C protein using His-tag affinity chromatography. Due to chromosomal expression of TolC, we used sucrose density gradient centrifugation to separate both the inner membrane and outer membrane. Since TolC is an outer membrane protein, the outer membrane fraction was solubilized in detergent Triton X-100 and then loaded onto Cu^{2+} charged His binding resin. TolC was eluted with increasing concentrations of imidazole. All fractions were separated on a 12% SDS-PA gel and visualized using silver staining. Purified TolC is detected as a band with a molecular weight of 55 kDa in the 500 mM imidazole fraction (Figure III.19). WT

strain was also processed simultaneously as a control to identify proteins binding non-specifically to the column. However, when compared to WT purification profile no unique TolC-specific proteins could be identified in purified TolC fractions (Figure III.19).

Co-purification did not identify proteins that might interact with TolC, possibly because of transient nature of interaction between TolC and other proteins. Therefore, we next used cross-linking approach, previously reported by Lobedanz *et.al* (Lobedanz *et al.,* 2007) to stabilize TolC-transporter complexes. In this approach, we used succinimidyl 3-(2-pyridyldithio)-propionate (SPDP) cross linker. SPDP is a thiol amine crosslinker with a short spacer arm of 6.8 Å and would cross link the amine group of proteins with cysteine thiol group of TolCS363C. TolCS363C strain was incubated with SPDP and TolC-transporter complexes were affinity purified and analyzed on 12% SDS-PA gel. As a negative control, TolCS363C without cross linker was also processed in parallel (Figure III.20A).

500 mM imidazole fractions of both cross-linked and non-crosslinked samples show several proteins co-purified along with TolCS363C. However, comparing the purification profiles of TolCS363C samples treated with cross-linker and samples without a cross-linker, SDS-PA gel could not detect proteins specifically co-purified with TolCS363C mutant. To confirm that cross linking was successful these fractions were transferred onto PVDF membranes. The membranes were probed with anti-AcrA, anti-AcrB and anti-TolC antibodies. Immunoblotting analysis showed that AcrA but not AcrB was crosslinked to TolCS363C and co-purified along with it

(Figure III.20B). Immunoblotting analysis of non-crosslinked samples also shows small amount of AcrA suggesting that AcrA is directly interacting with TolC.

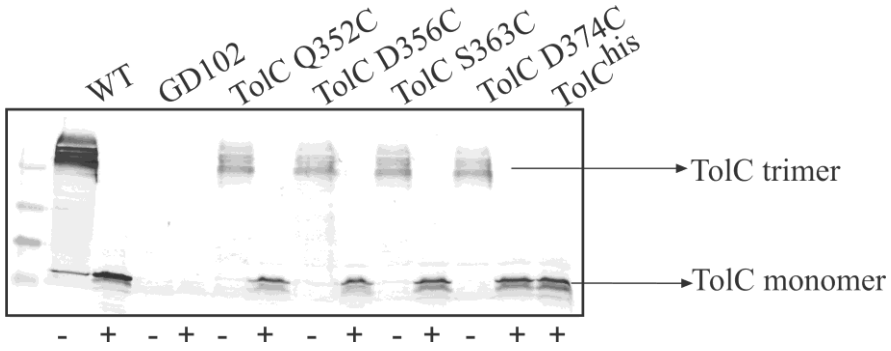

Figure III.18. Immunoblotting analysis of chromosomal TolC cysteine mutants. WT and Δ*tolC-ygiBC* strains were included as positive and negative controls respectively. 20 µg of total membrane proteins were separated on 12% SDS-PA gel. TolC is detected using polyclonal anti-TolC antibodies. + and – signs indicate boiled and un-boiled samples respectively.

Table 9. **MIC (µg/ml) of TolC cysteine mutants expressed from chromosome.**

Drug	**WT**	**GD100**	**TolC Q352C**	**TolC D365C**	**TolC S363C**	**TolC D374C**	**TolC^{his}**
Ery	32	1	32	32	32	32	32
Lin	312.5	39	312.5	312.5	1250	312.5	312.5
Nov	64	1	64	64	256	64	64
SDS	>10240	5	>10240	>10240	>10240	>10240	>10240

SDS: Sodium dodecyl sulfate, Nov: Novobiocin, Lin: Lincomycin, Ery: Erythromycin

Table 10. Colicin V secretion assay. Chromosomally expressed TolC cysteine mutant strains transformed with pHK11 plasmid.

Strain	**TolC Q352C**	**TolC D365C**	**TolC S363C**	**TolC D374C**	**TolC^{his}**	**GD100**
Diameter of halo (cm)	0.86	0.86	0.83	0.86	0.86	-

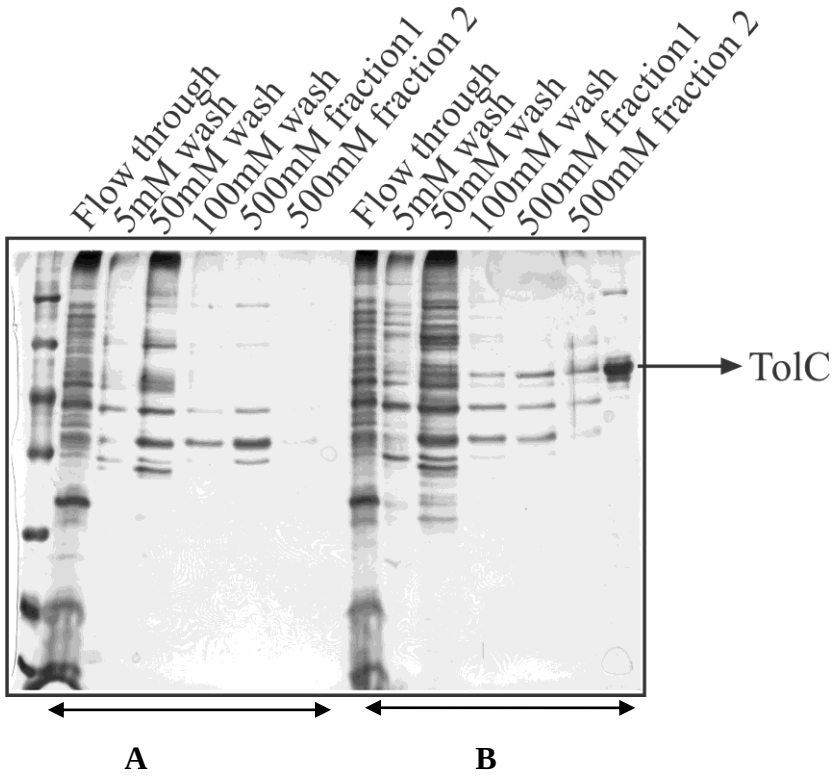

Figure III.19 Purification profiles of WT (A) and TolCD356C (B) strains. All fractions were boiled in SDS-loading buffer, separated by 12% SDS-PA gel and visualized by silver staining. Purified TolC loaded onto the last lane as a positive control.

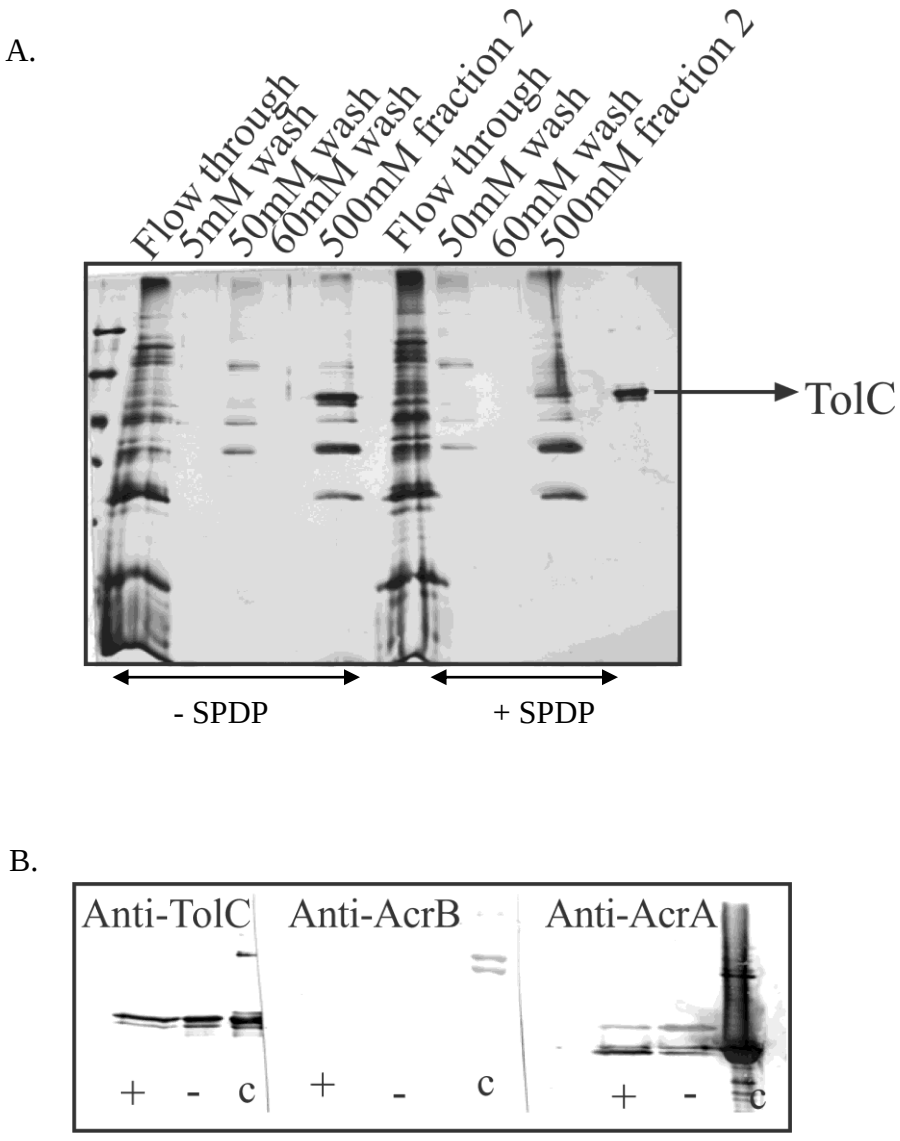

Figure III.20 Purification of TolC S363C after treatment with SPDP cross linker.

A. Purification profile of TolCS363C mutant in the presence (+SPDP) and absence (–SPDP) of cross linker. All fractions were resolved on 12% SDS-PA gel and proteins were visualized by silver staining. **B.** Western blotting analysis of 500 mM imidazole fractions. + SPDP, - SPDP, c- purified TolC, AcrB and AcrA included as positive controls for anti-TolC, anti-AcrB and anti-AcrA immunoblotting respectively.

III.3.2 Accessibility of TolC cysteine residues unaltered in the presence of additional transporters. In agreement with previous studies our cross linking results show that AcrA is in close association with TolCS363C. We hypothesized, that since this residue is involved in stable protein-protein interaction with AcrA it would not be accessible to a thiol reactive dye. To check the accessibility of this residue and other cysteine residues we used a thiol-reactive fluorophore, fluorescein 5 maleimide (F5M). The maleimide moiety of F5M reacts with thiol group of cysteine residue to form a stable thioether bond. Cells were incubated with 0.25 mM F5M for 30 min. The reaction was stopped with 1 mM DTT (see experimental procedures). Membrane fractions from each strain were isolated. WT and GD102 strains were included as positive and negative controls respectively. Membrane proteins were separated on a 12% SDS-PA gel. The gel was first scanned for fluorescence signal using Storm scanner and then stained with Coomassie Brilliant Blue to visualize proteins (Figure III. 21 top panel). To confirm equal levels of expression, immunoblotting using anti-TolC antibodies was also done with the same fractions (Figure III.21 bottom panel).

As expected, WT TolC and cysteineless TolC^{his} showed no fluorescence signal. TolC Q352C residue was also not labeled with F5M, indicating that either this residue is blocked by AcrA/ other protein(s) interacting with it or its physical orientation prevents its accessibility to F5M. Residue D374C at the periplasmic entrance did get labeled with F5M. Surprisingly, TolC S363C residue was also labeled with F5M indicating that this residue is not blocked by AcrA but freely available for labeling. This can be explained by two possibilities. First, TolC transiently interacts with chromosomally expressed AcrAB. If it transiently interacts with AcrAB at a give

time some molecules of TolC may be available for labeling whereas some TolC molecules may be blocked by the AcrAB proteins. Second, TolC may exist as a heterogeneous population, some TolC molecules are involved in stable association with AcrAB/ other proteins while the other molecules are freely available for labelling.

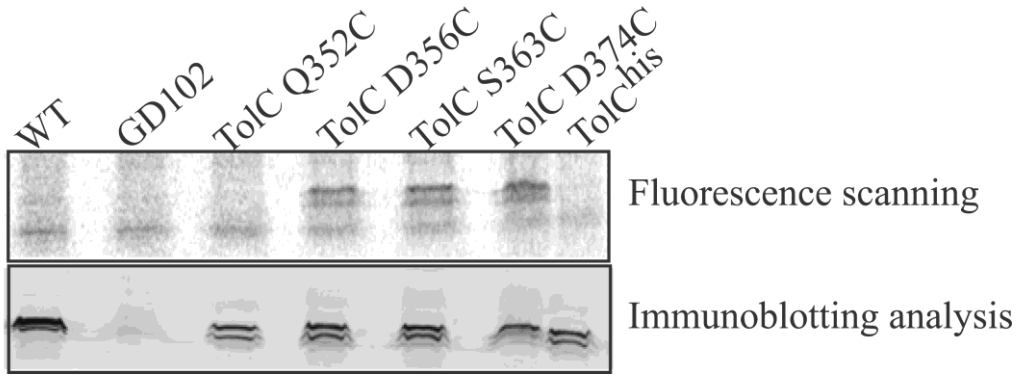

Figure III.21. In vivo labeling with F5M. Whole cells were labeled with F5M. Membrane fractions were isolated and 20 µg total membrane proteins were separated with 12% SDS-PA gel. The gel was first scanned for fluorescence and then the proteins were transferred onto PVDF membrane. The membrane was then probed with polyclonal anti-TolC antibody.

To test the above mentioned possibilities, TolC D356C, S363C and $TolC^{his}$ strains were transformed with plasmids expressing colicin V (pBR322 with *cvaABC* and *cvi* genes, pHK11) (Hwang *et al.*, 1997) and MacAB (pBAD with *macAB*, pBADMacAB (Tikhonova *et al.*, 2007). Colicin V is a 9 kDa antibacterial protein toxin and is active against many *E.coli* strains as well as other members of the

Enterobacteriaceae family. Colicin V is secreted by CvaABC type I system. In this complex, CvaB is an inner membrane ABC type transporter, with the ATP binding domain in the C-terminal cytoplasmic domain. CvaA belongs to the membrane fusion family of proteins and helps in the secretion of colicin V. It has been shown previously that CvaAB recruits TolC only in the presence of its substrate, colicinV (Hwang *et al.*, 1997). MacAB is an ABC type macrolide efflux transporter and confers resistance to macrolides composed of 14 and 15 membered lactones. It was shown recently that MacAB is also involved in the secretion of heat stable enterotoxin II in *E. coli* (Yamanaka *et al.*, 2008). Previous studies have shown that MacAB also requires TolC for its export function and that MacA can bind to TolC *in vivo*. We hypothesized that if indeed TolC exists as a heterogeneous population, then in the presence of an additional transporter the labeling of TolC cysteine residues will change.

For this purpose TolC D356C, S363C and D374C and $TolC^{his}$ transformed with either pHK11 plasmid or pBADMacAB plasmid were labeled with F5M. As controls the same strains without plasmids were also labeled with F5M. An aliquot of the cells was used to confirm active colicin V secretion (described in experimental procedures). MacAB expression was induced with 0.2% arabinose for 3 hr. Membrane fractions were isolated from all strains and the proteins were separated on 12% SDS-PA gel, scanned for fluorescence labeling and then stained with coomassie blue stain (Figure III.22). As expected cysteineless $TolC^{his}$ was not labeled with F5M, whereas D356C, S363C and D374C residues were accessible to F5M even in the presence of CvaAB. In case of MacAB, the signal resolution was poor due to over expression of MacAB proteins and no conclusion could be drawn from these

results. However, fluorescence scanning results show that cysteine accessibility pattern was unaltered even in the presence of CvaAB transporter. In this experiment we could not distinguish between the two explanations that TolC exists as a heterogeneous population or that AcrAB-TolC interactions are transient in nature. Also, from the results of these experiments we cannot rule out the possibility that different MFP-transporter complexes contact different surfaces on TolC and that residues D356C, S363C and D374C may not lie at interaction sites. Further experiments are needed to understand how TolC is engaged into complexes.

Next we constructed TolC cysteine mutants that lack AcrAB (Appendix A). These mutants will be used to check the cysteine accessibility pattern in the absence of AcrAB. AcrAB deletions in TolC cysteine strains were created using lambda red recombination. The deletion mutants were confirmed with PCR using primers specific to kanamycin gene and the region downstream of AcrB. Deletion of AcrA was also confirmed by western blotting analysis using anti-AcrA antibodies. These strains will be used to label TolC with F5M.

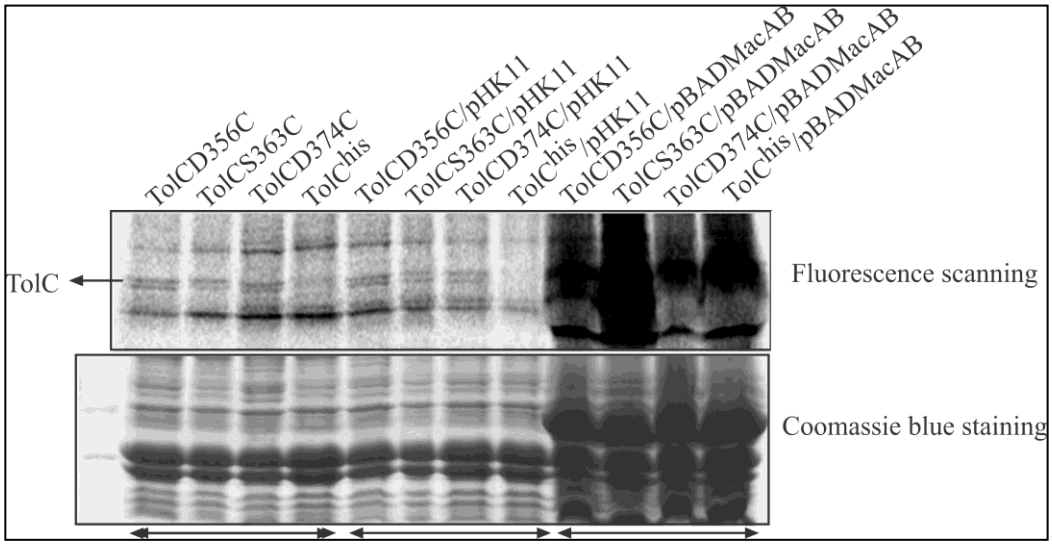

Figure III.22. Cysteine accessibility to F5M in the presence CvaAB and MacAB. Cells transformed with different plasmids were labeled with F5M in vivo. Membrane fractions were isolated and membrane proteins were separated with 12% SDS-PA gel. The gel was first scanned for fluorescence and then stained with coomassie blue stain.

III.3.3 Real time labeling of TolC cysteine residues. Previous studies with hemolysin transporter, HlyBD suggested that TolC may be recruited only in the presence of substrates (Koronakis *et al.,* 1995). Therefore we hypothesized that increasing concentrations of drug (substrate) would protect the cysteine residues from the thiol reactive probe and thus the rate of labeling of TolC cysteine residues would decrease proportionally. This competition between drug and probe would in turn help us determine the rate of efflux of substrates through the TolC channel. Rate of labeling of cysteine residues is a function of concentration of fluorophore, rate of entry of fluorophore into the cell and accessibility of the residue. With the concentration of the

fluorophore and rate of entry of fluorophore into the cell being constant for all strains, the rate of labeling will be solely determined by the position/accessibility of the cysteine residues. As all the cysteine residues are located in the periplasmic region of TolC, we were interested in determining the rate at which these residues get labeled and if the rate of labeling is altered in the presence of drugs.

For this purpose we used a thiol specific fluorescent dye, 7-diethylamino-3-(4'-maleimidylphenyl)-4-methylcoumarin (CPM). CPM is membrane permeable and like F5M, CPM is not fluorescent until after conjugation with a thiol group. This conjugate has an excitation and emission wavelength of 384 and 470 nm respectively. Two strains, WT cysteineless TolC as a negative control and TolCD374C strain were used to determine the optimum CPM concentration and specificity of labeling. In order to optimize CPM concentration for labeling we kept cell density constant at 0.2 OD_{600} and used five different concentrations of CPM (1-5 μM).

As expected TolCD374C showed higher rate of labeling than WT cysteineless TolC. Also, the rate of fluorescence increased with increasing concentrations of CPM and remained constant at concentrations of 2 μM and higher (Figure III.23A).

Next we wanted to check how the rate of labeling increases with increasing number of cells. For this purpose we used two concentrations of CPM, 1 μM and 5 μM and increased the number of cells from 0.05 OD_{600} to 0.6 $OD_{600.}$ As expected, the rate of fluorescence labeling increased proportionally with increasing number of cells (Figure III.23 B, C). Our results indicate that the rate of increase in fluorescence is specific to the rate of labeling of the TolC cysteine residue.

To check if different cysteine residues have different labeling rates, we used TolCQ352C, D356C, S363C, D374C and TolC^{his} strains. WT and GD102 were included as positive and negative controls respectively (Figure III.24). All strains showed similar rates of labeling except for TolCD374C strain (Table 11). TolCD374C strain showed slightly higher rate of labeling than WT or other TolC cysteine residues. This result indicates that residue 374C is more accessible to the fluorophore than other cysteine residues.

As this difference in labeling rates was small as compared to WT, we checked the labeling of TolCD374C and TolC^{his} expressed from plasmids. For this, we transformed GD102 (Δ*tolC-ygiBC*) strain with plasmids expressing TolCD374C (pTolCD374C) and cysteineless TolC^{his} (pTolC^{his}). Four strains, the chromosomally expressed TolCD374C and TolC^{his} and GD102/pTolCD374C and GD102/ pTolC^{his} were labeled with increasing concentrations of CPM. Both chromosomally expressed TolC^{his} and TolC^{his} expressed from plasmid showed similar rates of labeling. The rate of labeling increased proportionally between 1 μM and 5 μM CPM and then remained constant at higher concentrations of CPM (Figure III. 25A). Chromosomally expressed TolCD374C did show a slightly higher rate of labeling than TolC^{his}. Like TolC^{his} strain the rate of labeling of chromosomally expressed TolCD374C increased proportionally with increasing concentrations of CPM. As expected GD102/pTolCD374C strain showed the highest rate of labeling. Rate of labeling increased proportionally up to 10 μM CPM and then remained constant.

A.

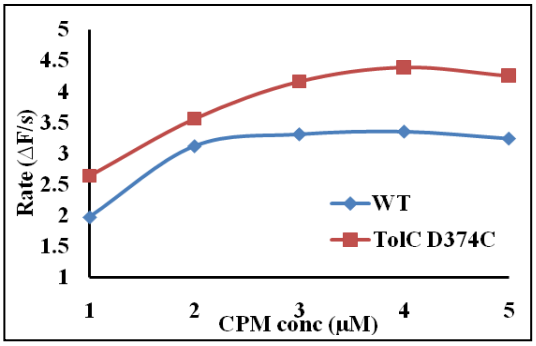

B.

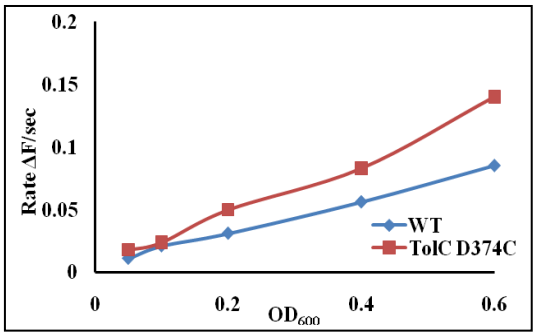

C.

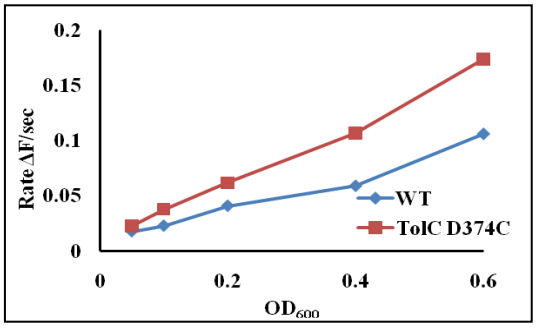

Figure III.23. In vivo labeling with fluorophore, CPM A. Rate of increase in labeling with increasing concentrations of CPM, cell density kept constant. B. Rate of labeling increases with increasing number of cells at CPM concentration constant at 1 μM and 5 μM (C)

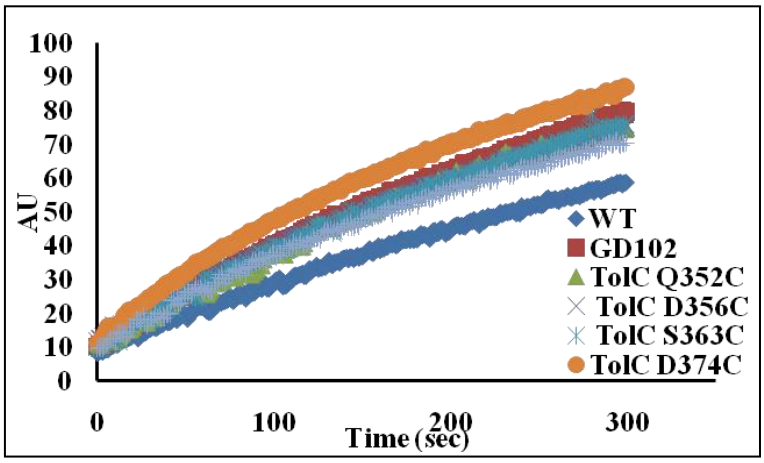

Figure III.24. Whole cell labeling with fluorophore, CPM. WT and GD102 strains were used as positive and negative controls. The rate of labeling is determined as the slope of the individual graphs.

Table 11. Rate of labeling of TolC cysteine mutants with CPM

Strain	Rate of labeling (ΔF/sec)
WT	0.19
GD102	0.28
TolC Q352C	0.26
TolC D365C	0.25
TolC S363C	0.27
TolC D374C	0.32
TolC^{his}	0.25

To check the effect of substrates on rate of labeling of TolC, we used GD102/pTolCD374C, GD102/pTolC^{his} strains. TolCD374C was chosen because it is located at periplasmic entrance aperture of TolC and is said to contact substrates. Puromycin was selected as substrate as puromycin's absorption spectrum does not interfere with the excitation and emission wavelengths of CPM and is an excellent substrate for the AcrAB-TolC multidrug efflux pump. The structure of puromycin is analogous to aminoacyl t-RNA. Puromycin binds to the ribosome releasing the nascent polypeptide chain and thus inhibits protein synthesis.

A.

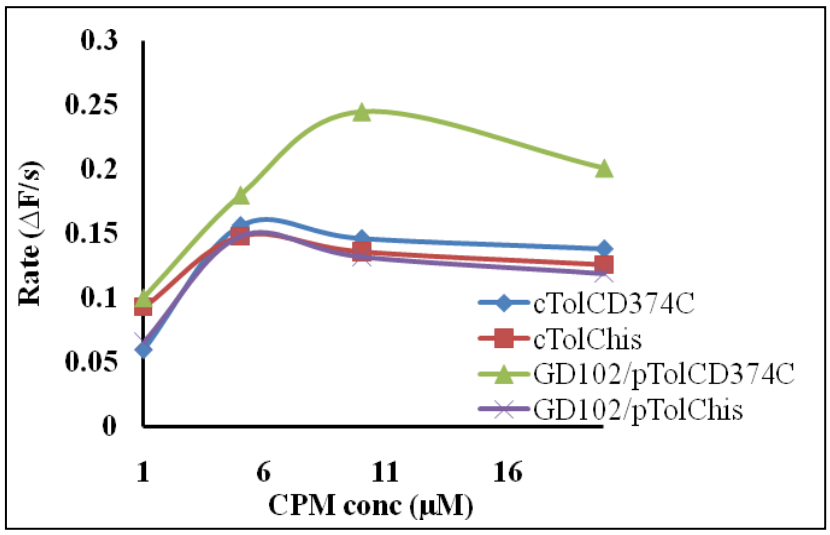

B.

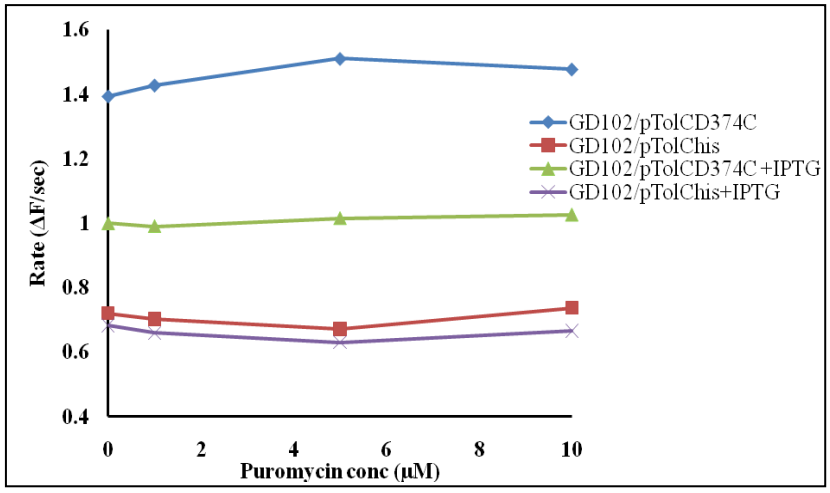

Figure III.25. Real time labeling of TolCD374C and TolC^{his} with CPM. A. Rate of labeling of TolCD374C and TolC^{his} expressed from plasmid. B. Rate of labeling of TolC D374C and TolC^{his} in the presence of increasing concentrations of puromycin.

GD102/pTolCD374C, GD102/pTolC^{his} strains were labeled in the presence of 5, 10, 15 and 20 μM puromycin (Fig III. 25B). Increasing concentrations of puromycin did not alter the rate of labeling of TolCD374C. To check if induction of expression of TolCD374C would have an effect on the labeling rate we induced pTolCD374C and pTolC^{his} with 0.1 mM IPTG at 0.3 OD_{600}. The cells were harvested at 0.6 OD_{600} and then labeled with CPM in the presence of increasing concentrations of puromycin. The rates of labeling were unaltered in the presence of increasing concentrations of puromycin. Induction of TolCD374C expression also did not affect the rate of labeling of pTolCD374C residue in the presence of increasing concentrations of puromycin. Unexpectedly in the presence of IPTG, pTolCD374 showed lower rate of labeling than in the absence of IPTG indicating that IPTG could inhibit the labeling reaction.

IV. Discussion

IV.1 ΔTolC strains are unable to efficiently metabolize glucose.

Through the course of these studies we found that ΔTolC strains have severe defects when growing in M9 medium. These growth defects manifest as reduced growth rates, extended lag phase and altered cell morphology (Figures III.8A and III.8B). Furthermore loss of YgiB, YgiC and their homologues further exacerbates this ΔTolC phenotype.

Growth defects in Δ*tolC*, Δ*tolC-ygiBC* and Δ*tolC*-Δ*ygiBC*-Δ*yjfMC* strains were only observed when these strains were grown in M9 medium with glucose as carbon source. In LB medium these strains showed the WT phenotype. LB medium is a rich source of vitamins, pyruvate and intermediates of amino acids and nucleotide biosynthetic pathways. Cells utilize these intermediates along with pyruvate to derive energy through gluconeogenesis (Isenberg & Newman, 1974). However, M9 medium is a chemically defined medium and cells must use M9 salts as a source of phosphates, ammonium, and sulfates. Glucose is supplied as carbon source and cells generate energy through glycolysis. The difference in growth phenotypes of these strains in LB and M9 medium strongly indicated that Δ*tolC* strains experience a metabolic deficiency. Indeed growth defects in Δ*tolC* strains can be completely compensated by the addition of amino acid L-serine to the growth medium (Figure III.6)

E.coli K12 strain cannot utilize L-serine as a carbon source but L-serine plays a central and important role in *E.coli* metabolism (Newman & Walker, 1982). L-

serine is required for the synthesis of phosphatidylserine, a minor phospholipid in the *E.coli* cytoplasmic membrane. However phosphatidylserine serves as the key intermediate for synthesis of phophatidylethanolamine the major lipid in the *E.coli* bilayer (Raetz, 1976) making it important for lipid biosynthesis. L-serine also serves as a precursor for the synthesis of L-glycine and L-cysteine. However neither glycine nor cysteine could restore the growth phenotype in Δ*tolC* strains indicating that growth defects observed were not due to deficiency of either of the amino acids. *E.coli* enzyme L-serine deaminase converts L-serine to pyruvate (Isenberg & Newman, 1974), an intermediate of the glycolysis/gluconeogenesis pathway. Therefore cells can utilize pyruvate and generate energy through glycolysis. In *E.coli*, L-alanine, L-cysteine and L-tryptophan are the only amino acids that can be converted to pyruvate (http://ecocyc.org) all other amino acids such as aspartate and glutamate are degraded to intermediates of the TCA cycle. Although we did see a small increase in the growth rates of Δ*tolC*-Δ*ygiBC*-Δ*yjfMC* strain in the presence of glutamate and aspartate the lag phase still persisted. Also, keeping the LB growth phenotypes in perspective, led us to the preliminary conclusion that the glycolysis pathway was inhibited in Δ*tolC* strains.

Phosphoenolpyruvate phosphotransferase system is the major pathway for transport of sugars in *E.coli*. Glucose, fructose, mannitol and sorbitol are PTS-dependent sugars whereas glycerol, xylose, maltose and lactose are non-PTS sugars (Meadow *et al.*, 1990). Therefore, *E.coli* encodes specific transporters for these non-PTS sugars. Results of our experiments with different carbon sources indicate that the metabolism of glucose is affected but not its transport in ΔTolC strains. Glucose is transported via the glucose-specific transporter of the phosphoenolpyruvate (PEP)-

dependent phosphotransferase system (PTS), PtsG and also has been demonstrated to be transported in a PTS dependent manner by mannose transporter ManZ (Meadow *et al.,* 1990 and García-Alles *et al.,* 2002). Glucose is immediately phosphorylated to yield glucose-6-phosphate, an intermediate of glycolysis. Similar to glucose, fructose is also transported by the PTS ManZ system and is phosphorylated to fructose-6-phosphate (Kornberg, 2001). However, fructose is also taken up by the fructose specific membrane spanning transporter FruA and is phosphorylated to fructose-1-phosphate. The fructose-1-phosphate formed is further phosphorylated by ATP and 1-phosphofructokinase (FruK) to fructose 1, 6-bis phosphate (Kornberg, 2001). As ΔTolC strains are able to utilize fructose, glycerol and xylose we believe that the bottleneck for the ΔTolC strains to utilize glucose is in the early stages of glycolysis. Our experiments indicate that the conversion of glucose-6-phosphate to fructose-6-phosphate and fructose-6-phosphate to fructose-1, 6-bis phosphate catalyzed by enzymes phosphoglucose isomerase and phosphofructokinase respectively may be affected.

Phosphoglucose isomerase encoded by the *pgi* gene participates in both glycolysis and gluconeogenesis. Previous studies have shown that *pgi* belongs to the SoxSR transcriptome (Pomposiello *et al.,* 2001 and Blanchard, 2007). Furthermore, Rungrassamee *et.al* show that both PtsG and Pgi are required for survival for *E.coli* during oxidative stress (Rungrassamee *et al.,* 2008) . Their data also shows that oxidative stress conditions induce the expression of both PtsG and Pgi. They further discuss that during oxidative stress Pgi redirects the carbon metabolism through the pentose phosphate pathway producing NADPH as reducing equivalents. The pentose phosphate pathway produces key intermediates like ribose-5-phosphate. Ribose-5-

phosphate is further converted to two molecules of fructose-6-phosphate and a molecule of glyceraldehyde-3-phosphate. The resulting fructose-6-phosphate and glyceraldehyde-3-phosphate can either be catabolized through glycolysis, or recycled via gluconeogenesis. Although not the most efficient pathway for producing energy but one molecule of glucose-6-phosphate through six cycles of pentose phosphate pathway and gluconeogenesis can produce 6 CO_2 and 12 NADPH (Rungrassamee *et al.,* 2008).

TolC like Pgi and PtsG belongs to the SoxS transcriptome and is required for survival *E.coli* under oxidative stress conditions (Rosner & Martin, 2009). Also, strong evidence suggests that normal glucose metabolism is affected when cells experience oxidative stress (Rungrassamee *et al.,* 2008). Taken together these findings and our results that ΔTolC strains are not able utilize glucose suggest that deletion of TolC induces oxidative stress like conditions in *E.coli* cells. This in turn leads to inefficient glucose metabolism as explained by slow growth rates and therefore does not affect their ability to survive.

IV.2 Inactivation of TolC leads to depletion of NAD^+.

To further investigate the reason for poor growth on glucose minimal medium we measured the NADH and NAD^+ concentrations in WT and Δ*tolC* strains. Significant differences were observed in NADH/NAD^+ ratios between WT and Δ*tolC* strains (Table 3a). In M9 medium stationary phase Δ*tolC* strain showed three-fold lower [NAD^+] than WT whereas Δ*tolC-ygiBC-yjfMC* strain had 14-fold lower concentration of NAD^+ leading to abnormal NADH/NAD^+ ratios.

NADH/NAD^+ ratios are tightly regulated in the cell as high NADH/NAD^+ ratios inhibit key enzymes of the TCA cycle such as citrate synthase and malate dehydrogenase (Prüss *et al.,* 1994). TCA cycle is a part of the metabolic pathway that is used to generate energy in the cell. In addition, TCA cycle also provides precursors for amino acid and nucleotide biosynthesis. High NADH/NAD^+ ratio has also been shown to inhibit pyruvate dehydrogenase complex of *E.coli* (Kim *et al.,* 2008). Pyruvate dehydrogenase complex connects glycolysis with TCA cycle and catalyses the conversion of pyruvate to acetyl CoA with the reduction of NAD^+ to NADH. Therefore abnormal NADH/NAD^+ ratios lead to inhibition of key metabolic enzymes which in turn leads to metabolic shut down.

Despite the dramatic drop in NAD^+ levels, NADH levels in Δ*tolC* strains still remained high (Table 3a). This indicates strongly that oxidation of NADH was inhibited. We found that rates of NADH oxidation in GD105 membranes decreased significantly upon entry into stationary phase and remained only at 50% level of the WT (Table 4). *E.coli* has two membrane bound NADH dehydrogenases, NDH-I and NDH-II (Pruss *et al*., 1994). NDH-I couples NADH oxidation to produce PMF. Previous studies showed that mutational inactivation of NDH-I leads to growth defects during transition into the stationary phase (Pruss *et al*., 1994). These growth defects could be suppressed by serine. Similarly presence of L-serine in M9 medium suppressed growth defects observed in Δ*tolC* cells. Taken together these findings suggest that TolC inactivation leads to inhibition of NDH-I, which in turn results in metabolic shutdown and dissipation of PMF.

NADH acts as an iron reductant in a Fenton reaction and drives DNA damage by iron and peroxide *in vivo* (Brumaghim *et al.*, 2003). Previous studies showed that raising the NADH level *in vivo* by eliminating or negatively regulating NADH dehydrogenase activity dramatically sensitizes *E. coli* to killing by peroxide (Imlay & Linn, 1988). Also, recently it was reported that cells lacking TolC overproduce SoxRS, Rob and MarA stress response factors (Rosner & Martin, 2009). SoxRS system is activated by exposure to superoxide and nitric oxide, MarA is activated by exposure to antibiotics and phenols and Rob, when cells are exposed to 2, 2-dipyridyl or bile salts (Rosner & Martin, 2009). Thus, high levels of NADH in GD105 cells could contribute significantly to oxidative stress in these cells. We suggest that inhibition of NDH-I and rising levels of NADH are the major reasons for the induction of SoxS, MarA and Rob stress responses in the cells lacking TolC. Therefore we believe that the poor growth of Δ*tolC* strains on M9 minimal medium is due to metabolic shut down and oxidative stress caused in the stationary phase.

IV.3 Inactivation of TolC leads to depletion of intracellular glutathione.

The growth defects in Δ*tolC* strains are exacerbated in the absence of YgiB, YgiC and their homologues, YjfMC. As YgiC and YjfC are predicted to be an enzyme glutathionylspermidine synthetase we further wanted to investigate if the defects in growth were due to lack of glutathionylspermidine. Therefore we measured the intracellular concentration of GSH in these strains. As Δ*tolC* strains had prolonged lag phase after inoculation into fresh medium, we collected samples during LB to M9 transition. Although we were not able to detect GSP even in WT cells our HPLC

analysis shows that in LB medium Δ*tolC* strains had WT levels of GSH. However, a significant drop in GSH level was seen after incubation for one hour in M9 medium. Levels of GSH further decreased as incubation time in M9 medium increased. The possible reasons for this dramatic drop in total GSH concentration could either be due to oxidation of GSH to GSSG by enzyme glutathione oxidoreductase or halt in GSH biosynthesis and degradation of GSH into its individual amino acids.

Glutathione reductase assay was used to measure the total intracellular glutathione (both oxidized and reduced) concentration. Consistent with results of HPLC experiments results of glutathione reductase assay confirmed that Δ*tolCygiBCyjfMC* strain had reduced levels of total glutathione when transferred to M9 medium. These results strongly indicate that the reduction in GSH levels was not due to oxidation of GSH to GSSG. The decrease in GSH levels in Δ*tolC* strains could be explained by halt in GSH biosynthesis and degradation of GSH into its individual amino acids. We believe that abnormal NADH/NAD^+ ratios in Δ*tolC* strains cause metabolic shut down in Δ*tolC* strains which results in halt in amino acid, nucleotide and GSH biosynthesis. A halt in amino acid biosynthesis requires degradation of the abundant intracellular GSH into γ-glutamyl and cysteinyl glycine residues. Previous studies have demonstrated that *E.coli* can use both these residues as an amino acid source (Suzuki *et al.,* 1993). GSH degradation is catalyzed by enzyme γ –glutamyltranspeptidase. Interestingly in *E.coli* this enzyme is localized in the periplasmic space (Suzuki *et al.,* 1993). Therefore for degradation of GSH, cytosolic GSH has to be transported to the periplasm and the degradation products need to be transported back into the cytoplasm. The transporters involved in this process remain unknown.

Glutathione reductase assay was also used to assay the GSH exported out from the cells. Surprisingly extracellular medium of M9 12 hour Δ*tolC* and Δ*tolCygiBCyjfMC* strains show ~8-fold and ~9-fold more GSH in extracellular medium than WT. From these results we can conclude that TolC is not required for export of GSH. We believe that the major reasons for depletion of GSH in Δ*tolC* strains could be halt in GSH biosynthesis, degradation of GSH and export of GSH. However the mechanism and reasons for trigger of GSH export in Δ*tolC* strains remains to be studied.

IV.4 Deletion of TolC induces stress on *E.coli* membranes.

Protein expression profiles of stationary phase ΔTolC cells show the presence of large amounts of protein PspA. PspA is a 25 kDa cytoplasmic protein, also found to be associated with the inner membrane. PspA is expressed in *pspABCDE* operon. In *E.coli*, *psp* operon is transcribed by σ^{54}-RNA polymerase and also requires activation by PspF (Hankamer *et al.,* 2004). PspF is a DNA binding transcriptional activator of the *psp* operon (Darwin, 2005) and is divergently transcribed from the *pspABCDE* operon. Brissette *et.al* in 1990 first reported that PspA was induced during filamentous phage infection (Brissette *et al.,* 1990). *psp* operon is also strongly induced by exposure to adverse conditions such as heat shock, osmotic shock, treatment with ethanol and proton ionophores such as carbonylcyanide-*m*-chlorophenylhydrazone (CCCP) (Weiner & Model, 1994). Mislocalization of membrane proteins and the inhibition of protein secretion by blockage of the Sec secretion machinery have also been shown to induce PspA expression (Darwin, 2005). Commonality of all of the above mentioned

conditions is that they lead to dissipation of the PMF (proton motive force). Kobayashi *et al.* demonstrated that PspA helps modulate this stress by binding to the inner membrane of *E.coli* and forming large oligomers which prevent proton leakage from damaged membranes (Kobayashi *et al.*, 2007). PspA is also known to bind to transcription factor PspF thereby negatively regulating its own expression. The model proposed for PspA induction is such that under normal conditions PspA binds to PspF and prevents activation of the *psp* operon. Under membrane stress proton motive dissipating conditions PspA binds to membrane and forms large oligomers thus freeing PspF. Free PspF in turn activates expression of the *psp* operon. Thus inner membrane localization and overproduction of PspA is a strong indication of membrane stress and proton motive force dissipating conditions.

Membrane fractions of stationary phase ΔTolC strains grown in M9 medium show the presence of PspA indicating that ΔTolC strains experience membrane stress in stationary phase. It has been demonstrated that the major stress experienced by cells during stationary phase is oxidative stress (Nystrom, 2004). Protein and lipid oxidation leads to production of reactive oxygen species (ROS) generated by the electron transport chain that can in turn damage DNA and membranes (Nystrom, 2004). As cells lacking TolC overproduce SoxRS, Rob and MarA stress response factors (Rosner & Martin, 2009) we believe that the TolC channel is required for the export of toxic metabolites, ROS generated due to oxidative stress in the stationary phase. In the absence of TolC these toxic metabolites accumulate in the periplasm, cause oxidation of membrane protein and lipids thus creating stress on the membrane. Our results of growth experiments with different carbon sources confirm this hypothesis. Although

glycerol, fructose and L-serine could complement the slow growth defects of ΔTolC strains, membrane fractions of ΔTolC strains grown in M9 medium either supplemented with glycerol or L-serine still showed the presence of PspA. These results strongly indicate that TolC is required to combat the oxidative stress experienced in the stationary phase.

Results of determination of colony forming units and LIVE/DEAD cell viability assay kit confirm that although Δ*tolC* strains experience membrane stress in stationary phase the viability of these cells is not affected. From this result we can conclude that the lag phase experienced by these strains is not due to lower number of viable cells in the stationary phase but due to the time required to replenish essential metabolites and repair membranes.

In summary, we propose the following model for the role of TolC and YgiBC in *E.coli* metabolism and physiology (Figure IV.1). Deletion of TolC inhibits NADH oxidases like Ndh-I. This in turn leads to increased concentrations of NADH and therefore an abnormal NADH/NAD^+ ratio which ultimately results in metabolic shutdown. Inhibition of NADH oxidases and accumulation of NADH induces the formation of reactive oxygen species (ROS) which in turn activates the expression of Mar, Sox, Rob regulon. Transcriptional activator SoxS induces the expression of phosphoglucose isomerase which redirects the carbon metabolism through the pentose phosphate pathway as evidenced by slow growth. Lastly, we believe that inhibition of NADH oxidases in ΔTolC strains probably occurs due to stress on *E.coli* membranes during stationary phase and that YgiBC and YjfMC proteins help in maintaining

membrane integrity. This stress on membranes is probably generated due to the accumulation of toxic metabolites as they are unable to exit the cells.

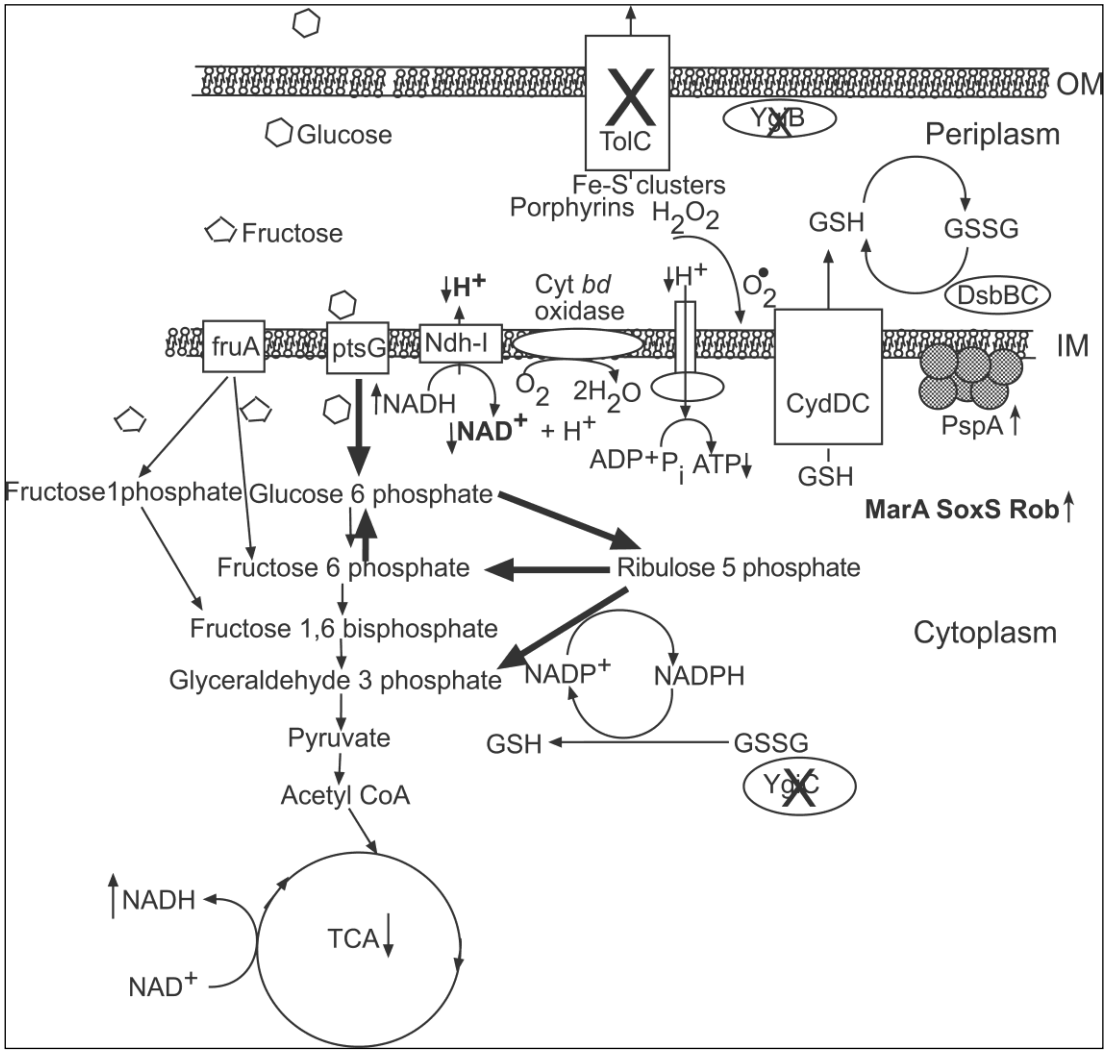

Figure IV.1 A model for the proposed role of TolC and YgiBC in *E.coli* physiology.

IV. 5 TolC mediated GSH protection against antibiotics.

As TolC is a key player in conferring antibiotic resistance we wanted to check if spermidine or glutathione affect drug susceptibilities in Δ*tolC* and Δ*ygiBC*-Δ*yjfMC* strains. Spermidine did not alter the drug susceptibility in WT and Δ*tolC-ygiBC* strains. Previous studies showed that GSH protects *E.coli* cells against harmful effects of norfloxacin (Goswami *et al.,* 2006). In accord with these results our results also show up to 32-fold increased resistance for norfloxacin. Norfloxacin is bactericidal drug and has been shown to generate free radicals thus causing oxidative stress inside cells (Kohanski *et al.,* 2007). Therefore, the proposed mechanism for this GSH mediated protection was that GSH acts as an anti-oxidant and scavenges the free radicals produced by norfloxacin. However our results as well as Goswami *et.al*'s results show up to 8-fold increase in resistance against erythromycin in the presence of 15 mM GSH in WT and Δ*ygiBC*-Δ*yjfMC* strains (Goswami *et al.,* 2007). Unlike norfloxacin, erythromycin is a bacteriostatic drug and does not induce free radical formation in *E.coli* cells (Kohanski *et al.,* 2007). The observation that GSH mediated protection against norfloxacin is 6-fold higher than that observed for erythromycin in WT cells, suggests that the GSH antioxidant property may in part protect cells against the effects of norfloxacin. However this protection mechanism is not restricted only to the antioxidant property of GSH.

Our results indicate that GSH mediated protection against antibiotics requires presence of functional TolC channel. In case of erythromycin, no protection by GSH was observed in the absence of TolC indicating importance of TolC in protection against erythromycin. However in case of norfloxacin, in the absence of TolC only up

to 4-8-fold protection was observed in presence of 10 mM GSH as compared to 16-32-fold in WT. As TolC is known to function with major efflux pumps such as AcrAB and AcrEF we next wanted to determine if AcrAB or AcrEF are involved in this GSH mediated protection against antibiotics. Like WT, Δ*acrAB-acrEF* strain also showed upto 32-fold protection against norfloxacin and 8-fold protection against erythroycin in presence of 15 mM GSH indicating that GSH mediated protection of antibiotics does not require functional AcrAB and AcrEF efflux pumps. Thus, in summary our results strongly indicate that mechanism of GSH mediated protection requires both a functional TolC channel as well as the anti-oxidant property of GSH. The exact mechanism of GSH mediated antibiotic protection is not known and requires further studies.

In eukaryotic cells glutathione conjugates of xenobiotics are exported out of the cell by specific transporters. This glutathione conjugation reaction is catalyzed by glutathione-S-transferases (Vuilleumier, 1997). *E.coli* does not possess such transferases; however the periplasmic enzyme glutathione transpeptidase has been shown to degrade GSH and transfer the γ-glutamyl group to amino acids and peptides (Suzuki *et al.*, 1993). Also, previous studies have demonstrated export of glutathione conjugates in *E.coli* cells (Kałuzna & Bartosz, 1997). Therefore we propose that γ-glutamyl or glutahtione conjugates of antibiotics are transported from the periplasm through the TolC channel in a manner independent of the AcrAB or AcrEF transporters.

IV.6 Dynamics of TolC-MFP interactions.

Functional TolC channel is required for GSH mediated protection against antibiotics. Therefore, we hypothesized that other proteins participate with TolC to aid in its function. For this purpose we constructed four TolC cysteine replacement mutants with cysteine replacements at residues Q352, D356, S363 and D374, as these residues have been demonstrated to lie at the TolC-AcrA interaction interface (Lobedanz *et al.*, 2007). Each of these mutant TolC proteins also had a six histidine tag at its C-terminal. A cysteineless TolC with six histidine tag at its C-terminal, $TolC^{his}$ was also constructed and served as a control. We were able to successfully express these proteins from the native TolC promoter from the *E.coli* chromosome. Functional analysis confirms that these mutants are functional.

Co-purification studies using TolCD356C mutant did not identify any specific proteins forming a stable complex with TolC indicating that TolC may form transient complexes with proteins interacting with it. To confirm this, we employed the cross-linking strategy used previously (Lobedanz *et al.*, 2007) and subject $TolCS363C^{his}$ strain to a thiol amine cross-linker, SPDP. In accord to previously published results we were able to detect AcrA in crosslinked samples as well as small amount of AcrA could also be detected in non-crosslinked samples indicating that AcrA is in close association with TolC. This difference in the amount of AcrA crosslinked and co-purified without a cross-linker suggests strongly that TolC-AcrA complexes are transient in nature. Indeed we observed that although AcrA is in close association with TolC all the cysteine residues except for residue 352C were accessible to F5M confirming the transient nature of interaction.

The results of these in vivo experiments are in agreement with the recently published in vitro experiments characterizing the MFP-TolC interactions (Tikhonova *et al.,* 2009). Tikhonova *et al.*'s results demonstrate that TolC-MFP interactions are highly dynamic in nature and the lifetime of these complexes range from seconds to minutes. Their data also shows that different MFP's bind to TolC with different affinities. Of the tested MFP's MacA of the MacAB macrolide efflux system has been shown to have maximum affinity followed EmrA and then AcrA.

Although our in vivo results correlate with the recently published in vitro results we cannot refute the possibility that TolC can exist as a heterogeneous population. We used two approaches to test this possibility. First, we systematically deleted AcrAB from chromosome of TolC cysteine mutant expressing *E.coli* strains. F5M labeling of these strains will give us a better understanding about the dynamics of TolC-MFP interactions. Second, we transformed these TolC cysteine expressing *E.coli* strains with plasmid expressing colicinV and its transporter, CvaAB. However as the F5M labeling pattern was unaffected in the presence of an additional transporter we were not able to distinguish between the two possibilities. Further experiments are required to understand how TolC is engaged into complexes.

Previous studies with HlyBD and CvaAB transporters have demonstrated that TolC is recruited by these transporters only in the presence of substrates therefore we hypothesized that increasing concentrations of drugs would protect the cysteine residues and the hence decrease the rate of labeling of these residues with a fluorophore. In the absence of drugs, in vivo real time CPM labeling studies showed that all the TolC

cysteine mutant strains had similar rates of labeling except for TolCD374C strain. TolC D374C strain showed approximately two-fold increase in the rate of labeling. This increase in rate of labeling can be attributed to the position of the residue. Residues D371 and D374 are shown to line the periplasmic constriction of the TolC channel (Andersen *et al.*, 2002). Andersen *et al.* show that mutation of D371 and D374 residues to alanine residues slightly enlarges the TolC channel. Therefore we believe that mutation of D374 residue to cysteine residue can moderately enlarge the TolC constriction which results in a leaky TolC channel thereby increasing the rate of labeling of the cysteine residue.

We attempted to determine rate of efflux of substrate through the TolC channel. For this we used TolCD374C and $TolC^{his}$ strains to detect competition between fluorophore and puromycin. We expected to see a decrease in labeling rate of the cysteine residue in the presence of increasing concentrations of drug, puromycin. However in our experiments increasing concentration of puromycin did not affect the rate of labeling of TolC D374C residue. Several reasons can account for this observation. First, as the life time of AcrA-TolC complexes is only a few seconds the drug efflux step probably takes place within seconds. Such a fast reaction would be difficult to monitor with this system. Some other technique such as stop-flow can be used to monitor the efflux of drug. Second, the ratio between fluorophore and drug may not have been optimal. Therefore further optimization with different concentrations of fluorophore and different drug needs to done. Although we were not able to determine the rate of efflux of drugs, these chromosomal TolC cysteine mutant strains provide a tool for studying TolC-protein/MFP interactions in the future.

References

Amabile-Cuevas, C. F., & Demple, B. (1991). Molecular characterization of the soxRS genes of *Escherichia coli*: two genes control a superoxide stress regulon. *Nucleic Acids Res. , 19*, 4479-4484.

Andersen, C., Koronakis, E., Hughes, C., & Koronakis, V. (2002). An aspartate ring at the TolC tunnel entrance determines ion selectivity and presents a target for blocking by large cations. *Molecular Microbiology , 44* (5), 1131–1139.

Andersen, C., Koronakis, E., Bokma, E., Eswaran, J., Humphreys, D., Hughes, C., Koronakis V. (2002). Transition to the open state of the TolC periplasmic tunnel entrance. *PNAS , 99* (17), 11103-11108.

Anderson, M. (1985). Determination of glutathione and glutathione disulfide in biological samples. *Methods in enzymology , 113*, 548-555.

Aono, R., Tsukagoshi, N., & Yamamoto, M. (1998). Involvement of outer membrane protein TolC, a possible member of the mar-sox regulon, in maintenance and improvement of organic solvent tolerance of *Escherichia coli* K-12. *J Bacteriol , 180* (4), 938-44.

Arnold, K., Bordoli, L., Kopp, J., & Schwede, T. (2006). The SWISS-MODEL Workspace: A web-based environment for protein structure homology modelling. . *Bioinformatics , 22*, 195-20.

Aslund F, Z. M. (1999). Regulation of the OxyR transcription factor by hydrogen peroxide and the cellular thiol-disulfide status. *Proc Natl Acad Sci U S A. , 96*, 6161-6165.

Augustus, A. M., Celaya, T., Husain, F., Humbard, M., & Misra, R. (2004). Antibiotic-Sensitive TolC Mutants and Their Suppressors. *Journal of Bacteriology , 186* (6), 1851–1860.

Baba, T., Ara, T., Hasegawa, M., Takai, Y., Okumura, Y., Baba, M., Datsenko K, Tomita M, Wanner B, Mori H. (2006). Construction of *Escherichia coli* K-12 in-frame, single-gene knockout mutants: the Keio collection. *Mol Syst Biol. ,* 1-11.

Balakrishnan, L., Hughes, C., & Koronakis, V. (2001). Substrate-triggered Recruitment of the TolC Channel-tunnel *Escherichia coli*. *J. Mol. Biol. , 313,* 501-510.

Blanchard JL, W. W. (2007). Rapid changes in gene expression dynamics in response to superoxide reveal SoxRS-dependent and independent transcriptional networks. *PLoS One , 2*, e1186.

Bleuel, C., Große, C., Taudte, N., Scherer, J., Wesenberg, D., Krauß, G. J., Nies DH, Grass G. (2005). TolC Is Involved in Enterobactin Efflux across the Outer Membrane of *Escherichia coli*. *Journal of Bacteriology , 187* (19), 6701–6707.

Bollinger JM Jr, Kwon DS, Huisman GW, Kolter R, Walsh CT. (1995). Glutathionylspermidine metabolism in *Escherichia coli*. Purification, cloning, overproduction, and characterization of a bifunctional glutathionylspermidine synthetase/amidase. *J Biol Chem. , 270* (23), 14031-41.

Boulos, L., Prévost, M., Barbeau, B., Coallier, J., & Desjardins, R. (1999). LIVE/DEAD® BacLight(TM): application of a new rapid staining method for direct enumeration of viable and total bacteria in drinking water. . *Journal of Microbiological Methods , 37*, 77-86.

Bowman, W. H., Tabor, C. W., & Tabor, H. (1973). Spermidine Biosynthesis. *Journal of Biological Chemistry , 248* (7), 2480-2485.

Brissette, J., Russel, M., Weiner, L., & Model, P. (1990). Phage shock protein, a stress protein of *Escherichia coli*. *Proc Natl Acad Sci USA , 87*, 862-866.

Brumaghim, J., Li, Y., Henle, E., & Linn, S. (2003). Effects of hydrogen peroxide upon nicotinamide nucleotide metabolism in *Escherichia coli*: changes in enzyme levels and nicotinamide nucleotide pools and studies of the oxidation of NAD(P)H by Fe(III). *J Biol Chem. , 278* (43), 42495-504.

Carmel-Harel, O., & Storz, G. (2000). Roles of the glutathione- and thioredoxin-dependent reduction systems in the *Escherichia coli* and saccharomyces cerevisiae responses to oxidative stress. *Annu Rev Microbiol. , 54*, 439-61.

Chattopadhyay, M. K., Tabor, C. W., & Tabor, H. (2009). Polyamines Are Not Required for Aerobic Growth of *Escherichia coli*:Preparation of a Strain with Deletions in All of the Genes for Polyamine Biosynthesis. *Journal of Bacteriology , 191* (17), 5549–5552.

Chesney, J., Eaton, J., & Mahoney, J. J. (1996). Bacterial Glutathione: a Sacrificial Defense against Chlorine Compounds. *Journal of Bacteriology , 178* (7), 2131–2135.

Darwin, A. (2005). The phage-shock-protein response. *Mol.Microbiology , 57* (3), 621–628.

Dastidar, V., Mao, W., Lomovskaya, O., & Zgurskaya, H. I. (2007). Drug-induced conformational changes in multidrug efflux transporter AcrB from Haemophilus influenzae. *J Bacteriol. , 189* (15), 5550-8.

Datsenko, K. A., & Wanner, B. L. (2000). One step inactivation of chromosomal genes in *Escherichia coli* K-12 using PCR products. *Proc Natl Acad Sci USA , 97*, 6640-6645.

Dubin, D. T. (1959). Evidence for conjugates between polyamines and glutathione in E. coli. *Biochem. Biophys. Res. Comm. , 1* (5), 262-265.

Fahey, R. C., & Newton, G. L (1987). Determination of Low-Molecular-Weight Thiols Using Monobromobimane Fluorescent Labeling and High-Performance Liquid Chromatography. *Methods In Enzymology , 143*, 85-96.

Fairlamb, A. H., Blackburn, P., Ulrich, P., Chait, B., & Cerami, A. (1985). Trypanothione: A Novel Bis(Glutathionyl)Spermidine Cofactor for Glutathione Reductase in Trypanosomatids. *Science , 227* (4693), 1485-1487.

Fairlamb, A. H., Henderson, G. B., & Cerami, A. (1986). The biosynthesis of trypanothione and N1-glutathionylspermidine in Crithidia fasciculata. *Mol Biochem Parasitol , 21*, 247-257.

Filip, C., Fletcher, G., Wulff, J., & Earhart, C. (1973). Solubilization of the cytoplasmic membrane of *Escherichia coli* by the ionic detergent sodium-lauryl sarcosinate. *J Bacteriol. , 115* (3), 717-22.

García-Alles, L., Zahn, A., & Erni, B. (2002). Sugar recognition by the glucose and mannose permeases of *Escherichia coli*. Steady-state kinetics and inhibition studies. *Biochemistry. , 41* (31), 10077-86.

German, G. J., & Misra, R. (2001). The TolC protein of *Escherichia coli* serves as a cell-surface receptor for the newly characterized TLS bacteriophage. *J.Mol Biol , 308* (4), 579-85.

Gilson, L., Mahanty, H., & Kolter, R. (1990). Genetic analysis of an MDR-like export system: the secretion of colicin V. . *Embo J , 9*, 3875-3884.

Goswami, M., Mangoli, S. H., & Jawali, N. (2007). Effects of Glutathione and Ascorbic Acid on Streptomycin Sensitivity of *Escherichia coli*. *Antimicrob Agents Chemother , 51* (3), 1119–1122.

Goswami, M., Mangoli, S. H., & Jawali, N. (2006). Involvement of reactive oxygen species in the action of ciprofloxacin against *Escherichia coli*. *Antimicrob Agents Chemother , 50*, 949-954.

Hankamer, B., Elderkin, S., Buck, M., & Nield, J. (2004). Organization of the AAA Adaptor Protein PspA Is an Oligomeric Ring. *The Journal of Biological Chemistry , 279* (10), 8862–8866.

Hayashi, S., & Wu, H. (1990). Lipoproteins in Bacteria. *Journal of Bioenergetics and Biomembranes , 22* (3), 451-471.

Helbig, K., Bleuel, C., Krauss, G. J., & Nies, D. H. (2008). Glutathione and transition-metal homeostasis in *Escherichia coli*. *J Bacteriol. , 190* (15), 5431-8.

Hiraga, S., Hironori, N., Ogura, T., Ichinose, C., Mori, H., Ezaki, B., Jaffé A. (1989). Chromosome Partitioning in *Escherichia coli*: Novel Mutants Producing Anucleate Cells. *Journal of Bacteriology , 171* (3), 1496-1505.

Hwang, J., Zhong, X., & Tai, P. (1997). Interactions of dedicated export membrane proteins of the colicin V secretion system: CvaA, a member of the membrane fusion protein family, interacts with CvaB and TolC. *J Bacteriol. , 179* (20), 6264-70.

Igarashi, K., & Kashiwagi, K. (2006). Polyamine Modulon in *Escherichia coli*: Genes Involved in the Stimulation of Cell Growth by Polyamines. *J. Biochem. , 139*, 11–16.

Igarashi, K., & Kashiwagi, K. (1999). Polyamine transport in bacteria and yeast. *Biochem. J. , 344*, 633±642.

Igarashi, K., & Kashiwagi, K. (2000). Polyamines: Mysterious Modulators of Cellular Functions. *Biochemical and Biophysical Research Communications , 271*, 559–564.

Imlay, J. A., & Linn, S. (1987). Mutagenesis and Stress Responses Induced in *Escherichia coli* by Hydrogen Peroxide. *Journal of Bacteriology , 169* (7), 2967-2976.

Ip, H., Stratton, K., Zgurskaya, H., & Liu, J. (2003.). pH-induced conformational changes of AcrA, the membrane fusion protein of *Escherichia coli* multidrug efflux system. *J Biol Chem , 278*, 50474-82.

Isenberg, S., & Newman, E. (1974). Studies on L-Serine Deaminase in *Escherichia coli* K-12. *Journal of Bacteriology , 118* (1), 53-58.

Kałuzna, A., & Bartosz, G. (1997). Transport of glutathione S-conjugates in *Escherichia coli*. *Biochem Mol Biol Int. , 43* (1), 161-71.

Kato, A., Tanabe, H., & Utsumi, R. (1999). Molecular characterization of the PhoP-PhoQ two-component system in *Escherichia coli* K-12: identification of extracellular Mg2+-responsive promoters. *J Bacteriol. , 181* (17), 5516-20.

Kelley, L. A., & Sternberg, M. (2009). Protein structure prediction on the web: a case study using the Phyre server. *Nature Protocols. , 4*, 363 - 371.

Kiefer, F., Arnold, K., Künzli, M., Bordoli, L., & Schwede, T. (2009). The SWISS-MODEL Repository and associated resources. *Nucleic Acids Research. , 37*, D387-D392.

Kim, Y., Ingram, L. O., & Shanmugam, K. T. (2008). Dihydrolipoamide Dehydrogenase Mutation Alters the NADH Sensitivity of Pyruvate Dehydrogenase Complex of *Escherichia coli* K-12. *J Bacteriol. , 190* (11), 3851–3858.

Kobayashi, N., Nishino, K., & Yamaguchi, A. (2001). Novel macrolide-specific ABC-type efflux transporter in *Escherichia coli*. *Journal of Bacteriology , 183* (19), 5639-44.

Kobayashi, R., Suzuki, T., & Yoshida, M. (2007). *Escherichia coli* phage shock protein A (PspA) binds to membrane phospholipids and repairs proton leakage of the damaged membranes. *Mol. Microbiol , 66*, 100-109.

Kohanski, M. A., Dwyer, D. J., Hayete, B., Lawrence, C. A., & Collins, J. J. (2007). A common mechanism of cellular death induced by bactericidal antibiotics. *Cell , 130* (5), 797-810.

Kornberg, H. L. (2001). Routes for Fructose Utilization by *Escherichia coli*. *J. Mol. Microbiol. Biotechnol. , 3* (3), 355-359.

Koronakis, E., Hughes, C., Milisav, I., & Koronakis, V. (1995). Protein exporter function and in vitro ATPase activity are correlated in ABC domain mutants of HlyB. *Mol. Microbiol. , 16*, 87–96.

Koronakis, V., Eswaran, J., & Hughes, C. (2004). Structure and function of TolC: the bacterial exit duct for proteins and drugs. *Annu Rev Biochem. , 73*, 467-89.

Koronakis, V., Sharff, A., Koronakis, E., Luisi, B., & Hughes, C. (2000). Crystal structure of the bacterial membrane protein TolC central to multidrug efflux and protein export. *Nature , 405* (6789), 914-9.

Kwon, D., Lin, C.-H., Chen, S., Coward, J., Walsh, C., & Bollinger, J. M. (1997). Dissection of Glutathionylspermidine Synthetase/Amidase from *Escherichia coli* into Autonomously Folding and Functional Synthetase and Amidase Domains. *272* (4), 2429–2436.

Lazdunski, C. J., Bouveret, E., Rigal, A., Journet, L., Lloubès, R., & Bénédetti, H. (1998). Colicin Import into *Escherichia coli* Cells. *Journal of Bacteriology , 180* (19), 4993-5002.

Leonardo, M. R., Dailly, Y., & Clark, D. P. (1996). Role of NAD in regulating the adhE gene of *Escherichia coli*. *J Bacteriol. , 178* (20), 6013-8.

Lin, C.-H., Kwon, D. S., Bollinger, M., & Walsh, C. T. (1997). Evidence for a Glutathionyl-Enzyme Intermediate in the Amidase Activity of the Bifunctional Glutathionylspermidine Synthetase/Amidase from *Escherichia coli*. *Biochemistry , 36* (48), 14930-14938.

Lin, E. (1976). Glycerol Dissimilation and its Regulation in Bacteria. *Annual Review of Microbiology , 30*, 535-578.

Lobedanz, S., Bokma, E., Symmons, M. F., Koronakis, E., Hughes, C., & Koronakis, V. (2007). A periplasmic coiled-coil interface underlying TolC recruitment and the assembly of bacterial drug efflux pumps. *Proc Natl Acad Sci U S A. , 1044* (11), 612-7.

Ma, D., Cook, D., Alberti, M., Pon, N., Nikaido, H., & Hearst, J. (1995). Genes acrA and acrB encode a stress-induced efflux system of *Escherichia coli*. *Mol Microbiol. , 16* (1), 45-55.

Martin, R., & Rosner, J. (2003). Analysis of microarray data for the marA, soxS, and rob regulons of *Escherichia coli*. *Methods Enzymol , 370*, 278-280.

Martin, R., Gillette, W., Rhee, S., & Rosner, J. (1999). Structural requirements for marbox function in transcriptional activation of mar/sox/rob regulon promoters in *Escherichia coli*: sequence, orientation and spatial relationship to the core promoter. *Mol Microbiol , 34,* 431–441.

Masip, L., Veeravalli, K., & Georgiou, G. (2006). The Many Faces of Glutathione in Bacteria. *Antioxidants & Redox Signaling , 8* (5, 6).

Matsumura, H., & Miyachi, S. (1980). Cycling assay for nicotinamide adenine dinucleotides. *Meth. Enzymol. , 69,* 465-470.

Meadow, N. D., Fox, D. K., & Roseman, S. (1990). The Bacterial Phosphoenolpyruvate:Glycose Phosphotransferase System. *Annu. Rev. Biochem , 59,* 497-542.

Newman, E., & Walker, C. (1982). L-Serine Degradation in *Escherichia coli* K-12: a Combination of L-Serine, Glycine, and Leucine Used as a Source of Carbon. *Journal of Bacteriology , 151* (2), 777-782.

Nikaido, H. (1998). Antibiotic resistance caused by gram-negative multidrug efflux pumps. *Clin Infect Dis: , 27* (1), S32-41.

Nikaido, H., & Takatsuka, Y. (2009). Mechanisms of RND multidrug efflux pumps. *Biochimica et Biophysica Acta , 1794* (5), 769–781.

Nishino, K., & Yamaguchi, A. (2001). Overexpression of the response regulator evgA of the two-component signal transduction system modulates multidrug resistance conferred by multidrug resistance transporters. *J Bacteriol. , 183* (4), 1455-8.

Nystrom, T. (2004). Stationary-Phase Physiology. *Annu.Rev.Microbiol , 58*, 161–81.

Okusu, H., MA, ,. D., & Nikaido, H. (1996). AcrAB Efflux Pump Plays a Major Role in the Antibiotic Resistance Phenotype of *Escherichia coli* Multiple-Antibiotic-Resistance (Mar) Mutants. *Journal of Bacteriology , 178* (1), 306–308.

Osborn, M. J., Gander, J. E., Parisi, E., & Carson, J. (1972). Mechinism of assembly of the outer membrane of Salmonella typhimurium. Isolation and characterization of cytoplasmic and outer membrane. *J.Biol.Chem , 247* (12), 3962-72.

Pai, C.-H., Chiang, B.-Y., Ko, T. P., Chou, C.-C., Chong, C.-M., Yen, F.-J., Chen S, Coward JK, Wang AH, Lin CH. (2006). Dual binding sites for translocation catalysis by *Escherichia coli* glutathionylspermidine synthetase. *The EMBO journal , 25*, 5970–5982.

Peitsch, M. C. (1995). Protein modeling by E-mail . *Bio/Technology , 13*, 658-660.

Pomposiello, P., Bennik, M., & Demple, B. (2001). Genome-wide transcriptional profling of the *Escherichia coli* responses to superoxide stress and sodium salicylate. *Jornal of Bacteriology , 183*, 3890-3902.

Prüss, B. M., Nelms, J. M., Park, C., & Wolfe, A. J. (1994). Mutations in NADH:ubiquinone oxidoreductase of *Escherichia coli* affect growth on mixed amino acids. *J Bacteriol. , 176* (8), 2143-50.

Raetz, C. (1976). Phosphatidylserine Synthetase Mutants of *Escherichia coli*. *Journal of Biological Chemistry , 251* (11), 3242-3249.

Rosner, J. L., & Martin, R. G. (2009). An excretory function for the *Escherichia coli* outermembrane pore TolC: upregulation of marA and soxS transcription and Rob activity due to metabolites accumulated in tolC mutants. *J Bacteriol , 191* , 5283-5292.

Rungrassamee, W., Liu, X., & Pomposiello, P. J. (2008). Activation of glucose transport under oxidative stress in *Escherichia coli*. *Archives in Microbiology , 190* (1), 41–49.

Sauer, U., Hatzimanikatis, V., Hohmann, H.-P., Manneberg, M., van Loon, A. P., & Bailey, J. E. (1996). Physiology and Metabolic Fluxes of Wild-Type and Riboflavin-Producing Bacillus subtilis. *Applied And Environmental Microbiology , 62* (10), 3687–3696.

Seeger, M., Schiefner, A., Eicher, T., Verrey, F., Diederichs, K., & KM, P. (2006). Structural asymmetry of AcrB trimer suggests a peristaltic pump mechanism. *Science. , 313* (5791), 1295-8.

Song, S., & Park, C. (1998). Utilization of D-ribose through D-xylose transporter. *FEMS Microbiol Lett. , 163* (2), 255-61.

Stanley, P., Koronakis, V., & Hughes, C. (1998). Acylation of *Escherichia coli* Hemolysin: A Unique Protein Lipidation Mechanism Underlying Toxin Function. *Microbiology and Molecular Biology reviews , 62* (2), 309–333.

Stroud, R. M., Miercke, L. J., O'Connell, J., Khademi, S., Lee, J. K., Remis, J., Harries, W., Robles, Y., Akhavan, D. (2003). Glycerol facilitator GlpF and the associated aquaporin family of channels. *Current Opinion in Structural Biology , 13*, 424–431.

Suzuki, H., Hashimoto, W., & Kumagai, H. (1993). *Escherichia coli* K-12 can utilize an exogenous gamma-glutamyl peptide as an amino acid source, for which gamma-glutamyltranspeptidase is essential. *Journal of Bacteriology , 175*, 6038–6040.

Tabor, C. W. (1960). *Biochem. Biophys.Res. Commun , 2*, 117-20.

Tabor, H., & Tabor, C. W. (1975). Isolation, characterization, and turnover of glutathionylspermidine from *Escherichia coli*. *J Biol Chem. , 250* (7), 2648-54.

Tabor, H., Tabor, C. W., & Irreve, F. (1973). Quantitative determination of aliphatic diamines and polyamines by an automated liquid chromatography procedure. *Analytical Biochemistry , 55* (2), 457-467.

Tikhonova, E. B., & Zgurskaya, H. I. (2004). AcrA, AcrB, and TolC of *Escherichia coli* Form a Stable Intermembrane Multidrug Efflux Complex. *Journal of Biological Chemistry , 279* (31), 32116–32124.

Tikhonova, E. B., Devroy, V. K., Lau, S. Y., & Zgurskaya, H. I. (2007). Reconstitution of the *Escherichia coli* macrolide transporter: the periplasmic membrane fusion protein MacA stimulates the ATPase activity of MacB. *Mol Microbiol. , 63* (3), 895-910.

Tikhonova, E., Dastidar, V., Rybenkov, V., & Zgurskaya, H. (2009). Kinetic control of TolC recruitment by multidrug efflux complexes. *Proc Natl Acad Sci U S A. , 106* (38), 16416-21.

Vaccaro, L., Scotta, K. A., & Sansom, M. (2008). Gating at Both Ends and Breathing in the Middle: Conformational Dynamics of TolC. *Biophysical Journal , 95* (12), 5681-5691.

Voet, D., & Voet, J. G. (1996). Chapter 19. Citric acid cycle. *Biochemistry 2nd Edition, John Wiley & sons Inc.*

Vuilleumier, S. (1997). Bacterial glutathione S-transferases: what are they good for? *J Bacteriol. , 179* (5), 1431-41.

Wandersman, C., & Delepelaire, P. (1990). ToIC, an *Escherichia coli* outer membrane protein required for hemolysin secretion. *Proc. Nati. Acad. Sci. USA , 87*, 4776-4780.

Weiner, L., & Model, P. (1994). Role of an *Escherichia coli* stress-response operon in stationary-phase survival. *PNAS , 91*, 2191-2195.

Wiriyathanawudhiwong, N., Ohtsu, I., Li, Z. D., Mori, H., & Takagi, H. (2009). The outer membrane TolC is involved in cysteine tolerance and overproduction in *Escherichia coli*. *Appl Microbiol Biotechnol , 81*, 903-913.

Yamanaka, H., Kobayashi, H., Takahashi, E., & Okamoto, K. (2008). MacAB is involved in the secretion of *Escherichia coli* heat-stable enterotoxin II. *J Bacteriol. , 190* (23), 7693-8.

Yoshida, M., Kashiwagi, K., Shigemasa, A., Taniguchi, S., Yamamoto, K., Makinoshima, H., Ishihama, A., Igarashi, K. (2004). A Unifying Model for the Role of Polyamines in Bacterial Cell. *The journal of Biological Chemistry , 279* (44), 46008–46013 .

Zgurskaya, H. I., & Nikaido, H. (1999 a.). AcrA is a highly asymmetric protein capable of spanning the periplasm. *J Mol Biol , 285*, 409-20.

Zgurskaya, H., & Nikaido, H. (1999). Bypassing the periplasm: reconstitution of the AcrAB multidrug efflux pump of *Escherichia coli*. *Proc Natl Acad Sci U S A , 96,* 7190-5.

Zhang, A., Rosner, J., & Martin, R. (2008). Transcriptional activation by MarA, SoxS and Rob of two tolC promoters using one binding site: a complex promoter configuration for tolC in *Escherichia coli*. *Molecular Microbiology , 69* (6), 1450–1455.

Appendix A. List of strains

Strain name	Genotype	Kanamycin resistance gene (locus)	Primers used for PCR confirmation		Size of PCR product (bp)
			Forward Primer	Reverse Primer	
BW25113/ WT	*lacI*^{q} *rrnB*$_{T14}$ Δ*lacZ*$_{WJ16}$ *hsdR514* Δ*araBAD*$_{AH33}$ Δ*rhaBAD*$_{LD78}$	-	-	-	-
GD100	*ΔtolC*	-	ftolCstart	rygiCkan	
GD101	*ΔygiBC*	-	ftolCstart	rygiCkan	
GD102	*ΔtolC ΔygiBC*	-	ftolCstart	rygiCkan	
GD103	*ΔyjfMC*	+ *yjfMC*	fyjfL	rygiCkan	1800
GD104	*ΔygiBC ΔyjfMC*	+ *yjfMC*	fyjfL	rygiCkan	1800
GD105	*ΔtolC ΔygiBC ΔyjfMC*	+ *yjfMC*	fyjfL	rygiCkan	1800
GD106	*ΔspeE ΔtolC*	+ *tolC*	k2	rygiA	1204
GD107	*ΔgshB ΔtolC*	+ *tolC*	k2	rygiA	1204
GD108	*ΔygiBC ΔyjfMC ΔgspS*	+ *gspS*	k2	rPitB	1556
GD109	*ΔspeE ΔygiBC*	+ *ygiBC*	TolCS1	rygiCkan	1905
GD110	Δ*speE,* Δ*gshB*	+ *gshB*	k2	ryqgE	1303

GD111	*ΔyjfMC ΔtolC*	+ *tolC*	k2	rygiA	1204
GD112	*ΔgshA ΔtolC*	+ *tolC*	k2	rygiA	1204
GD113	MG1655 but *ΔtolC*	+ *tolC*	k2	rygiA	1204
JW0117-1	Δ*speE*	+	k2	rspeD	856
JW2914-1	Δ*gshB*	+	k2	ryqgE	983
			frsmE	ryqgE	1692
JW2956-1	Δ*gspS*	+	k2	rpitB	1556
JW2663-1	Δ*gshA*	+	EmrB forward primer	rygaA	3343
GD201	GD101 but TolCQ352C^{his} in *tolC-ygiBC* locus	NA	TolC start	TolChis	1505
GD202	GD101 but TolCD356C^{his} in *tolC-ygiBC* locus	NA	TolC start	TolChis	1505
GD203	GD101 but TolCS363C^{his} in *tolC-ygiBC* locus	NA	TolC start	TolChis	1505
GD204	GD101 but	NA	TolC	TolChis	1505

	TolCD374C^{his} in *tolC-ygiBC* locus		start		
GD205	GD101 but TolC^{his} in *tolC-ygiBC* locus	NA	TolC start	TolChis	1505
GD206	GD201 but Δ*acrAB*	+ *acrAB*	k2	rAcrABdownstr	1184
GD207	GD202 but Δ*acrAB*	+ *acrAB*	k2	rAcrABdownstr	1184
GD208	GD204 but Δ*acrAB*	+ *acrAB*	k2	rAcrABdownstr	1184

Appendix B. Growth rates of strains

Growth medium	WT	GD100	GD102	GD105
M9 + CAA	0.76 ±0.16	0.96 ±0.03	0.83± 0.06	0.86 ±0.05
M9 + Riboflavin	0.652	0.25	0.58	0.21
M9 + Thiamine	0.628	0.40	0.47	0.21
M9 + Aspartate	0.61	ND	ND	0.57
M9 + Glutamate	0.6 ±0.04	ND	ND	0.38 ±0.16
M9 + Methionine	0.58	ND	ND	0.51
M9 + 0.4g/L Alanine	1.2	ND	ND	1.4
M9 + Serine	0.54 ±0.03	ND	ND	0.61± 0.042
M9 + Glycine	0.66± 0.06	ND	ND	0.36 ±0.085
M9 + Glycerol	0.38± 0.05	0.41 ±0.007	ND	0.43± 0.07
M9 + Fructose	0.46± 0.03	0.43 ±0.03	ND	0.42± 0.06
M9 + Xylose	0.41± 0.03	0.41± 0.04	ND	0.41 ±0.007
M9 + 2mM GSH	0.64	0.5	ND	0.23
Cells transformed with pTolC^{his} plasmid (M9 medium)	ND	0.59	0.58	0.49±0.05
LB +5 mM GSH	1.0 ± 0.09	0.97	ND	0.98±0.05
LB + 10 mM GSH	0.87±0.1	0.65	ND	0.53±0.07
LB + 15 mM GSH	0.64±0.07	No growth	ND	No growth
LB + 1 mM L-cys	1.2	1.14	ND	1.14

LB + 5 mM L-cys	1.2	1.17	ND	1.12
LB + glucose	1.2	ND	ND	1.4

ND- not determined

Appendix C. List of primers

Primer name	Sequence 5'→3'
fTolCKana	ATC GGC CTG AGC CTT TCT GGG TTC AGT TCG TTG AGC TGT GTA GGC TGG AGC TGC TT
rTolCKana	CGG TTT GCT CAG CGC ATT GTT CTG TCC CCA GAG CTG ACC ATA TGA ATC CTC CTT AG
K2	CGG TGC CCT GAA TGA ACT GC
TolC start	AAT GCA AAT GAA GAA ATT GC
ftolcstart	AGT TTG ATC GCG CTA AAT ACT GCT TCA CCA CAA GGA ATG CAA ATG AAG AAA TTG CT
rtolC	TAC GTT CAG ACG GGG CCG AAG CCC CGT CGT CGT CAT CAG TGG TGG TGG TGG TGG TG
rtolChis2	TAC GTT CAG ACG GGG CCG AAG CCC CGT CGT CGT CAT CAG TGG TGG TGG TGG TGG TGG TTA

	CGG
rygiA	TGG CTG GTC GAA ATT GAA GC
fygiAkan	GCT TCG GCC CCG TCT GAA CGT AAG GCA ACG TAA AGA TGT GTA GGC TGG AGC TGC TT
rygiCkan	ATA TGT GGA TAA AAC CGA GAC ATA TCC TGG GTG ATC CAT ATG AAT ATC CTC CTT AG
fygiBkan	AGA GTG ATG AAA CAG TGT CTC TCT ATC AAA ATG CTG TGT GTA GGC TGG AGC TGC TT
fyjfMkan	AAC AGT AAA ATT GGT CAC GGA GCG ATT AGT CGC ATT TGT GTA GGC TGG AGC TGC TT
ryjfCkan	CAA TCT GCG GTT TCT CGC CAT CGA ACC AGG ACG CAA CAT ATG AAT ATC CTC CTT AG
fyjfL	GAG TAT TCC AGA CTA TTT CG
raidB	ACG GTG TGA GTT TGC CAG TG
raid2	GCG CAA TAA TTC AGG CGG AT
rYqgE	CCA GCG GCT TGT TGA CGA TG
ryqaA	TGG CAC TAA TTG TAG GCC TGC AC
rSpeD	CGG CAG TTT TGG CGT AGC AG

rPitB	CGC AAT GAC CAG GCC GAC GA
fRsmE	GAT ATC CTG TTG GGA CCT CGC G
LP gsp	TAA TCA GTA CGG GGT TGC TAC
RP gsp	ACA ACA ATT ACG CCA ACT GCT TAG
RygiBRT	CAT CAT GTA ACC GGC CAT CAG
yyqgE2	GGC CGT TAG CCA CGC GTT ATC
rygiBRT#2	GTA TCA GCC ACC CAT TGA ACG
rygiCRT	GAT GTA GAG GAA CTC AGT AGC
TolCD1	CAA AGC TCA TTA TGC GCG ATG GAA GCG
TolCS2	CGC GTA CCG ACG CAG TAG CCC GCT TC
fAcrABKanDisrptn	TTT TGA CCA TTG ACC AAT TTG AAA TCG GAC ACT CGA GGT GTA GGC TGG AGC TGC TTC
rAcrABKanDisrptn	AGG CCG CTT ACG CGG CCT TAG TGA TTA CAC GTT GTA TCC ATA TGA ATA TCC TCC TTA G
rAcrABdownstr	ACT AAT ACC AGG ATT GCT CGT